

2012

Experimental study of the effect of drilling fluid contamination on the integrity of cement-formation interface

Nnamdi Charles Agbasimalo

Louisiana State University and Agricultural and Mechanical College, agbasimalo@gmail.com

Follow this and additional works at: https://digitalcommons.lsu.edu/gradschool_theses



Part of the [Petroleum Engineering Commons](#)

Recommended Citation

Agbasimalo, Nnamdi Charles, "Experimental study of the effect of drilling fluid contamination on the integrity of cement-formation interface" (2012). *LSU Master's Theses*. 2403.

https://digitalcommons.lsu.edu/gradschool_theses/2403

This Thesis is brought to you for free and open access by the Graduate School at LSU Digital Commons. It has been accepted for inclusion in LSU Master's Theses by an authorized graduate school editor of LSU Digital Commons. For more information, please contact gradetd@lsu.edu.

EXPERIMENTAL STUDY OF THE EFFECT OF DRILLING FLUID CONTAMINATION ON
THE INTEGRITY OF CEMENT-FORMATION INTERFACE

A Thesis

Submitted to the Graduate Faculty of the
Louisiana State University and
Agricultural and Mechanical College
in partial fulfillment of the
requirements for the degree of
Master of Science in
Petroleum Engineering

in

The Craft and Hawkins Department of Petroleum Engineering

by
Nnamdi Charles Agbasimalo
B.Eng., Federal University of Technology, Owerri, 2005
August 2012

ACKNOWLEDGMENTS

I wish to express my deepest gratitude to Dr Mileva Radonjic for her patience, guidance and support throughout this study. I would like to thank Dr Richard Hughes, Dr Julius Langlinais, and Dr Andrew Wojtanowicz for graciously accepting to serve on my thesis committee.

I thank all members of the Sustainable Energy and Environmental Research (SEER) group for their contributions and support in the course of this study. I sincerely appreciate the resourcefulness of Fenelon Nunes, Gerry Masterman, Darryl Bourgoyne and Janet Dugas. I am grateful to Dr Clinton Willson, Dr Kyungmin Ham, Dr Dongmei Cao, Dr Varshni Singh and Wanda LeBlanc for their help with material characterization. I am immensely grateful to the Craft & Hawkins Department of Petroleum Engineering for providing me with assistantship for two years during this study. I also wish to thank all my friends and colleagues at LSU for their encouragement through the years. My heartfelt gratitude goes to Jidekene Atuchukwu for her support and encouragement.

I wish to express my profound gratitude to my parents, Sir Okey and Dr (Lady) Ngozi Agbasimalo, and my siblings, Ikechukwu, Onyinye, Byron and Arinze, for their love and support.

TABLE OF CONTENTS

ACKNOWLEDGMENTS	ii
LIST OF TABLES	v
LIST OF FIGURES	vi
NOMENCLATURE	x
ABSTRACT.....	xi
CHAPTER 1. INTRODUCTION	1
1.1 Background	1
1.2 Objective	2
1.3 Methodology	3
1.4 Overview of Thesis	3
CHAPTER 2. LITERATURE REVIEW	5
2.1 Well Cements	5
2.1.1 Portland Cement Chemistry and Classification.....	5
2.1.2 Process of well cementing	7
2.1.3 Problems in well cementing	8
2.1.4 Cement Behavior in low pH environment.....	9
2.1.5 Studies on Cement Interaction with Low pH Environment	11
2.2 Drilling Fluid (Mud).....	17
2.2.1 Drilling Fluid Composition and Usage.....	17
2.2.2 Mud Removal and Displacement Efficiency.....	18
2.2.3 Bentonite Chemistry and its Behavior in Low pH Environment.....	19
2.2.4 Studies on Effect of Mud Contamination on Cement Properties	20
2.3 Cement-Formation Interface in the Wellbore	21
2.3.1 Nature of Cement-Formation Interface	21
2.3.2 Factors affecting the cement-rock bond	22
2.3.3 Studies on Effect of Mud Contamination on Cement-Formation Bond.....	23
CHAPTER 3. EXPERIMENTAL SETUP AND PROCEDURE.....	27
3.1 Experimental Program.....	27
3.2 Composite Core Preparation	27
3.3 Experimental Fluids	29
3.4 Experimental Setup	32
3.4.1 Biaxial Type Core Holder.....	32
3.4.2 Syringe Pump	32
3.4.3 Back-pressure Regulator (BPR)	32
3.4.4 Pressure Data Acquisition System.....	34
3.5 Material Characterization Techniques	35
3.5.1 Surface Profilometry.....	35

3.5.2 X-Ray Computed Tomography (Low Resolution CT).....	35
3.5.3 X-Ray Microtomography (High Resolution CT)	36
3.5.4 Image Based Porosity	39
3.5.5 Light (Optical) Microscopy	40
3.5.6 Scanning Electron Microscopy (SEM).....	41
3.5.7 X-Ray Diffraction (XRD).....	42
3.5.8 Inductively Coupled Plasma-Optical Emission Spectroscopy (ICP-OES)	43
CHAPTER 4. RESULTS AND DISCUSSION.....	44
4.1 Surface Profilometry	44
4.2 X-Ray Computed Tomography (Low Resolution CT)	45
4.3 Micro-CT (High Resolution CT) and Image Based Porosity.....	47
4.3.1 Mud Contamination Experiment [0%]	49
4.3.2 Mud Contamination Experiment [5%]	54
4.3.3 Mud Contamination Experiment [10%]	59
4.4 Pressure Profile	64
4.5 pH Measurements.....	65
4.6 X-ray Diffraction (XRD) Data	66
4.7 Scanning Electron Microscopy (SEM) Images	68
4.8 Light (Optical) Microscopy.....	70
4.9 Inductively Coupled Plasma-Optical Emission Spectroscopy (ICP-OES)	73
4.10 Discussion of Results	74
4.10.1 pH Increase	74
4.10.2 Pressure Drop Increase	75
4.10.3 Porosity Increase.....	77
4.10.4 Summary of Observations	79
CHAPTER 5. CONCLUSIONS AND RECOMMENDATIONS	83
5.1 Conclusions from the Experimental Findings	83
5.2 Recommendations for Future Work	84
REFERENCES	85
APPENDIX.....	92
VITA	93

LIST OF TABLES

Table 2.1: Mineralogical composition of unhydrated cement ¹⁵	5
Table 2.2: Major cement hydration products ^{3,16}	6
Table 3.1: Composite core design for flow-through experiments.....	28
Table 3.2: Brine composition used in experiments ⁶⁰	31
Table 4.1: Properties of typical Berea sandstone core used for each composite core	64
Table 4.2: ICP-OES analysis of influent and effluent brine samples showing the concentration of different cations present. The brine samples analyzed were for the 1 st , 15 th and 30 th day of each flow-through experiment.	73
Table 4.3: Pre core-flood porosity of cement in the composite cores	81
Table 4.4: Post core-flood porosity of the cement at the inlet of the composite cores.....	81
Table 4.5: Post core-flood porosity of the cement at the outlet of the composite cores.....	82

LIST OF FIGURES

Figure 3.1: Preparation procedure for composite cores	
A: Half cylinder Berea sandstone cores showing the flat longitudinal surface of the cores roughened with coarse Norton® emery cloth	
B: Mud-contaminated cement poured on the half-cylinder Berea Sandstone	
C: Side view of mold with sandstone placed inside and neat cement poured into the mold	
D: Top view of mold with sandstone placed inside	
E: Top view of mold with sandstone placed inside and neat cement poure	30
Figure 3.2: Cement-sandstone composite core	31
Figure 3.3: Schematic of experimental setup.....	33
Figure 3.4: Experimental setup showing the vertically oriented core holder and syringe pumps.....	34
Figure 3.5: Sample preparation procedure for microtomography showing the sections of the composite core where the mini cores were drilled from and also images of mini cores	37
Figure 3.6: Schematics of composite cores showing the orientation utilized during the drilling of mini cores. The mini cores are represented with dotted lines and the green arrows indicate direction of drilling	38
Figure 3.7: Sample preparation procedure for scanning electron microscopy and optical microscopy showing where the samples were taken from.....	40
Figure 4.1: Surface profile of 113 μm x 149 μm section of Berea sandstone showing the peaks and the valleys. The red represents peaks in both plots while the white and blue represent valleys in the 2D and 3D plots respectively. The large red patch on the plots indicates quartz crystal while the white and blue regions indicate where pores are present.....	44
Figure 4.2: Plot showing how the surface roughness values were obtained.....	45
Figure. 4.3: Low resolution CT images of 1 in by 12 in cement-sandstone composite cores. The brighter half is the cement while the darker half is the sandstone. Longitudinal and cross sectional views of the image reveal effective bonding between the cement and the rock before and after core-flooding.....	46
Figure 4.4: Schematics of composite cores showing the orientation utilized during the drilling of mini cores and the resultant cross sections after drilling. The mini cores are represented with dotted lines and the green arrows indicate direction of drilling.....	48
Figure 4.5a: Micro-CT images of 3 mm diameter mini cores drilled from the cement of the 0% mud contaminated cement-sandstone composite core (inlet and outlet) after 30 days of core-flood and also from a control sample. The control sample mini core shows uniform density (uniform brightness). The post core-flood mini cores (inlet and outlet) on the other hand reveal presence of	

lower density cement (dark gray color) close to the sandstone. The black spots in the lower density region indicate increased porosity. The zones numbered 1,2, and 3 are where the axial slices in Figure 4.5b were taken from. 50

Figure 4.5b: Axial slices of Micro-CT images of 3 mm diameter mini cores drilled from the cement of the 0% mud contaminated cement-sandstone composite core (inlet and outlet) after 30 days of core-flood and also from a control sample. The control sample mini core shows uniform density (uniform brightness). The post core-flood mini cores (inlet and outlet) on the other hand reveal presence of lower density cement (dark gray color) close to the sandstone. The black spots in the lower density region indicate increased macroporosity. 51

Figure 4.6a: Micro-CT images of 3 mm diameter mini cores drilled from the cement-sandstone interface of the 0% mud contaminated cement-sandstone composite core (inlet and outlet) after 30 days of core-flood and also from a control sample. The cement in the control sample show uniform density (uniform brightness). The post core-flood mini cores (inlet and outlet) on the other hand reveal presence of lower density cement (dark gray color) close to the sandstone. The black spots in the lower density region indicate increased macroporosity. 52

Figure 4.6b: Axial slices of Micro-CT images of 3 mm diameter mini cores drilled from the cement-sandstone interface of the 0% mud contaminated cement-sandstone composite core (inlet and outlet) after 30 days of core-flood and also from a control sample. The cement in the control sample show uniform density (uniform brightness). The post core-flood mini cores (inlet and outlet) on the other hand reveal presence of lower density cement (dark gray color) close to the sandstone. The black spots in the lower density region indicate increased macroporosity. Axial slices were chosen to represent typical features in the mini cores. 53

Figure 4.7a: Micro-CT images of the mini cores drilled from the cement of the 5% mud contaminated cement-sandstone composite core (inlet and outlet) after 30 days of core-flood and also from a control sample. The neat cement and contaminated cement in the control sample show no significant density difference (no difference in brightness levels). The post core-flood mini cores (inlet and outlet) on the other hand reveal presence of lower density cement (dark gray color) close to the sandstone. The black spots in the lower density region indicate increased macroporosity. 55

Figure 4.7b: Axial slices of Micro-CT images of the mini cores drilled from the cement of the 5% mud contaminated cement-sandstone composite core (inlet and outlet) after 30 days of core-flood and also from a control sample. The neat cement and contaminated cement in the control sample do not show identifiable density difference (no difference in brightness levels). The post core-flood mini cores (inlet and outlet) on the other hand reveal presence of lower density cement (dark gray color) close to the sandstone. The black spots in the lower density region indicate increased macroporosity. Axial slices chosen to represent typical observations in the mini cores. 56

Figure 4.8a: Micro-CT images of the mini cores drilled from the cement-sandstone interface of the 5% mud contaminated cement-sandstone composite core (inlet and outlet) after 30 days of core-flood and also from a control sample. The neat cement and contaminated cement in the control sample show no significant density difference (no difference in brightness levels). The

post core-flood mini cores (inlet and outlet) on the other hand reveal presence of lower density cement (dark gray color) close to the sandstone. The black spots in the lower density region indicate increased macroporosity..... 57

Figure 4.8b: Axial slices of Micro-CT images of the mini cores drilled from the cement-sandstone interface of the 5% mud contaminated cement-sandstone composite core (inlet and outlet) after 30 days of core-flood and also from a control sample. The neat cement and contaminated cement in the control sample show no significant density difference (no difference in brightness levels). The post core-flood mini cores (inlet and outlet) on the other hand reveal presence of lower density cement (dark gray color) close to the sandstone. The black spots in the lower density region indicate increased macroporosity..... 58

Figure 4.9a: Micro-CT images of the mini cores drilled from the cement of the 10% mud contaminated cement-sandstone composite core (inlet and outlet) after 30 days of core-flood and also from a control sample. The neat cement and contaminated cement in the control sample show slight density gradation between them (difference in brightness levels). The post core-flood mini cores (inlet and outlet) on the other hand reveal presence of large pores in the contaminated cement. The large pores are indicated by black spots in the contaminated cement..... 60

Figure 4.9b: Axial slices of Micro-CT images of the mini cores drilled from the cement of the 10% mud contaminated cement-sandstone composite core (inlet and outlet) after 30 days of core-flood and also from a control sample. The neat cement and contaminated cement in the control sample show slight density gradation between them (difference in brightness levels). The post core-flood mini cores (inlet and outlet) on the other hand reveal presence of large pores in the contaminated cement. The large pores are indicated by black patches in the contaminated cement. A reduced density zone is also observed around some of the large pores. 61

Figure 4.10a: Micro-CT images of the mini cores drilled from the cement-sandstone interface of the 10% mud contaminated cement-sandstone composite core (inlet and outlet) after 30 days of core-flood and also from a control sample. The neat cement and contaminated cement in the control sample show slight density gradation between them (difference in brightness levels). The post core-flood mini cores (inlet and outlet) on the other hand reveal presence of large pores in the contaminated cement. The large pores are indicated by black patches in the contaminated cement. 62

Figure 4.10b: Axial slices of Micro-CT images of the mini cores drilled from the cement-sandstone interface of the 10% mud contaminated cement-sandstone composite core (inlet and outlet) after 30 days of core-flood and also from a control sample. The neat cement and contaminated cement in the control sample show slight density gradation between them (difference in brightness levels). The post core-flood mini cores (inlet and outlet) on the other hand reveal presence of large pores in the contaminated cement. The large pores are indicated by black patches in the contaminated cement. A reduced density zone is also observed around some of the large pores..... 63

Figure 4.11: Pressure profile of the core-flood experiments. The pressure drop periodically increased and leveled off as the experiments progressed. The periods of pressure drop stability were longer in the 5% and 10% mud contamination experiments..... 65

Figure 4.12: Plot of pH measurements of effluent samples taken daily. The pH values for effluent brine from 0% contamination experiment were generally lower than those of 5% and 10% contamination experiments. 66

Figure 4.13: XRD plot for Berea Sandston showing presence of Quartz, Albite and clays. 67

Figure 4.14: Inlet of cement-sandstone composite core showing
(a) A clean surface at the inlet at the beginning of the flow-through experiment
(b) Presence of brown layer at the inlet at the end of flow-through experiment 67

Figure 4.15: XRD plot for the brown deposit observed at the inlet of the composite cores at the end of core-flood. The plot has no identifiable peaks showing that the substance is amorphous. Amorphous silica gel is the final product of cement degradation. 67

Figure 4.16: Secondary Electron Microscopy images of fresh Berea sandstone showing quartz crystals surrounded by clays. 68

Figure 4.17: Back scattered electron microscopy images of 0% mud contaminated core showing a low density region in the cement closest to the cement-sandstone interface in the post core flood sample; this zone is clearly absent in the pre core-flood sample
(a) Pre core-flood composite core (b) and (c) Post core-flood composite core 69

Figure 4.18: Back scattered electron microscopy images of 10% mud contaminated core showing large pores filled with resin in the cement closest to the cement-sandstone interface in the post core flood sample. The pre core-flood sample clearly shows absence of large pores
(a) Pre core-flood composite core (b) and (c) Post core-flood composite core 70

Figure 4.19: Optical Images of cement-sandstone composite cores. Pink coloration indicates areas with high calcium content and red to purple indicates carbonated areas
(a) Pre core-flood 0% mud contamination (b) Post core-flood 0% mud contamination
(c) Pre core-flood 10% mud contamination (d) Post core-flood 10% mud contamination . 72

Figure 4.20. Schematics of typical axial slices of the Micro-CT images of the interface-evaluation mini cores at the end of the flow-through experiments. 80

NOMENCLATURE

m_i = Molality, m (number of moles per 1 kg of aqueous solution)

k = Permeability, D or m^2

ϕ = Porosity, %

P = Pressure, psi or MPa

T = Temperature, °C or °F

Q = Flow rate, ml/min

μ = Viscosity, cp

PV = Pore volume

ABSTRACT

Well cementing is one of the key processes performed during drilling and completion of wells. The main objective of primary cementing is to provide zonal isolation. Failure of cement to provide zonal isolation can lead to contamination of fresh water aquifers, sustained casing pressure, or blowout. For effective cementing, the cement slurry should completely displace the drilling fluid. In practice, this is hard to achieve and some mud is left in the wellbore where it contaminates the cement after cement placement.

This study investigates the effect of mud contamination of cement on the integrity of cement-formation interface. Flow-through experiments were conducted over 30-day periods using cement-sandstone composite cores and brine (salinity ~20,000 ppm) at 2100 psi (14.48 MPa) confining pressure, temperature of 72°F (22.22°C) and flow rate of 1 ml/min. Each cylindrical composite core was composed of half-cylinder Berea sandstone and half-cylinder Portland cement paste, with dimensions 12 in (30.48 cm) in length and 1 in (2.54 cm) in diameter. One composite core had no contaminated layer and each of the two other cores had a ~1.27 mm (0.05 in) thick layer of contaminated cement with 5% or 10% mud contamination by volume.

Image based techniques used to characterize the composite cores revealed the presence of large non-circular pores (with as much as ~750 μm length and ~150 μm thickness) in the mud contaminated cement at the end of the core-flood. The large pores were higher in number in the 10% than in the 5% mud contaminated cement. The pores did not appear to be interconnected at the end of 30-day core-flood although leaching of the cement surrounding the large pores was observed. The porosity of the 10% mud contaminated cement was found to have increased from 0.65% to 12.53%.

Based on the observations, we can conclude that large pores are created in cement due to the presence of mud contamination and the pores increase in number as level of mud contamination increases. Leaching of the cement surrounding the large pores may lead to interconnectivity of the large pores in the long run and result in loss of zonal isolation.

CHAPTER 1 INTRODUCTION

1.1 Background

Wellbore cementing has come a long way since Frank Hill first used Portland cement to seal off a water bearing formation in 1903 at the Lompoc field in California¹. Cement job design and placement has evolved over the years but the primary objectives of wellbore cementing have remained the same. Primary cementing is carried out to provide zonal isolation, provide structural support for the casing, and protect the casing from attack by corrosive fluids². The most critical function of wellbore cement is to provide zonal isolation^{3,4} and failure of cement to provide this function can result in one or more of the following: contamination of fresh water aquifers, loss of hydrocarbon reserves in producing wells, loss of injected fluids in injector wells, sustained casing pressure or even a blowout. Various studies have shown that cement failure can occur in both active and abandoned wells and provide pathways for leakage of wellbore fluids⁵⁻⁷. The pathways could be created by failure at the cement-casing interface, cement-formation interface or even within the bulk cement (due to channels or fractures)³. To prevent a leakage path from being created at the cement-formation interface, a good bond is required between the cement and the formation. The bond should be good enough to withstand the effects of cyclic loading and exposure of cement to corrosive fluids. Unfortunately, poor cement bond exists in a large number of wells and it has been identified as one of the leading causes of sustained casing pressure (SCP)⁸. Currently, more than 8000 wells in the Gulf of Mexico exhibit sustained casing pressure⁹. This figure is alarming considering the safety, environmental and financial implications of having so many leaking wells. About \$50 million is spent annually in the USA for fixing cement failures⁷ and it costs an average of \$639,000 to plug and abandon a well in the Gulf of Mexico¹⁰. These have motivated several studies to be carried out to provide better

understanding of cement-rock bond issues. These studies have shown that poor cement-formation bond is usually caused by poor primary cementing which includes inadequate mud displacement³. When a well is being drilled, partially dehydrated-gelled drilling fluid and mud cake are deposited on the wall of the wellbore¹¹. These are usually difficult to displace, leaving mud channels through the cement. Several studies on mud displacement efficiency have shown that displacement efficiency can range between 37% and 99.7% depending on mud conditioning, casing centralization, cement-mud density difference, and flow regime^{3, 12, 13}. The presence of mud channels have been shown to reduce cement-formation bond strength and create pathways for fluid migration. Some of the residual mud contaminate the cement in the wellbore altering its properties and consequently its ability to provide zonal isolation and this is the basis of this study.

1.2 Objective

The objectives of this study are to assess the effect of drilling fluid contamination of cement on cement's ability to provide zonal isolation and investigate the physicochemical alterations at the interface transition zone. The ability of cement to provide zonal isolation is determined by the integrity of both the cement and the cement-formation interface³. The bond between the cement and the rock is defined by the mechanical interlocking of cement hydration products with the rock grains and the chemical reaction between the cement paste and rock grains. The contamination of the cement by drilling fluid alters the properties of the cement and this in turn affects the character of the bond between the cement and the rock. To delineate the extent of the effect of the contamination of cement slurry on the integrity of the cement-rock interface, experimental and material characterization techniques were employed.

1.3 Methodology

To realize the objectives of the study, 30-day flow-through experiments were conducted using 1 in (2.54 cm) by 12 in (30.48 cm) cement-sandstone composite cores. Class-H cement (water to cement ratio-w/c=0.38) and 300 mD Berea sandstone were used for the composite cores. The composite cores used for the flow-through experiments had 0%, 5% and 10% drilling fluid contamination of the cement respectively. Experiments were performed using brine (salinity ~20,000 ppm) at a flow rate of 1 ml/min, overburden pressure of 2100 psi (14.48 MPa) and temperature of 72 °F (22.22 °C). The pressure drop across each composite core was recorded throughout the core-flood to observe the changes in permeability of the composite cores. Extensive quantitative and qualitative material characterization of the cement-sandstone cores were carried out to evaluate the alterations at the cement-sandstone interface and also ascertain the reaction mechanisms that produced the alterations. Influent and effluent brine samples were analyzed to corroborate observations from other analysis techniques.

1.4 Overview of Thesis

Chapter 1 deals with the importance of good cementing to the life of a well. It also presents the objectives and methodology of the study.

Chapter 2 covers the literature review on pertinent areas including cementing, cement chemistry, mud displacement efficiency, drilling fluid contamination of cement and cement-formation interface.

Chapter 3 lays out the experimental design and procedures followed in the study. It explains the equipment used, the sample preparation process and the material characterization techniques employed.

Chapter 4 presents the data collected from the flow-through experiments and from the characterization of pre and post core-flooded composite cores. It also provides a discussion of the results with comparison to similar studies.

Chapter 5 presents the conclusions reached at the end of the study. It also outlines the recommendations made for future work on drilling fluid contamination of cement-formation interface.

CHAPTER 2 LITERATURE REVIEW

The study was undertaken to investigate the effect of drilling fluid contamination of cement on the integrity of the cement-rock interface and to understand the physicochemical processes occurring at the interface. A thorough literature review covering the three major components of the interface - cement, drilling fluid and the formation – as well as their behavior as a system, was carried out and is presented below.

2.1 Well Cements

2.1.1 Portland Cement Chemistry and Classification

Portland cement is the dominant cement used in wellbore construction³. It is used for primary cementing, remedial cementing and plug and abandonment of wells. Unhydrated Portland cement is comprised of four major compounds as shown in Table 2.1. The compounds are anhydrous and react chemically with water forming hydrated products. The major products of cement hydration are shown in Table 2.2. Ettringite ((CaO)₆(Al₂O₃)(SO₃)₃.32H₂O) is also produced during cement hydration. Hardened cement paste still contains unhydrated cement grains and the degree of hydration of cement does not change substantially after 28 days¹⁴.

Table 2.1: Mineralogical composition of unhydrated cement¹⁵.

Oxide Composition	Cement Notation	Common Name	Concentration (wt%)
3CaO.SiO ₂	C ₃ S	Alite	55-65
2CaO.SiO ₂	C ₂ S	Belite	15-25
3CaO.Al ₂ O ₃	C ₃ A	Aluminate	8-14
4CaO.Al ₂ O ₃ .Fe ₂ O ₃	C ₄ AF	Ferrite phase	8-12

Table 2.2: Major cement hydration products^{3, 16}.

Chemical Formula	Cement Notation	Common Name	Concentration (wt%)
3CaO·2SiO ₂ ·3H ₂ O	C-S-H	C-S-H	50-70
Ca(OH) ₂	CH	Portlandite	15-25

Calcium silicate hydrate (C-S-H) is poorly crystalline and acts as a binder in cement. It gives the cement its strength. Calcium hydroxide (CH) helps to maintain the pH of cement at ~13. Cement is a porous material and the pores, filled with highly alkaline solution (pH ~13), are grouped into gel (nano) pores, capillary pores, hollow-shell pores and air voids depending on the size and mechanism of formation¹⁶. The pore sizes range from 0.5 nm to several millimeters. The lower range of the pore sizes is made up of nano and capillary pores while the higher range is mainly isolated air voids that were entrapped during cement mixing and placement.

Cement is used for several purposes in a wellbore and is placed at different depths and conditions in a wellbore. This exposes cement to a wide range of temperatures and pressures and attack by formation fluids which can be corrosive in nature. Several cement formulations are available to satisfy the requirements of these different conditions. API specification 10A established 8 classes of Portland cement based on the conditions for which they are most suitable. The cement classes are designated A to H. Cement is also grouped into 3 grades based on their sulfate resistance capability: O (Ordinary), MSR (Moderate Sulfate Resistant) and HSR (High Sulfate Resistant). Sulfate resistance level is based on the C₃A (tricalcium aluminate) content, which influences the durability of cement under sulfate attack. Class A, G, and H cements have been used extensively in wellbores but Class G and H are the most commonly used today. Class G is the most frequently used class of cement outside the USA while class H is the most popular in the USA (apart from California, the Rocky Mountain region and Alaska)¹⁴. Class

A cement is intended for use up to a depth of 6,000 ft (1,830 m) and in less aggressive environments, where special cement properties are not required. It is only available in Ordinary grade. Class G and H are intended to use up to a depth of 8,000 ft (2,440 m) as manufactured but can be modified by addition of various additives to make them suitable for use in greater depths and more challenging downhole conditions. Class G and H are essentially identically in terms of chemical composition but Class H has larger particles (blaine fineness = 1600 cm²/g) than Class G (blaine fineness = 1800 cm²/g)³. Class G (w/c 0.44) hydrates faster than Class H (w/c 0.38) due to the larger surface area of its smaller particles. Both are available in MSR and HSR grades.

2.1.2 Process of well cementing

The process of well cementing involves gathering information for cement job design, designing the cement slurry, calculating the cement volume and cementing time requirements, selecting cement placement technique, and placing the cement. The quality of a cement job is heavily dependent on how good the cement job design was. Information about wellbore configuration and environment are crucial to a cement job design as they affect the cement slurry design and determine the cement placement technique to be utilized. The wellbore configuration information includes measured depth, open-hole size, and casing properties. These strongly influence the slurry volume required, hydrostatic pressure and friction pressure. Information about the wellbore environment includes the pore and fracture pressure profiles, type of formation being cemented, temperature profile, presence of gas, and mud properties. All the information listed above are processed prior to cement slurry design. During slurry design, additives are added to basic Class H or G cement to provide the cement with the desired properties. The additives include retarders, dispersants, fluid loss additives, and viscosifiers. Retarders (e.g. lignosulfonates) extend the setting time of cement while dispersants (e.g.

polynaphthalene sulfonate), reduce the viscosity of the cement. The slurry design process is a complex process involving additives that interfere with the performance of each other. Once the slurry design is available and the cement volume and cementing time required for the cement job are calculated, the process of cement placement can be initiated. Several primary cement placement techniques like normal displacement method, stage cementing, multiple string cementing etc. are available¹⁷. The cement placement technique selected for a cement job depends on various factors like the objectives of the cementing, string type to be cemented, and pressure profile of the well section.

2.1.3 Problems in well cementing

The basic functions of cement are to provide zonal isolation, structural support for the wellbore and casing protection against corrosive fluids. An unsuccessful cement job will lead to failure of cement to perform these functions and a secondary cement job may be carried out. Even when a good cement job is accomplished, cement can still fail in the long term due to several other factors. Consequently, wellbore cement problems can be grouped into two:

1. Short term cement problems

- i. Incomplete cementing due to casing eccentricity. Thus occurs when the casing is not properly centered in the wellbore causing preferential flow of the injected cement through the wider section on the casing-formation annulus. This results in the smaller annulus not being cemented.
- ii. Inadequate drilling mud removal. Gelled mud or mud cake in the wellbore are usually difficult to remove leaving residual mud on the wellbore wall. The residual mud interferes with the bonding of the cement to the formation resulting in a weak cement formation bond.

iii. Influx of formation fluids during cement setting. During the transition from cement slurry to hardened cement, the cement loses some of its ability to transmit hydrostatic pressure and this may allow gas influx into the wellbore from the formation.

2. Long term cement problems

i. Mechanical stress and strain on the cement due to pressure and temperature cycles over the life of the well. These occur during completion, pressure testing, and production.

The differences in thermal expansion and elasticity coefficients of casing, cement, and formation can induce creation and propagation of micro-annulus at the casing-cement interface, formation of a micro-annulus at the cement-formation interface, or creation of micro fractures in cement sheath.

ii. Geochemical degradation of the cement over time due to acid and sulfate attack.

Geochemical downhole conditions vary from well to well. Some environments are acidic due to the presence of relatively high concentrations of H₂S and CO₂. These have been shown to attack the cement affecting its mechanical properties. Sulphates are also present in some wellbore environments and these react with the cement to form ettringite and gypsum. The ettringite and gypsum have greater bulk volume than the cement from which they form. This causes compression of the surrounding sections of the cement, inducing stresses in the cement that result in cement fracturing^{2, 18}.

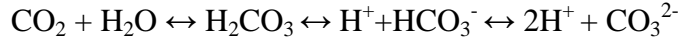
2.1.4 Cement Behavior in low pH environment

The incompatibility between the pH of cement pore solution and pH of the environment in which the cement is placed leads to chemical interaction between the cement and the environment. The cement pore solution is strongly alkaline with pH ~13. In an undisturbed state, the cement pore solution is in thermodynamic equilibrium with the hydrated cement^{19, 20}. When

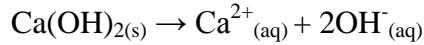
the cement is exposed to a lower pH solution like pure water, the thermodynamic equilibrium is disturbed. The concentration gradient between the cement pore water and surrounding water will induce diffusion of Na^+ , K^+ , and OH^- ions from the cement pore water to the pure water to equilibrate the environment. The outward diffusion of Na^+ , K^+ , and OH^- ions from the cement pore water reduces its pH which in turn induces the dissolution of CH accompanied by gradual decalcification of C-S-H^{19, 21}. Decalcification of C-S-H usually occurs in areas where CH is depleted and therefore unable to provide a buffer for the C-S-H. Depletion of the CH increases the porosity of the cement and consequently the permeability; this increases the rate of diffusion of the calcium leading to increased leaching of the calcium. In a typical cement leaching process by low pH environments, the inner front is characterized by dissolution of CH and the outer region is laced with progressive decalcification of C-S-H gels¹⁹. The decalcification of the C-S-H leads to the formation of silica gel with attendant reduction in mechanical strength.

The presence of CO_2 in the cement environment leads to degradation of the cement by a more convoluted mechanism. When CO_2 dissolves in water it forms carbonic acid. If cement is placed in such water, there would be dissolution of CH leading to outward diffusion of Ca^{2+} from the cement. Reaction between the carbonic acid and the diffusing calcium ions precipitates CaCO_3 (a process known as carbonation)²². As more CH is dissolved, the pH of the cement pore solution drops. When the pH drops below 10.5, the precipitated CaCO_3 becomes unstable and starts dissolving²³. Water soluble bicarbonates start forming and leaching out of the cement. The dissolution of CaCO_3 leaves the C-S-H with no buffer and the decalcification of C-S-H progresses with resultant formation of amorphous silica gel. The chemical equations describing the whole process are shown below²²⁻²⁵.

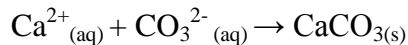
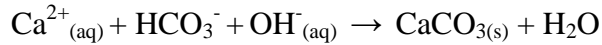
CO₂ dissolves in water to form carbonic acid



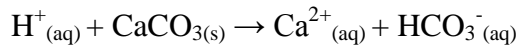
Calcium dissolves in water to maintain thermodynamic equilibrium



Calcium ions react with carbonic acid to precipitate calcium carbonate



As calcium hydroxide is depleted, pH drops and calcium carbonate starts dissolving



Depletion of calcium carbonate promotes decalcification of C-S-H resulting in formation of amorphous silica gel



2.1.5 Studies on Cement Interaction with Low pH Environment

Numerous lab and field studies have been carried out to characterize the behavior of cement in low pH environments. Some of the notable studies are presented below.

Jain and Neithalath²¹ conducted experiments to evaluate the behavior of neat and modified cements in pure water. Silica fume, fly ash and fine glass powder were added to the modified cement samples. The batch experiments were done with deionized water at liquid-solid ratio of 1000 for 90 days with intermittent sample analysis. Porosity of all cement samples increased with leaching duration. At the end of the experiment, the porosity of neat cement was found to be the highest. The porosity of the glass powder modified cement was found to be the lowest and the authors believed the Na₂O may have provided NaOH that buffered the cement. The dissolution of CH was lower in fly ash modified and glass powder modified cement

compared to neat cement. The authors confirmed CH dissolution as the main cause of porosity increase but stated that C-S-H decalcification contributed as well.

Yang et al¹⁹ performed experiments to predict calcium leaching behavior in low pH environments. They also tried to establish a relationship between leaching duration and changes in cement mechanical properties. Cylindrical cement specimens of 1.97 in (50 mm) diameter were used for batch experiments that lasted for 140 days with intermittent analysis of the cement samples. Three zones - leached, transition and sound- were established. Leaching depths increased with leaching duration and a linear relationship existed between leaching depth and square root of time. Extrapolation of the leaching rate predicted that the dissolution front of CH will reach the core of the cement sample (w/c 0.30) after 14 years. Dissolution of CH and decalcification of C-S-H in the leached zone adversely affected the mechanical properties of the cement. Compressive strength of the samples dropped drastically initially but the rate of reduction slowed down later. The hardness of the samples was low within the first few millimeters but leveled off towards the interior of the samples.

Yurtdas et al²⁶ investigated the effect of degradation of well cement by acidic fluids on cement's hydro-mechanical behavior. Core samples measuring 1.46 in (37 mm) diameter and 1.57 in (40 mm) were prepared with Class G cement. Ammonium nitrate solution was used as the leaching solution. The batch experiments were performed at 194°F (90°C) for 50 days. Uniaxial and triaxial compression tests were carried out on control and degraded samples with confining pressures of 435, 1450, 2900 psi (3, 10 and 20 MPa) for the triaxial test. Degraded cement exhibited higher volumetric compaction due to pore collapse. The pore collapse was inferred from acceleration of strain rate and examination of tested samples. The uniaxial

compression strength of the control sample was 4206 psi (29 MPa) while that of degraded cement was 1638 psi (11.3 MPa), showing a 63% decrease.

Shao et al²⁷ analyzed the coupled and decoupled effects of compressive stress and chemical degradation of class G cement. The cement samples measured 1.42 in (36 mm) diameter and 3.94 in (100 mm) height. For the decoupled chemical degradation tests, 6 mol/l ammonium nitrate solution was used for batch leaching tests. For the coupled degradation test, varying degrees of triaxial stress were maintained as 4 mol/l of ammonium nitrate was injected. Unreacted cement samples, leached samples from a batch experiment and degraded samples from coupled experiments were each subjected to compressive stresses of 14.50, 43.51, 87.02, 145.04, 290.08 psi (0.1, 0.3, 0.6, 1.0 and 2.0 MPa). The chemical degradation of the cement resulted in remarkable reduction of mechanical strength and plastic yield stresses. It was also observed that the mechanical deformation of the sample during the coupled test affected the chemical process by reducing the cement permeability; the authors proposed that this should be taken into consideration during modeling.

Duguid and Scherer²³ investigated the effect of carbonated brine on class H cement. The cement samples measuring 0.30 in (7.5 mm) in diameter by 7.87 in (200 mm) in height were exposed to carbonated brine of pH 2.4 or 3.7 at temperatures of 68°F (20°C) or 122°F (50°C) and pressures of 1450.38 psi (10 MPa) for 31 days. Degradation of the cement by carbonated brine was observed during the experiment with higher rate of degradation recorded in samples immersed in pH 2.4. Different zones of carbonation and leaching were observed on the samples. The leached area showed marked reduction in calcium content and significantly reduced mechanical strength. Brown and orange layers were observed at the outer region of degraded cement samples.

Duguid²⁸ also performed experiments to estimate the time to totally degrade a sheath of cement in a wellbore. He used class H cement samples enclosed by sandstone. The batch experiments were done with CO₂ saturated NaCl brine at 68°F (20°C) or 122°F (50°C) for one year. The pH of the brine was 3.4 and 5. The depth of reaction of the cement with the brine was measured intermittently. The data collected was plotted and analyzed. Duguid concluded that it would take 30,000 to 700,000 years to degrade 0.98 in (25 mm) of neat cement paste in a sandstone reservoir.

Kutchko et al²² carried out experiments to assess the effect of temperature and pressure on the degradation of class H cement when exposed to CO₂ saturated brine under static conditions. The cement cores were cured in 1% NaCl solution for 28 days at 71.6°F (22°C) or 122°F (50°C) and 14.50 psi (0.1 MPa) or 4394.64 psi (30.3 MPa). Batch experiments were performed for 9 days at 4394.64 psi (30.3 MPa), 122°F (50°C) and pH of 2.9. The experiment also showed that there was variation in depth of invasion of the degradation from sample to sample. Samples cured at high temperature and pressure showed shallower depth of degradation. The authors attributed it to higher degree of hydration of the cement at the high temperature and pressure.

Kutchko et al²⁹ also investigated the rate of CO₂ degradation of class H cement. Cement samples were exposed to supercritical CO₂ and CO₂ saturated brine for one year at 4394.64 psi (30.3 MPa). The depth of cement degradation was recorded intermittently. The data collected from the experiments were extrapolated with Fick's second law of diffusion and the Elovich equation to see what the penetration depth will be after 30 years. The values obtained were 1.00 ± 0.07 mm for the CO₂ saturated brine and 1.68 ± 0.24 mm for the supercritical CO₂.

Bachu and Bennion³⁰ performed two sets of experiments using class G cement and J55 steel casing to evaluate the possible mechanisms that would determine well leakage in the presence of CO₂. In the first set of experiments, cement cores each measuring 3.8 cm diameter and 3 cm length were exposed to CO₂ saturated brine for 90 days at 65°C. The pressure drop across the length of the cores was 15,160 kPa (2198.77 psi) and the confining pressure 28,940 kPa (4197.39 psi). In the second set of experiments, cement-casing pairs having perfect bond (no annular gap), small annular gap, small cracks and large cracks respectively were used. The cement-casing samples were exposed to supercritical ethane and CaCl₂ solution at an overburden pressure of 24,100 kPa (3495.41 psi) and pore pressure of 13,780 kPa (1998.62 psi) at 60°C. In the cement only experiments, the permeability of the cement decreased rapidly within the first 5 days from 0.116 - 0.232 μD to 0.01 μD and then stabilized at the low level. In the second set of experiments, the cement/casing pair with perfect bond had permeability of 1 nD, while the samples with annular gaps or cracks measuring 0.01–0.3 mm showed increased permeability of about 0.1–1 mD. The authors concluded that good cement job would likely provide a reliable barrier against CO₂ leakage but that presence of cement cracks or annular gaps would provide pathways for CO₂ leakage.

Yalcinkaya et al²⁴ conducted experiment to evaluate the effect of CO₂ saturated brine on fracture conductivity. Two flow-through experiments were conducted using CO₂ saturated brine and cylindrical Class H cement cores. Each cylindrical cement core measured 1 in diameter by 12 in length and was comprised of two half cement cylinders thereby creating an artificial fracture in the middle of the core. The flow-through experiments were conducted using confining pressures of 600 psi (4.14 MPa) and 1800 psi (12.41 MPa). The experiments lasted for 30 days and 10 days respectively. Computed tomography, mercury intrusion porosimetry (MIP) and

environmental scanning electron microscopy were used to analyze the cement cores at the end of the flow through experiments. Density variation in the cement due to cement dissolution was observed. MIP revealed reduction in the porosity for small pore sizes in the 600 psi (4.14 MPa) experiment while porosity increase was observed in medium pore sizes in the 1800 psi (12.41 MPa) experiment. Different reaction products with varying Fe content were observed at the fracture wall surfaces. Secondary fracture networks also developed at the outlet section of in the 600 psi (4.14 MPa) experiment and the authors concluded that these were likely created and propagated by expansive secondary mineralization.

Brandvoll et al³¹ conducted batch and flow-through experiments to evaluate long term cement integrity with exposure to CO₂-water mixture. Samples measuring 2.5 cm diameter by 5 cm length were prepared from class G cement and cured for 28 days. The batch and flow-through experiments were carried out using 16wt% and 3.5wt% salinity fluids respectively. Both were conducted at 36 °C and 1,450 psi (100 bar). Batch experiments lasted for 7-43 days. For the flow-through experiments, 1 mm holes were drilled through the cement samples. The flow-through experiments lasted between 4 and 12 days and were carried out under a confining pressure of 435 psi (30 bar) using flow rates ranging from 0.1 and 0.4 ml/min. In the batch experiments, clear evidence of carbonation was observed. Alteration depth did not correlate with duration of experiment. Decalcification of cement and deposition of carbonates were observed along the 1 mm hole. The inlet of the hole contained layer of silica gel which is totally decalcified. Analysis of the effluent brine revealed extensive leaching of silica from the cement.

Carey et al³² analyzed casing, cement and shale samples obtained from a 55 year old well in a 30 yr old CO₂-flooding site in West Texas. The samples were obtained 13.12-19.69 ft (4-6 m) above the caprock-reservoir contact. The recovered cement had about 0.1 mD air

permeability. 0.1–0.3 cm thick carbonate precipitate was observed near the casing. The cement adjacent to the shale had a carbonated orange colored area measuring 0.1-1 cm and had an orange colored region. The authors stated that the CO₂ may have migrated up the casing-cement interface or penetrated through corroded points on the casing. They also indicated that the filter cake may have provided a channel for CO₂ to migrate along the cement-shale interface. They concluded that even with the degradation of the cement, the Portland cement retained its structural integrity and would still provide hydraulic seal against significant migration of the CO₂.

2.2 Drilling Fluid (Mud)

2.2.1 Drilling Fluid Composition and Usage

Drilling fluid, or mud, is used during drilling of wells. The fluid is pumped from the surface, down the drill string, through the bit, and back to the surface via the annulus. This is done for the following reasons³³:

- 1 To remove the drill cuttings from under the bit and transport them to the surface
- 2 To cool and lubricate the bit and drillstring
- 3 To exert hydrostatic pressure to prevent influx of formation fluids into the wellbore
- 4 To maintain stability of open hole

Different drilling fluids are available and they are classified according to the base fluid in the mud. The types of mud include oil based mud (OBM), water based mud (WBM), synthetic based mud (SBM) and gaseous drilling fluid³⁴. The type of drilling fluid to be used is selected based on properties of the formation being drilled, environmental considerations, and cost. Gaseous drilling fluid is usually used in drilling hard well consolidated formations. OBMs give very good rate of penetration in shales but do not allow for easy detection of kicks. WBMs are cheap but do

not perform well in shales and under very high temperatures. SBMs have higher initial cost but disposal costs can be considerably low as they are less toxic³⁴. WBM is widely used in the Gulf of Mexico but recently, Internal Olefin (IO) SBMs with densities between 9 and 15 lb/gal have become the most commonly used muds in Gulf of Mexico^{35, 36}. WBM's usually contain water, barite, bentonite, caustic soda, and lignosulfonates.

2.2.2 Mud Removal and Displacement Efficiency

When a well is being drilled, there is formation of mud cake (2-5mm thick)³⁷ and partially dehydrated gelled mud on the formation wall due to static and dynamic filtration. The mud cake and gelled mud are difficult to displace during well cementing and there is usually channeling through the mud which can eventually promote gas migration. Scratchers in conjunction with casing movement are usually used to remove the mud before cement placement but they do not remove all the mud. Displacement of mud by cement in turbulence has been shown to enhance mud removal but this is limited by the formation fracture pressure³. Mud displacement efficiency is the ratio of the volume of the cement in the cemented annulus to the volume of the annulus. The uncemented annulus volume is filled with mud. The aim of a cementing operation is to completely fill the annulus with cement therefore the mud displacement efficiency is a quantification of the quality of the cement job. Several studies have shown that mud displacement efficiency varies widely depending on mud conditioning, casing centralization, cement-mud density difference, and flow regime³. Displacement efficiency values ranging from 37% to 99.7% have been reported in literature^{12, 13}. Some of the undisplaced mud contaminates the cement affecting its mechanical and chemical properties. Mud contamination has also been identified as a major cause of cement plug failure³⁸⁻⁴⁰.

2.2.3 Bentonite Chemistry and its Behavior in Low pH Environment

Bentonite is used extensively in water based muds. It is added in the mud to increase its viscosity, density and gel strength. The gel strength helps to suspend cuttings and other solids like barite in the mud. Drilling fluid made with fresh water and bentonite will have a pH of 8 to 9 unless it is contaminated. Bentonite typically has particle sizes less than 2 μm and is mainly composed of sodium montmorillonite^{33, 41}. Sodium montmorillonite has high cation exchange capacity. The cation exchange capacity is its ability to exchange cations located within its structure for other cations present in surrounding solution. The simplified chemical formula for montmorillonite is $4\text{SiO}_2 \cdot \text{Al}_2\text{O}_3 \cdot \text{H}_2\text{O}$. A good proportion of the Al^{3+} is usually replaced making the formula more complex. Sodium montmorillonite has the chemical formula $\text{Na}_{0.66}(\text{OH}_4)\text{Si}_8(\text{Al}_{3.34} \text{Mg}_{0.66})\text{O}_{20}$ and swells when mixed with water⁴¹⁻⁴³. Bentonite behavior when exposed to hyperalkaline conditions, e.g. cement, has been studied extensively due to its use for containment of radioactive waste. Studies have shown that the interaction of bentonite with cement is a very complex reaction with formation of secondary minerals that interact with each other^{44, 45}. When bentonite is exposed to hyperalkaline fluids $\text{pH} > 12$, there is collapse of its 2:1 structure altering its properties⁴⁶. Dissolution of the bentonite occurs with resultant precipitation of other minerals^{47, 48}. The precipitation of a mineral like tobermorite will hinder further dissolution of bentonite while the precipitation of analcime will accelerate the dissolution of bentonite⁴⁵. Calcium (aluminum) silicate hydrates (C(A)SH), zeolites, feldspars, hydroxides, carbonates, polymorphs of silica and other amorphous precipitates are all possible products of cement-bentonite interaction depending on pH, silica activity and presence of certain minerals^{44, 45}. Interaction between clays and cement has been shown to cause reduction in aluminum, silicon

and magnesium content of the clay and corresponding increase in the calcium content of the clay due to diffusion from the cement⁴⁹.

2.2.4 Studies on Effect of Mud Contamination on Cement Properties

Studies done on mud contamination of cement show that thickening time, compressive strength and rheological properties of the cement are altered by the mud. The alteration in compressive strength of the cement tends to be more pronounced during the initial setting time but tends to be less critical later.

El Sayed⁵⁰ investigated the effect of mud contamination of cement on cement properties. Three different mud types: oil based mud, water based mud and polymer based mud, were used. The cement properties measured were thickening time, compressive strength, consistency and rheological properties. Class G cement slurry having 15.9 ppg density, 144 cp plastic viscosity and 7 lb/100 ft² yield stress, was used as the base slurry. The cement was contaminated by 10, 20, 30, 40, 50% mud by volume with the three different mud types. For the compressive strength tests, the cement slurry was poured in 2 in steel cubes and cured at 80°C for 12 and 24 hrs. The rheological properties, consistency development, thickening time and compressive strength were all altered by the mud contamination. The compressive strength showed remarkable reduction as the mud contamination increased. After 12 hrs, the compressive strength in the neat cement was about 330 psi while some of the highly contaminated cement had almost unmeasurable compressive strength. After 24 hrs the compressive strength in neat cement was 1170 psi while that of some highly contaminated cement was about 200 psi. The 24-hr compressive strength of cement dropped by about 300 psi for every 10% increase in water based mud contamination. Oil based mud contamination reduced the 24-hr compressive strength of cement by about 200 psi for every 10% increase in mud contamination. 10% mud contamination of the cement by polymer

based mud reduced the compressive strength from 1170 psi to 300 psi and the compressive strength stayed almost constant at 300 psi as the mud contamination level was increased.

Bradford⁵¹ also tested cement samples for alteration in compressive strength due to mud contamination. Three different types of cement slurries were used. Class H cement, normal slurry and reduced water slurry containing dispersants. Cement samples with different degrees of mud contamination ranging from 5% to 50%, were made and cured at 170-230°F before being subjected to compressive strength tests. All the slurries showed reduction in compressive strength as degree of mud contamination increased. The Class H cement slurry was tested after 8 hrs and after 16 hrs. For the 8-hr test, 10% mud contamination caused the compressive strength to decrease by about 44% while during the 16-hr test the reduction was by 23%.

2.3 Cement-Formation Interface in the Wellbore

2.3.1 Nature of Cement-Formation Interface

The cement-formation bond is critical in preventing inter-zonal communication and maintaining wellbore stability but very few studies have been done with samples taken from wells for the purpose of understanding alterations in the cement-formation bond over the life of wells^{32, 37}. Most of the studies on the nature of the cement-rock bond have been done in civil engineering. Based on these studies, bonding mechanisms of the cement to the formation have been shown to be a combination of mechanical interlocking of cement hydration products with the rock grains and the chemical reaction between the cement paste and rock grains⁵²⁻⁵⁴. The bonding due to mechanical interlocking of rock grains increases with increasing surface roughness. Greater surface roughness also provides larger surface area for bonding thereby increasing the bond strength⁵². This means that the roughness of the wellbore wall increases the bond strength between the cement and the formation. The chemical reaction component of the

cement formation bond is more complicated as different formations possess different minerals with different reaction mechanisms and products when brought in contact with the cement.

At the cement-formation interface, there exists a zone of increased porosity. This zone is referred to as interfacial transition zone (ITZ). The boundary of the ITZ is not well defined since it is a transition zone. The interface zone is created by a phenomenon known as the wall effect. The wall effect occurs because of the size difference between the cement grains and formation grains. Cement grains are general between 5 and 60 μm while the size of a sand grain can be between 70 and 2000 μm ^{14,41}. The huge disparity in size makes the sand grains appear as walls when placed beside cement grains and this interferes with the packing of the cement grains near the sand grains. The resultant packing at the interface causes accumulation of water and increased porosity at the interface. The wall effect is most pronounced within 15-20 μm of the sand grains⁵⁵. Initially the ITZ has a porosity that is about 40% higher than the bulk cement. Due to the high porosity of this region, calcium ions being dissolved from the interior of the cement paste migrate to the ITZ and form CH. This creates a thin film of CH on the sand grain. Other cement hydration products like C-S-H and ettringite are produced at the ITZ further reducing the porosity. At later times the porosity of the ITZ is about the 10-20% higher than the bulk cement⁵⁵.

2.3.2 Factors affecting the cement-rock bond

Factors that affect the cement-formation bond include; inadequate mud displacement, mechanical stress and strain on the interface due to pressure and temperature cycles over the life of the well, geochemical attack by corrosive formation fluids and disruptions in the subsurface geology. Disruptions in the subsurface geology are due to tectonic movements and subsidence

(caused by fluid removal). The occurrence of one or more of the processes listed above can lead to debonding of the cement from the formation thereby creating a pathway for fluid migration.

2.3.3 Studies on Effect of Mud Contamination on Cement-Formation Bond

Becker et al⁵⁶ evaluated the effect of mud cake and mud contamination of cement on the cement-formation bond. Shear bond experiments were performed using cement-sandstone composites with either the presence of mud cake at the interface or the contamination of the cement by mud. Sandstone samples and cement class TZ 1 were used. In the mud cake tests, the mud types used were fresh water bentonite mud, salt water bentonite mud and red mud. The interface was tested in four different modes: with presence of mud cake, with mud cake scrapped off, with mud cake scrapped off plus the surface washed with water, and mud cake scraped off plus the surface washed with surfactant. The mud thickness was 1 mm. The bond strength of the cement-sandstone composite without mud cake was 185 psi (13 kp/cm²) and no significant bond strength could be measured in the presence of mud cake. For the various mud cake treatments, the highest bond strength was recorded with mud cake scraped off plus the surface washed with surfactant (average bond strength = 148 psi (10.4 kp/cm²)) while the lowest bond strength was obtained with mud cake scrapped off only (average bond strength = 73 psi (5.13 kp/cm²)). Amongst the mud types, the fresh water bentonite mud gave overall highest bond strength (average bond strength = 127 psi (8.9 kp/cm²)) while the red mud gave the lowest bond strength (average bond strength = 101 psi (7.13 kp/cm²)). For the mud contaminated cement tests, the mud types used were fresh water bentonite mud, salt water bentonite mud, red mud and oil emulsion mud. The cement was contaminated by 0%, 1%, 5%, 10% and 20% mud by volume respectively before being placed on the sandstone. The cement-sandstone samples were subjected to shear stress and a bond strength of ~171 psi (~12 kp/cm²) was obtained for the

uncontaminated cement-sandstone composite. The bond strength of the composites decreased with increasing mud contamination. Oil emulsion mud gave the overall lowest bond strength while bentonite fresh water mud gave the overall highest bond strength. At 10% mud contamination of cement, the bentonite fresh water mud had reduced the cement-sandstone bond strength to 141 psi (9.88 kp/cm²) while the oil emulsion mud gave a bond strength of 82 psi (5.75 kp/cm²).

Ladva et al³⁷ investigated the effect of different mud systems on the cement-formation bond. Effect of mud cake on porous formations and effect of mud treatment on shale were studied. Clashach sandstone was used as the porous media while Oxford shale and Catoosa shale were used for the shale experiments. Oxford shale is a swelling shale while Catoosa is a non-swelling shale. The rock samples measured 25.4 mm diameter and 20 mm long. They were embedded in annular cement with outer diameter of 48 mm and height of 44 mm. A Class G cement was used and cement-rock samples were cured for 1-8 days at 20°C - 85°C. The cement-rock bond strength was measured for all uncontaminated cement-rock sample types after curing for 24 hrs at 85°C. For the cement-sandstone sample, the cement fractured at 120 psi (>0.8 MPa) before the interface could be sheared. For the Oxford and Catoosa shales, the bond strengths were determined to be 0.4 MPa (58 psi) and 0.48 MPa (70 psi) respectively. When the Oxford shale was debonded, a film of shale was left on the cement but debonding of Catoosa was through the interface. As curing time increased, the bond strengths generally increased with cement fracturing observed in many cases. Oil based mud and water based muds were used for the mud cake experiments. Mudcake was built on the sandstone core by applying a pressure of 0.7 MPa (101.5 psi) for 24 hr at 25°C (77°F). The WBM reduced the cement-sandstone bond strength to 10⁻³ MPa (0.145 psi) while OBM reduced it to <10⁻⁵ MPa (<0.00145 psi). When

chemical wash was used on the WBM mud cake before cementing, the bond strength was 3 times greater than when it was unwashed. The failure mode for the mud cake experiments was through the mud cake. The Oxford shale was also pretreated with OBM, silicate mud, low inhibitive glycol mud, and polyacrylamides to increase the bond strength but no increase in bond strength was recorded.

Evans et al⁵⁷ carried out hydraulic bond tests using 1 mD Indiana limestone and 100 mD Berea Sandstone. The formation specimens tested had a length of 1.875 in. and a diameter of either 1.75 in. or 5.25 in. API class A cement was used and samples were cured at 100°F for 24 hrs under 1600 psi pressure. The cement was either squeezed on to the formation or just placed on it. The squeezing was done at 100 psi (0.69 MPa). Mud cake used was made by squeezing a 6% bentonite mud against the formation for 1 hr at 100 psi (0.69 MPa) pressure and then reducing the cake size to a thickness of 0.125 in. The hydraulic bond test was performed with a specially designed apparatus. The hydraulic bond of cement to dry limestone core was found to be about 10,300 psi (71 MPa). The bond strength of the cement to the sandstone could not be obtained as the core failed before the interface. The hydraulic bond strength for the mud contaminated sandstone-cement interface was 165 psi (1.14 MPa) and 260 psi (1.79 MPa), with squeezed cement having higher bond strength. Hydraulic bond strength of 130 psi (0.9 MPa) and 160 psi (1.1 MPa) were obtained for the limestone-cement interface with the squeezed cement also having higher bond strength. The authors stated that sandstone showed higher bond strength because the higher permeability of the sandstone allowed for greater dehydration of cement which resulted in higher cement strength.

Yong et al⁵⁸ evaluated the effect of mud cake produced by different types of drilling fluids on the shear bond strength of the cement-rock interface. The core was made from

arenaceous quartz and measured 1.97 in length and 0.98 in diameter. The permeability was between $500 \times 10^{-3} \mu\text{m}^2$ (507 mD) and $600 \times 10^{-3} \mu\text{m}^2$ (608 mD). The drilling fluids used were polymer-sulfo drilling fluid, polymer drilling fluid and polymer silicon-based drilling fluid. The mud cake was produced using a HPHT filter press and applying a pressure of 500 psi at 194°F for 30 mins. Curing was done for 24 hrs in water bath at 194°F. Shear bond test performed on uncontaminated core gave a bond strength value of 537.01 psi (3.7 MPa). The tests on the samples with mud cake gave shear bond strength of 192.07, 170.30, and 367.20 psi (1.32, 1.17 and 2.53 MPa) for polymer-sulfo drilling fluid, polymer drilling fluid and polymer silicon-based drilling fluid respectively. This not only shows that mud cake reduces the bond strength but that the bond strength varies with the drilling fluid type.

CHAPTER 3 EXPERIMENTAL SETUP AND PROCEDURE

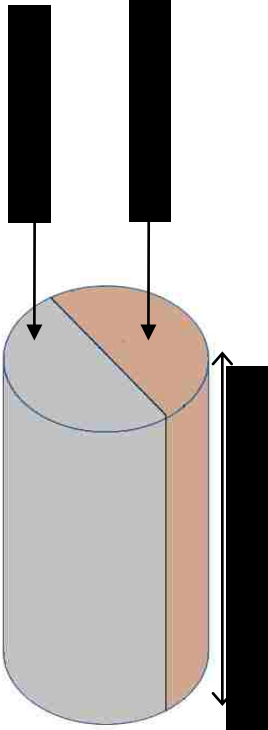
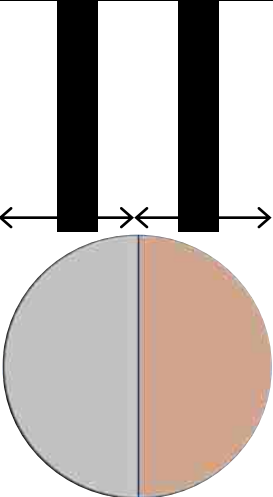
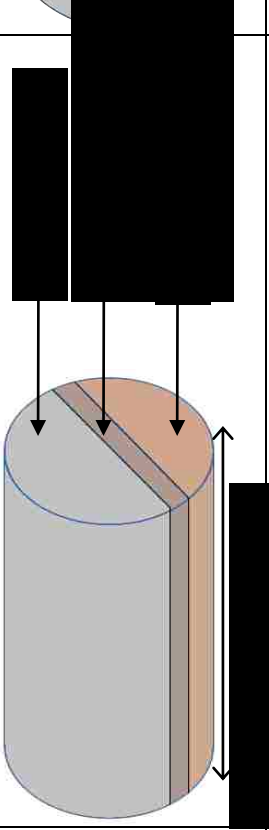
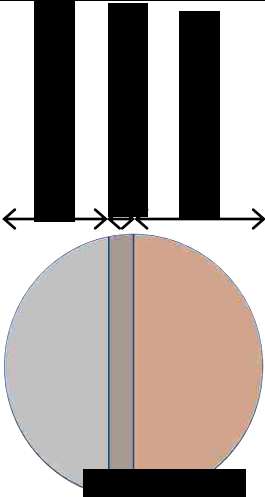
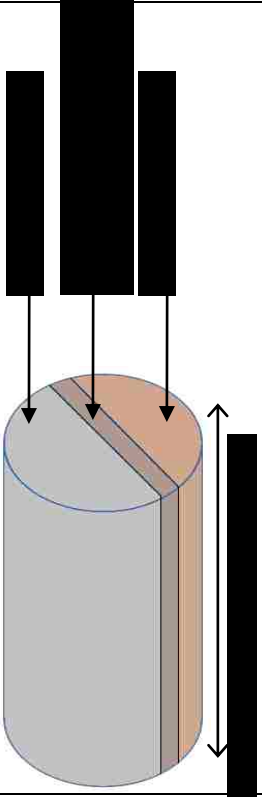
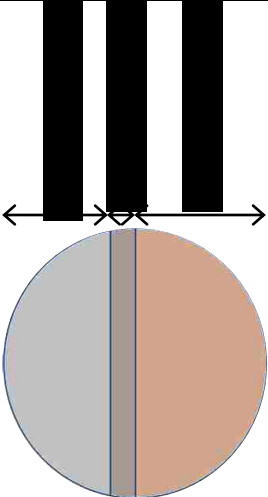
3.1 Experimental Program

To effectively study the effect of drilling fluid contamination, three different flow-through experiments were conducted as shown in Table 3.1. The confining pressure used was 2100 psi (14.48 MPa). This value was chosen to mimic a field case where there is a 1 psi/ft (22,620.59 Pa/m) pressure gradient at a depth of 3000 ft (914.4 m) with 70% horizontal pressure transfer. The pore pressure gradient was assumed to be 0.45 psi/ft (10,179.27 Pa/m) giving a pore pressure of 1350 psi (9.31 MPa) at 3000 ft (914.4 m). This gives a net overburden pressure of 750 psi (5.17 MPa). Each experiment was run for 30 days at 1 ml/min injection rate and temperature of 72°F (22.22°C).

3.2 Composite Core Preparation

All samples were prepared using 300 mD Berea sandstone and Class H cement. The 1 in diameter by 12 in long Berea sandstone core was cut longitudinally into two halves, each half measuring 12 in length. The flat longitudinal surface of each half was roughened with coarse Norton emery cloth to create a surface that is more representative of a wellbore. The sandstone was then immersed in distilled water before being placed in a Teflon mold. The wetting of the sandstone was to prevent loss of water from the cement to the sandstone when the cement is placed adjacent the sandstone. The class H cement was mixed following API Recommended Practice for Testing Oil Well Cements, API RP-10B⁵⁹. To prepare 600 ml of class-H cement slurry, 860 of class H cement and 327 grams of distilled water were mixed. The mixing was done with Hamilton Beach Mixer at 4,000 RPM for the first 15 seconds and 12,000 RPM for the next 35 seconds. After mixing, the slurry was degassed using a vacuum pump. The cement slurry was



Name	Sample design		Curing Time
	Longitudinal View	Cross Sectional View	
0% mud contamination			100 days
5% mud contamination			200 days
10% mud contamination			150 days

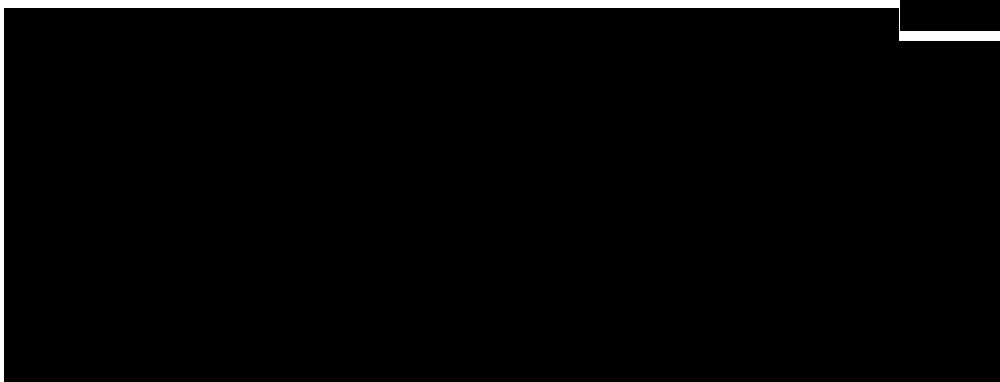
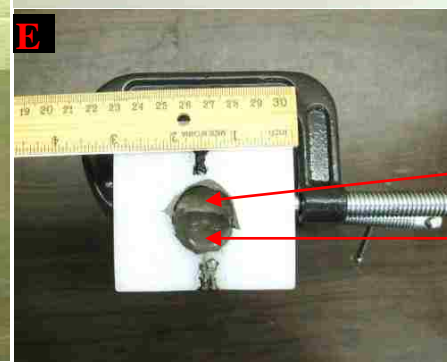
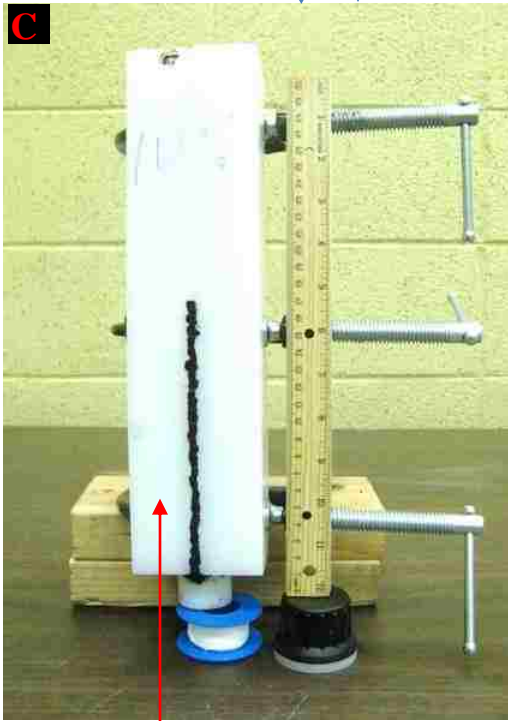
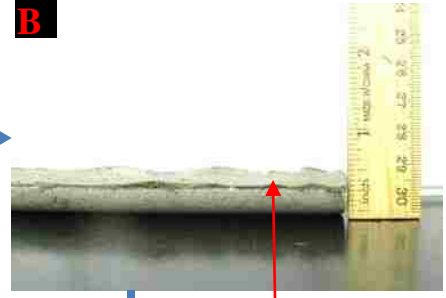
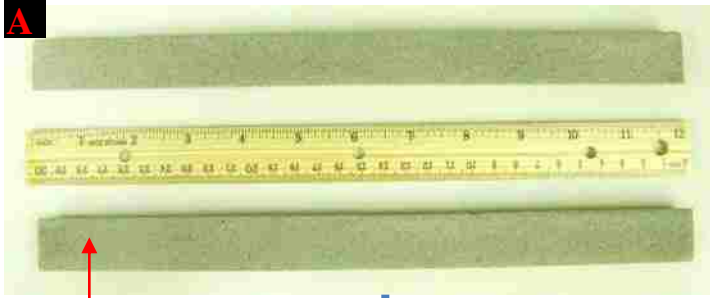


then poured into the Teflon mold where a wet sandstone half was already placed as shown in Figure 3.1. The wait on cement (WOC) period was 24 hrs. The composite core was then de-molded and cured in tap water for 100 days, as shown in Table 3.1, to achieve extensive hydration of the cement (the degree of hydration of cement does not change substantially after 28 days¹⁴).

For composite cores with drilling fluid contamination, fresh water mud was also prepared. 350 ml of distilled water was mixed with 15 g of bentonite, 0.5 g of carboxymethyl cellulose (CMC) and 0.2 g of NaOH. The mixing was done with Hamilton Beach Mixer at 8,000 RPM for 10 minutes. 10 ml and 5 ml of mud were mixed with 90 ml and 95 ml of cement slurry respectively using a whisk to achieve 10% and 5% mud contamination. About 100 ml of mud-cement mixture was poured on the flat longitudinal surface of horizontally placed half cylindrical sandstone to obtain ~1.27 mm (0.05 in) thick layer of contaminated cement. The 1.27 mm (0.05 in) is 10% of the total cement thickness of 12.7 mm (0.5 in). The mud-cement mixture was allowed to set for two hours to prevent mixing with neat cement when the neat cement was placed beside the contaminated cement. The sandstone with the layer of mud contaminated cement was then placed in a Teflon mold and neat class H cement slurry was poured into the mold as shown in Figure 3.1. The wait on cement (WOC) period was 24 hrs. The composite core was then de-molded and cured in tap water for 150 to 200 days, as shown in Table 3.1.

3.3 Experimental Fluids

The brine composition shown in Table 3.2 was used in all the flow-through experiments. The brine was originally designed to simulate West Texas formation fluids⁶⁰. The West Texas





formation brine contained some Mg and CaCO₃. The brine composition was reduced to include only NaCl and KCl so that the reactions during the experiments could be easily delineated. The salinity of the brine was about ~20,000 ppm. After mixing the brine, two levels of filtration were utilized before the brine was delivered to the pump to prevent solids from plugging the flow channels. The pH of the brine was 6.2 ± 0.2, throughout the flow-through experiments. The slightly acidic pH is probably due to atmospheric CO₂ that dissolved in the brine.

Table 3.2: Brine composition used in experiments⁶⁰.

Salts	Amount mixed with 1L of Distilled Water	Molality (mol/kg)
Sodium Chloride (NaCl)	20.196 g	0.3455 m
Potassium Chloride (KCl)	0.345 g	0.0046 m

3.4 Experimental Setup

The following equipment were used for the experiments: biaxial-type core holder, syringe pump, pressure data acquisition system, back pressure regulator, hydraulic pump, and pressure gauges. A schematic of the experimental setup is shown in Figure 3.3.

3.4.1 Biaxial Type Core Holder

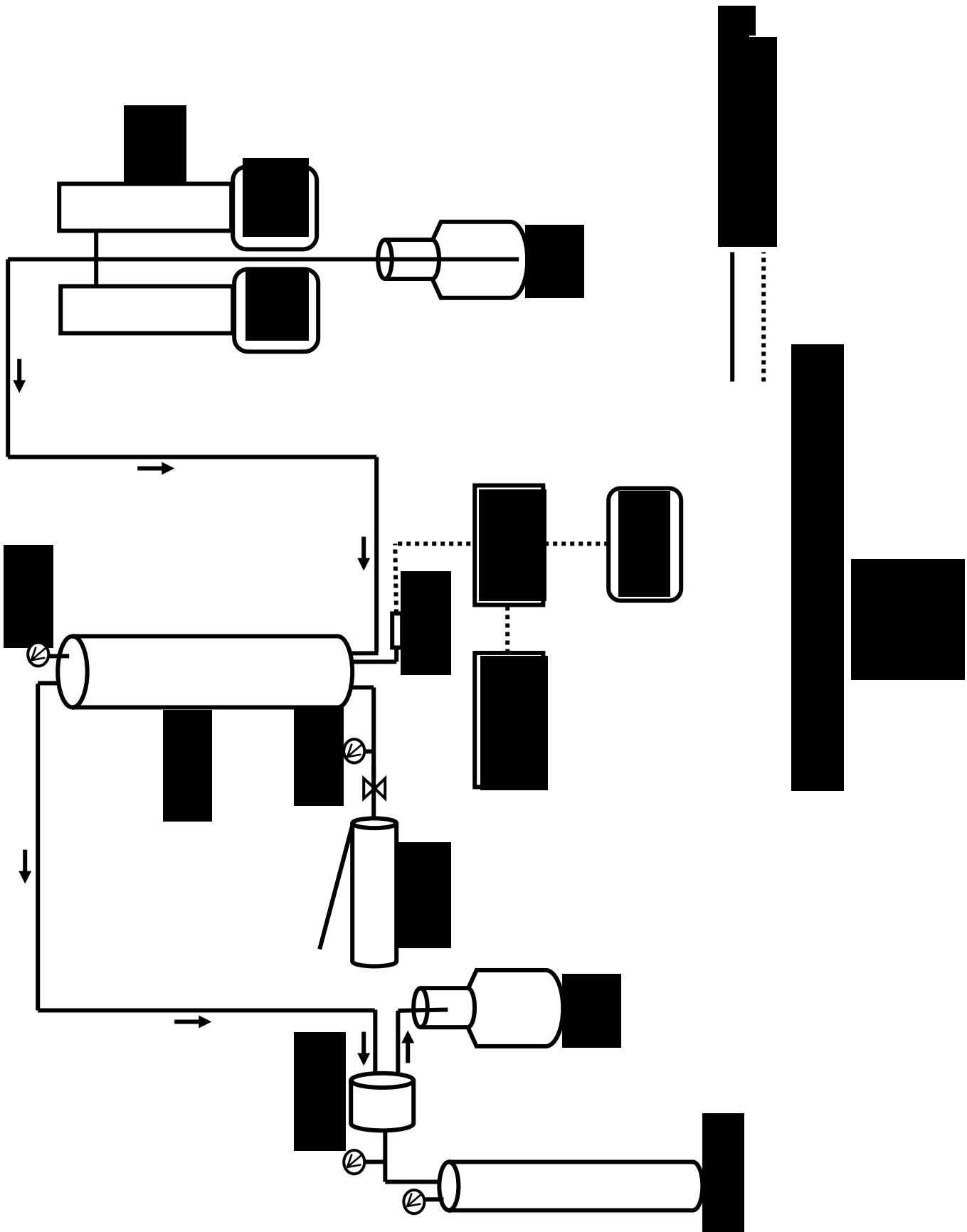
A Temco biaxial type core holder was used. The core holder contains a Viton® rubber sleeve that houses the composite cores during the experiment. The core holder and rubber sleeve were designed to accommodate cores with maximum dimensions of 1 in diameter and 12 in length. The core holder also has a maximum working pressure of 3500 psi and 500 psi net overburden pressure was required to seal the annulus between the core and the rubber sleeve to prevent annular flow. The confining pressure was applied by using an Enerpac hydraulic pump to deliver hydraulic oil into the core holder. The core holder was mounted in a vertical position and brine was injected from the bottom to simulate the upward flow of formation fluids at the cement-formation interface in a vertical wellbore.

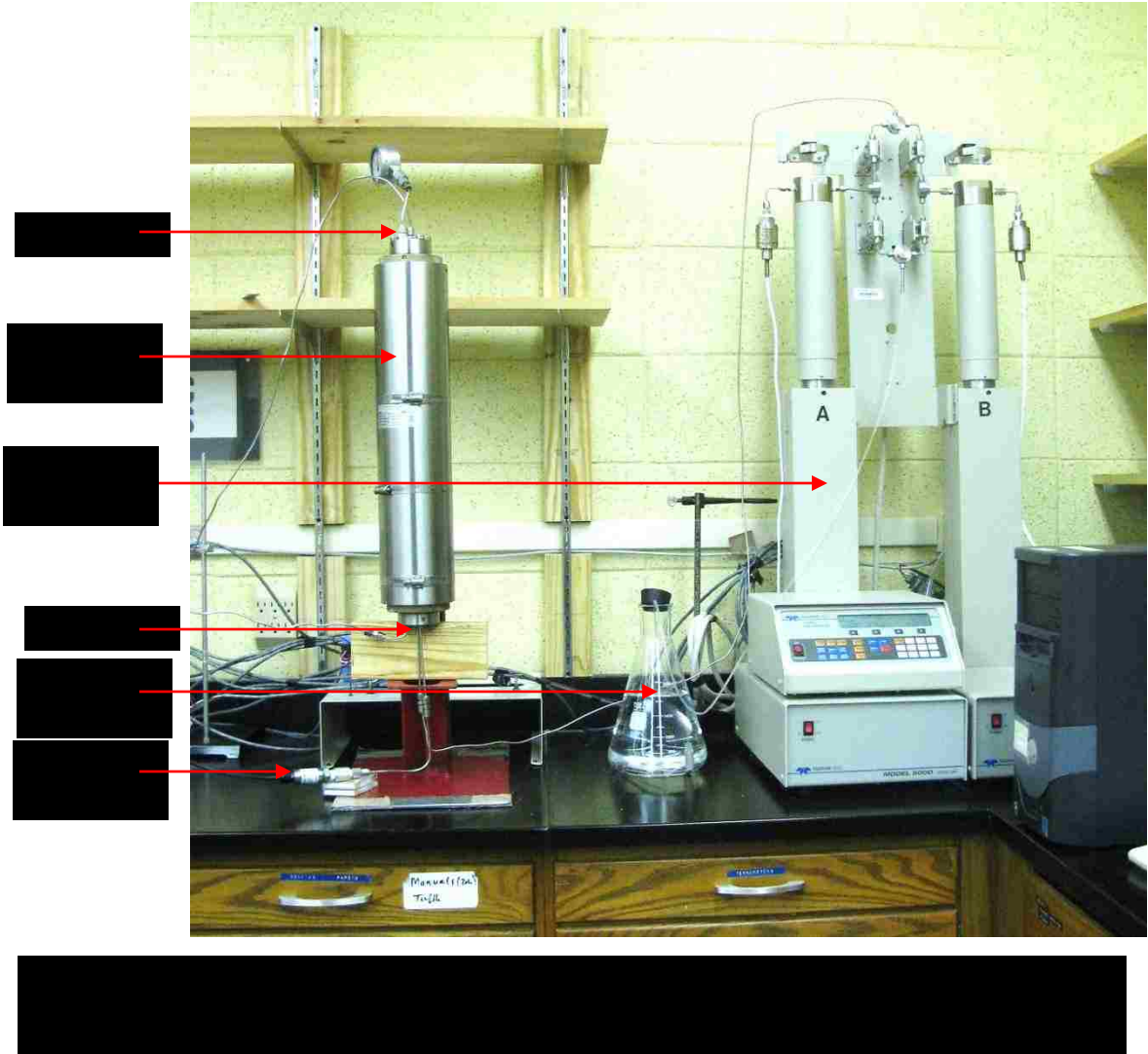
3.4.2 Syringe Pump

A syringe pump system was used for the experiments and it comprised of two Teledyne Isco 500D syringe pumps coupled to a D series pump controller. The two pumps, each having a capacity of 507 ml, utilize an electric valve manifold to deliver constant continuous flow. Each pump can deliver flow rates of 0.001 ml/min to 204 ml/min at a maximum pressure of 3750 psi.

3.4.3 Back-pressure Regulator (BPR)

An externally dome-loaded back-pressure regulator was used to supply a back-pressure of 1350 psi during the experiment. The BPR is designed for a maximum pressure of 5000 psi and maximum flow rate of 10 ml/min. The dome was charged with nitrogen gas (N₂).





3.4.4 Pressure Data Acquisition System

The pressure data acquisition system consists of an Omegadyne pressure transducer, Omega digital transmitter, 5V DC power supply, Microsoft Excel[®] data logging program and a computer. The transducer (rated 0-5000 psi with accuracy of 0.25% FS) was used to read the varying injection pressure at the inlet core face. The voltage signals from the transducer were sent to the digital transmitter where the signals were converted to digital data with a microprocessor-controlled integrating A/D converter. The digital data was then transmitted via RS 485 wires to the computer where the data is logged using the data logging program developed

by Darryl Bourgoyne, Louisiana State University Petroleum Engineering Research and Technology Transfer (PERTT) Laboratory Director.

3.5 Material Characterization Techniques

Pre and post core-flood analysis were carried out to characterize the physical and chemical processes leading to the varied permeability of the composite core. The following material characterization techniques were employed.

3.5.1 Surface Profilometry

Surface profilometry is a technique used for surface texture analysis^{61, 62}. It provides a quantification of the surface roughness of an object. The surface roughness is given in units of length. Modern profilometers also create 3D topographical maps of the sample surface⁶¹. An optical non-contact profilometer was used in the study. It uses a filtered white light beam to scan the surface of the sample. The reflected beam is captured, combined with a reference beam and processed to obtain the surface roughness. The surface roughness of the Berea sandstone used in the study was obtained to allow for effective comparison of experimental results with other studies as surface roughness affects the quality of cement-formation bond. The sandstone surface was scanned after the surface was roughened with Norton® emery cloth. The surface profiling was performed with WYKO NT3300 surface profiler at a vertical resolution of <1 nm. The profiling was performed at the micro-fabrication unit of the Center for Advanced Microstructures and Devices (CAMD) at Louisiana State University.

3.5.2 X-Ray Computed Tomography (Low Resolution CT)

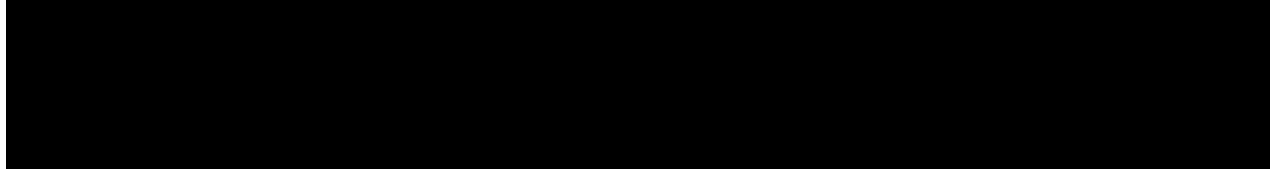
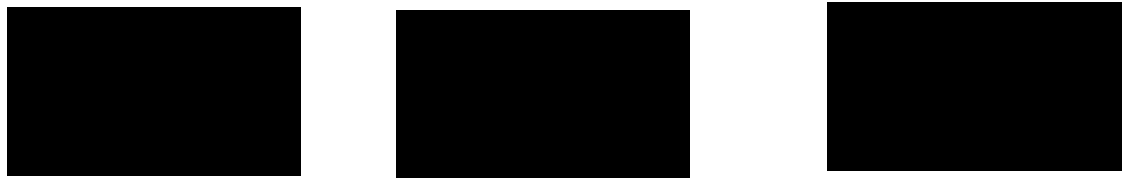
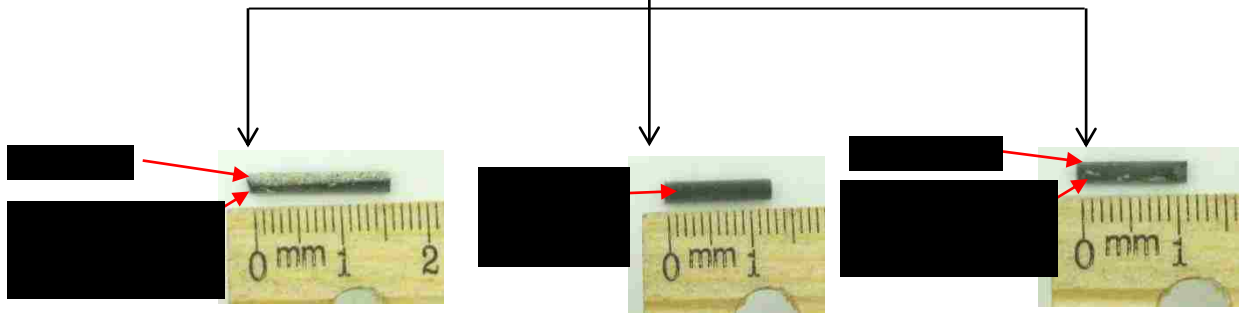
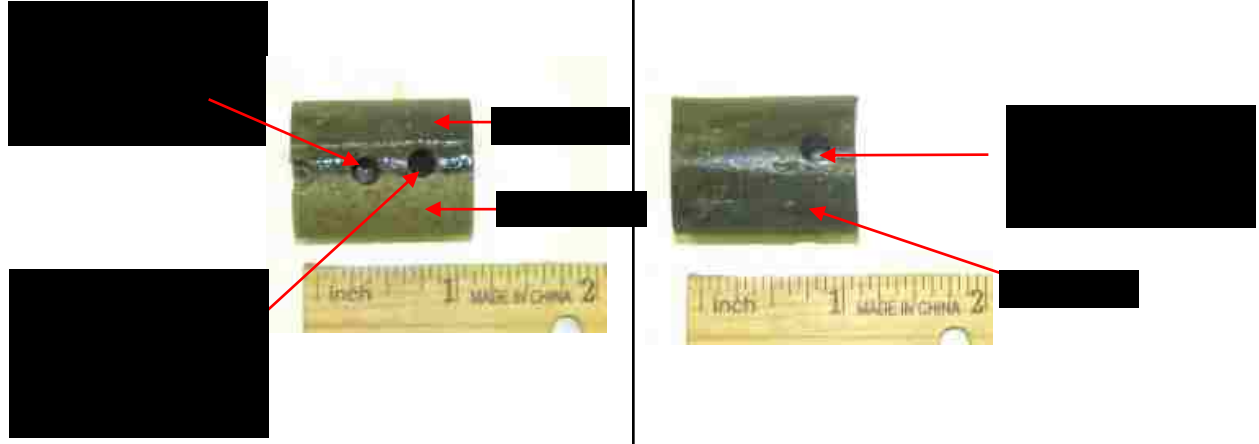
X-Ray computed tomography is a non-destructive imaging technique that utilizes the x-ray attenuation coefficient of different components of an object to reconstruct the object⁶³. Its most common application has been in diagnostic medicine but it has found use in several other

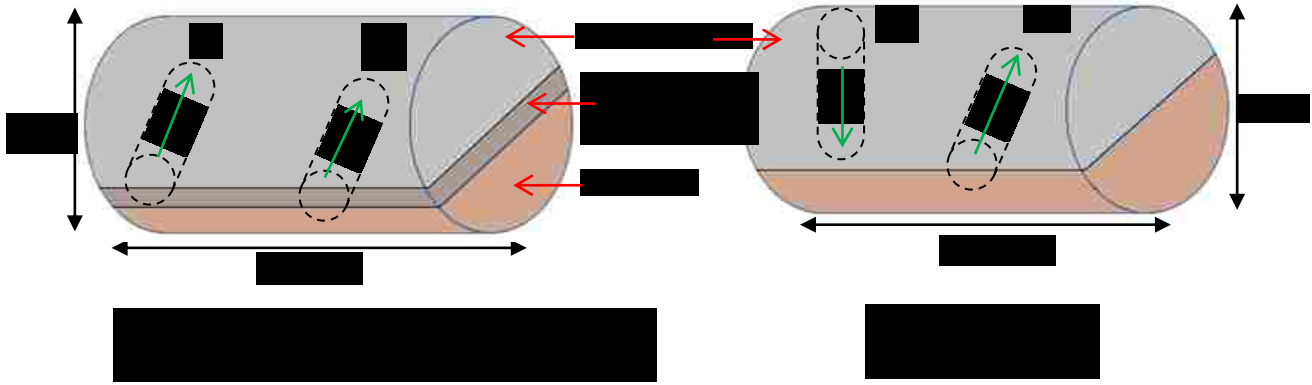
disciplines including Geology, Petroleum Engineering and Civil Engineering. In the current study, CT scans were carried out on composite cores as it provided a non-destructive and quick means to observe the density of different sections of the composite core and evaluate the quality of the bond along the interface. CT images of the composite cores were obtained pre and post flow-through experiments for identification of areas where alterations have occurred in the composite due to the core-flood so that further analysis could be carried out on those sections of the cores. The composite cores were scanned at Weatherford Laboratories using Toshiba Aquilion 64 slice Helical CT-scanner at a voxel size of $300\ \mu\text{m} \times 300\ \mu\text{m} \times 500\ \mu\text{m}$. The scanner was operated at 135 kVp and 200 mA. The composite cores were scanned at the same orientation before and after the flow-through experiments to allow for easy comparison of the resultant images.

3.5.3 X-Ray Microtomography (High Resolution CT)

Microtomography (Micro-CT), like low resolution CT, uses the x-ray attenuation property of different elements in a sample to construct virtual 3D model of the object⁶⁴. Micro-CT scanners are generally smaller than CT scanners and they also possess much higher resolution; resolution of Micro-CT can be as high as $<1\ \mu\text{m}$ ⁶⁵ while that of low resolution CT is usually in hundreds of micron. In petroleum engineering, Micro-CT is usually employed in pore network modeling. Small diameter samples are required to allow for complete beam penetration of the sample, consequently sample size is usually restricted to a few centimeters.

In the study, Micro-CT enabled examination of the composite cores at a much finer scale. Density variations and presence of pores in the cement that could not be identified using low resolution CT were observed using micro-CT. To obtain high resolution images from the Micro-CT scan, 3 mm diameter mini cores drilled from composite cores were used. Two sets of mini





1 and 3: Cement-evaluation mini cores
 2 and 4: Interface-evaluation mini cores

cores were drilled at the inlet and outlet of the post core-flood composite cores and also from the control samples as shown in Figure 3.5. The first set of mini cores was drilled to examine the cement-sandstone interface (interface-evaluation mini cores) and the second was drilled to evaluate the depth of cement degradation (cement-evaluation mini cores). For the 0% contaminated composite core, the cement-evaluation mini cores were drilled from the top of the cement half of the composite core down to the cement-sandstone interface as shown in Figure 3.5 and Figure 3.6b. This provides a cement mini core that spans the thickness of the cement in the composite core. The cement-evaluation mini cores for the 5% and 10% contaminated cores could not be drilled in the same way the 0% contaminated core was drilled because there was possibility of not obtaining the 1.27 mm thick contaminated cement layer at the interface. The cement-evaluation mini cores were however drilled from the side of the mini cores near the interface as shown in Figure 3.5 and Figure 3.6a. The interface-evaluation mini cores were drilled from the side of the mini cores; the same orientation was used for all the composite cores

as shown in Figure 3.5 and Figure 3.6. The drilling of the mini cores was carried out at the Rock Preparation Laboratory in the Department of Geology & Geophysics at Louisiana State University using a coring bit attached to a drill press. The mini cores were scanned using x-ray energy of 30 KeV at a spatial resolution of 2.5 μm and 0.5 degree increments. The scanning was performed at the Center for Advanced Microstructures and Devices (CAMD) at Louisiana State University. The scans were performed in 1.28 mm steps along the height of the samples and each 1.28 mm height contained one about 1 GB of data after the images were reconstructed and cropped.

3.5.4 Image Based Porosity

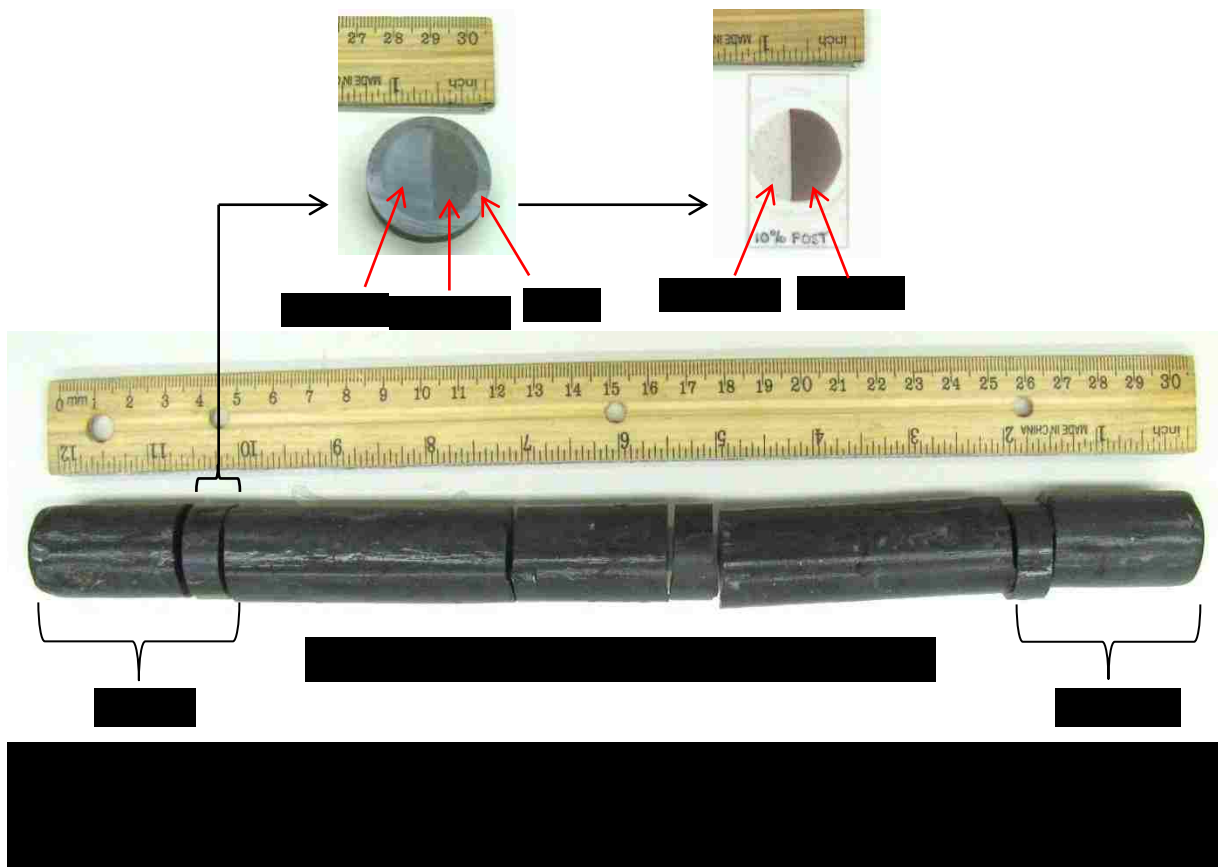
After the Micro-CT images were processed, sub-volumes were extracted from different sections of interest in the 3D gray scale images for image based porosity evaluation. Increased porosity of the cement at the end of the core-flood indicates increased leaching of the cement. The evaluated porosity provided a quantification of the degree of leaching that occurred in the different regions of the cement.

To obtain the porosity of the different sections, the 3D gray scale images were first segmented. Segmentation is the process of converting the gray scale images to binary images by isolating two distinct phases based on their intensity values⁶⁶. Threshold intensity values are usually used to separate the two phases. In the current study an indicator based krigging algorithm was used for the segmentation. Indicator krigging uses two threshold intensity values⁶⁶; intensity values above the higher threshold value were assigned as one phase (matrix) while intensity values below the lower threshold value were assigned as the second phase (pores). Intensity values between the two threshold values were assigned to either phase (matrix or pores) based on the best estimate obtained by using an algorithm. Threshold values were

selected from a 0-255 scale since an 8-bit gray scale image contains 256 (2^8) shades of gray. To complete the segmentation, each voxel in the first phase (matrix) was assigned a value of one and each voxel in the second phase (pores) was assigned a value of zero effectively converting the image into a binary image with one representing matrix and zero representing pores. The Pelican high performance computer at LSU visualization center was used for the segmentation. Thereafter, the histogram tool in ImageJ⁶⁷ software was used to process the resultant binary images and obtain the porosity by evaluating the ratio of the number of 0's to the total number of 0's and 1's. The porosity obtained was dependent on the resolution of the Micro-CT images. Since the resolution was 2.5 μm , only pores larger than 5 μm could be identified⁶⁶.

3.5.5 Light (Optical) Microscopy

Light (optical) microscopy uses visible light and assortment of lenses to magnify images of small objects⁶⁸. Some of the parts of a light microscope are objective lens, ocular lens, light



source, stage etc. Modern microscopes are usually equipped with cameras to capture digital images. In this study, optical microscopy was performed with Leica DM2500 M equipped with a Leica DFC450 C digital camera. It was employed for two main purposes. One use was for quick examination of samples to identify sections of interest so that further analysis could be performed on those areas. The second purpose was to obtain color images of stained thin sections of composite cores so that calcium distribution and carbonation in the cement could be observed. The optical microscope also provided larger field of view than the scanning electron microscope so that larger surface areas of the composite core could be observed, allowing capturing images of entire contaminated region. The thin sections were stained with alizarin red which turns calcium rich areas pale pink and carbonated areas purple or deep red. Figure 3.7 shows where the samples for the thin sections were obtained from. The optical microscopy was performed at the Sustainable Energy and Environmental Research (SEER) Laboratory in the Department of Petroleum Engineering, Louisiana State University.

3.5.6 Scanning Electron Microscopy (SEM)

Scanning Electron Microscopy uses a beam of electrons instead of light to generate magnified images of small objects. The SEM has an advantage over the light microscope because it has larger depth of field, much higher magnification and finer gradation in magnification levels. The magnification can be up to 500,000x producing a resolution as high as 1 nm. The object of interest is placed in the microscope and scanned with an electron beam. The interaction of the electrons with the object generates secondary electrons, backscattered electrons and X-rays⁶⁹. These signals are detected and processed to provide information about the object's topography and composition. To detect the different signals, the microscope needs to be equipped with secondary electron detector, back scatter electron detector and energy

dispersive x-ray spectroscopy (EDS) system respectively. The secondary electron imaging mainly provides information about the topography of the object. The reflection of backscattered electrons from the object is a function of the atomic number of the elements on the surface and therefore provides some information about the elemental composition of the object. EDS uses the characteristic x-rays emitted by the object to determine the elemental composition of the object. SEM can also be performed in a low vacuum mode called Environmental Scanning Electron Microscopy (ESEM). ESEM allows for imaging of uncoated non-conductive and wet materials which means that materials are imaged in their unaltered states. The secondary electron microscopy allowed for general observation on the Berea sandstone and identification of clays in the sandstone. The backscattered electron microscopy mode provided density contrast between areas that are calcium rich (Ca=40) and areas that are silicon rich (Si=28). With the impregnation of the composite core with resin, it enabled the confirmation of connectivity between the large pores created in the contaminated layer and the pores in the sandstone. Some samples were polished and coated with platinum to achieve improved imaging quality. The SEM images were captured using Hitachi S-3600N Scanning Electron Microscope at the Material Characterization Center in the Department of Mechanical Engineering, Louisiana State University.

3.5.7 X-Ray Diffraction (XRD)

XRD is a material analysis technique used in identification and quantification of the crystalline phases in a sample. In this analysis technique, X-rays are emitted onto the sample being analyzed and the atoms of the sample diffract the x-rays⁷⁰. The diffracted rays are captured, usually by a film, and the resulting spectra are analyzed to identify the crystalline phases in the sample. It was used for two purposes during the research. First was to evaluate the Berea Sandstone mineralogical composition which confirmed the presence of clays that were

also observed in the Scanning Electron Microscopy images. Second was to investigate the crystallinity of the brown layer observed at the inlet of the composite core. A Rigaku Corporation Miniflex located at the Louisiana State University Material Characterization Center was used for XRD of the Berea sandstone. It was operated at SCHV of 630 and scan speed of 4° per minute from 5° to 70°. To obtain the x-ray diffractogram of the brown layer, a Bruker/Siemens D5000 X-Ray diffractometer with dual goniometer located in the Department of Geology and Geophysics at Louisiana State University was used. It was operated at 40 KV, 30 mA and 0.02 degree step per 2.0 degree seconds from 2 to 70 degrees.

3.5.8 Inductively Coupled Plasma-Optical Emission Spectroscopy (ICP-OES)

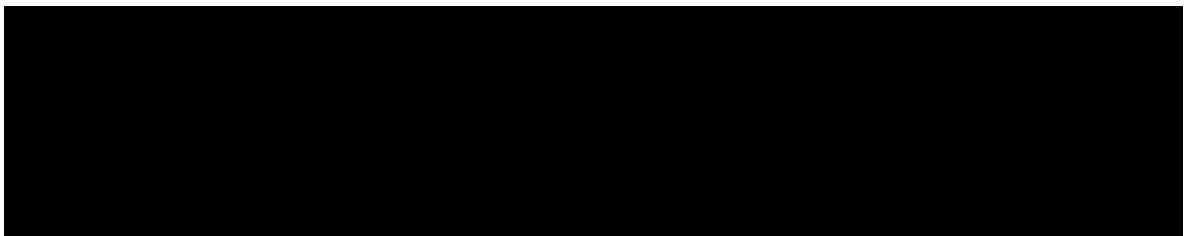
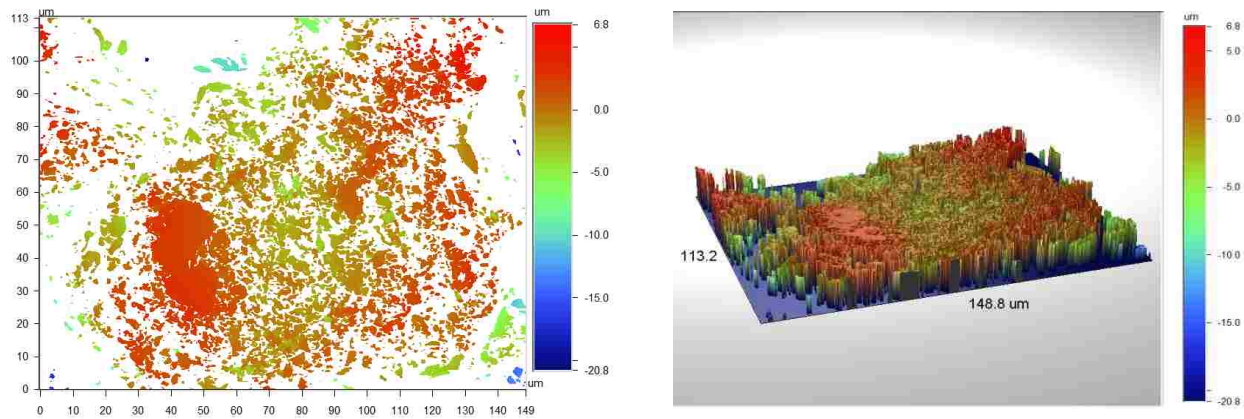
ICP-OES is a technique used in analysis of solutions to identify elements that are present. The solution of interest is exposed to very high temperature in the core of inductively coupled argon plasma (ICP). At very high temperatures, the elements in the solution become excited and emit light at the elements characteristic wavelength. The emitted light is used to identify and quantify the elements present in the sample. ICP-OES was used to analyze the influent and effluent brine samples taken daily throughout the experiment. This enabled the identification and quantification of the chemical composition of the brine to evaluate the dissolution/precipitation of different minerals from the cement/sandstone. The samples were analyzed in the LSU School of Plant, Environmental and Soil Sciences using a Spectro Ciros^{CCD} ICP-OES machine.

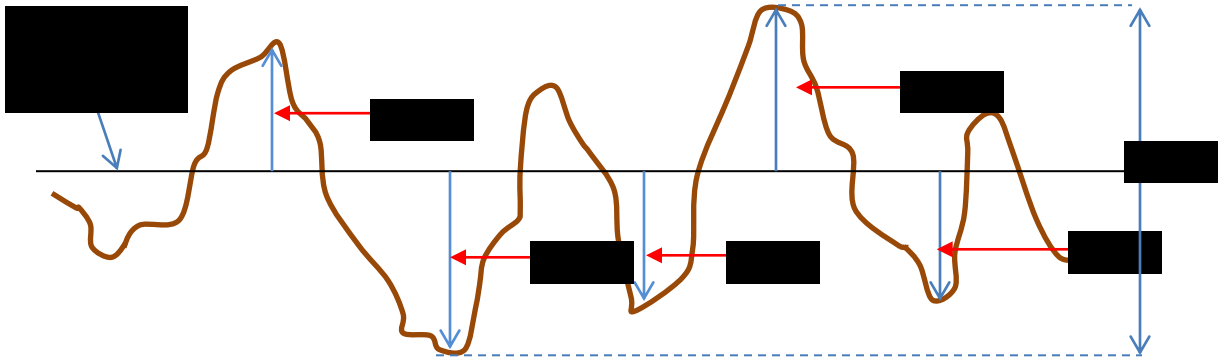
CHAPTER 4 RESULTS AND DISCUSSION

Results obtained from the flow-through experiments and from the analysis techniques described in Chapter 3 are presented in this chapter. These results are presented according to the experimental techniques. Discussion of the results is presented along with the results.

4.1 Surface Profilometry

The surface profile of the Berea sandstone was obtained before cement was placed on the sandstone to obtain a quantification of the roughness of the sandstone. High surface roughness provides larger surface area for cement to bond to the rock creating a more effective bond. The 2D and 3D surface profiles are shown in Figure 4.1. In the 2D profile, red represents peaks while white represents valleys. In the 3D profile, red represents peaks while blue represents valleys. Figure 4.2 explains the roughness values obtained from the surface profile. The root mean square value (R_q) of the peaks and valleys is normally accepted as the roughness value⁷¹ and it was obtained to be $2.33 \mu\text{m}$. The arithmetic mean of the peaks and valleys (R_a) was $1.70 \mu\text{m}$ while the distance between the highest peak and lowest valley (R_t) was $27.59 \mu\text{m}$.





R_p: Peak distance from mean line

R_v: Valley distance from mean line

R_a: Arithmetic mean of R_p's and R_v's

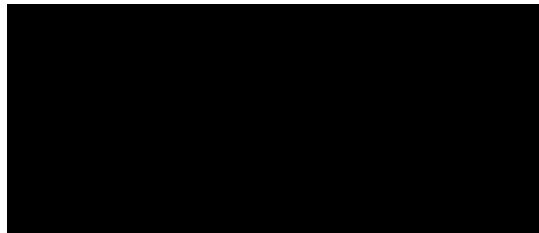
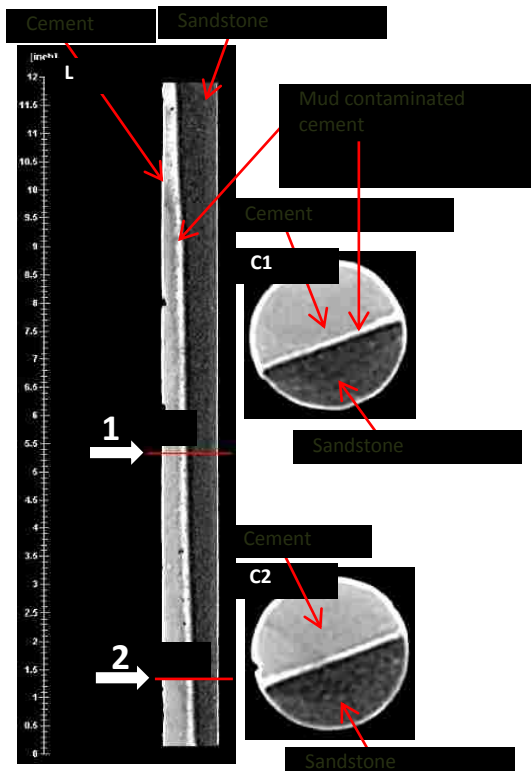
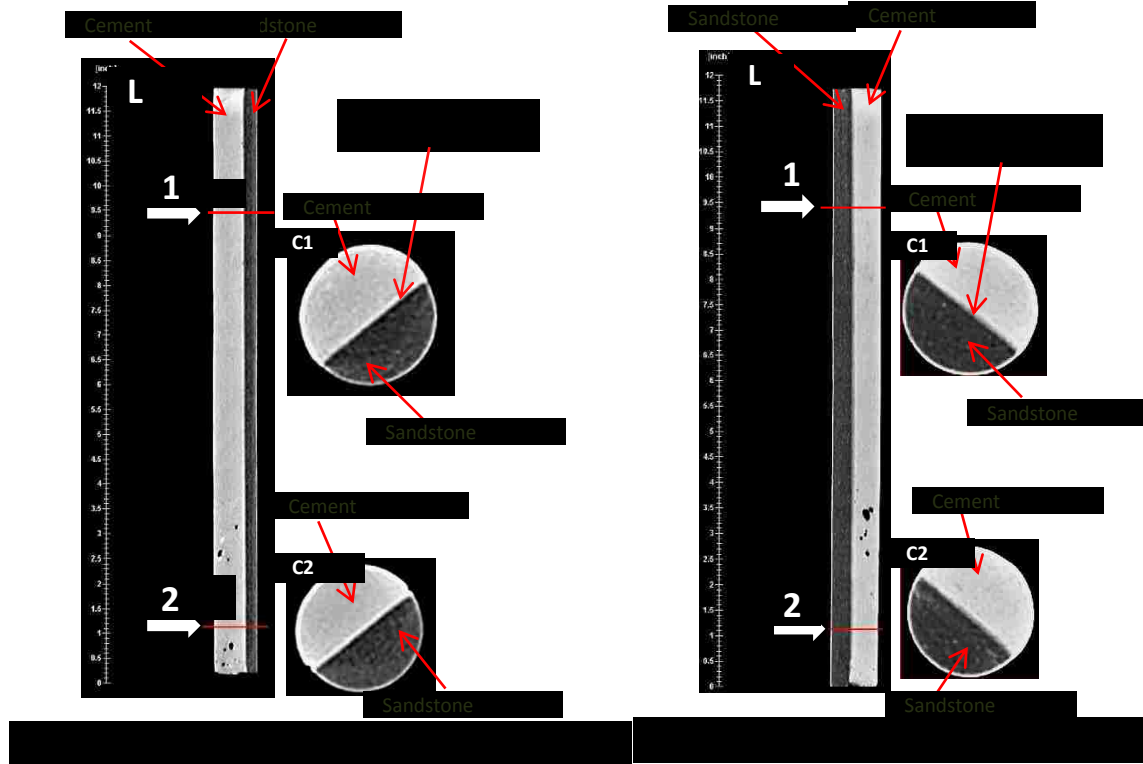
R_q: Root mean square value of the R_p's and R_v's

R_t: Distance between the highest peak and lowest valley



4.2 X-Ray Computed Tomography (Low Resolution CT)

X-Ray Computed Tomography images of whole composite cores were obtained to evaluate the nature and quality of the bond between the cement and the sandstone. The images were obtained before and after the core-flood to identify areas that have been altered during the flow-through experiments so that further analysis could be carried out on those sections. The images obtained are shown in Figure 4.3. The different shades of gray in a CT image correspond to the x-ray attenuation coefficient of the different sections of the scanned sample. This attenuation coefficient is dependent on the density and atomic mass of the volume of the sample; areas with high density or atomic mass are bright while voids are black. The white bands found on the edges of axial slices of the images are products of beam hardening effect caused by loss of the lower-energy parts of the x-ray spectrum as the x-ray beam penetrates the sample⁷². The cross sectional slices (C1 and C2) were taken from approximately the same points on the pre and



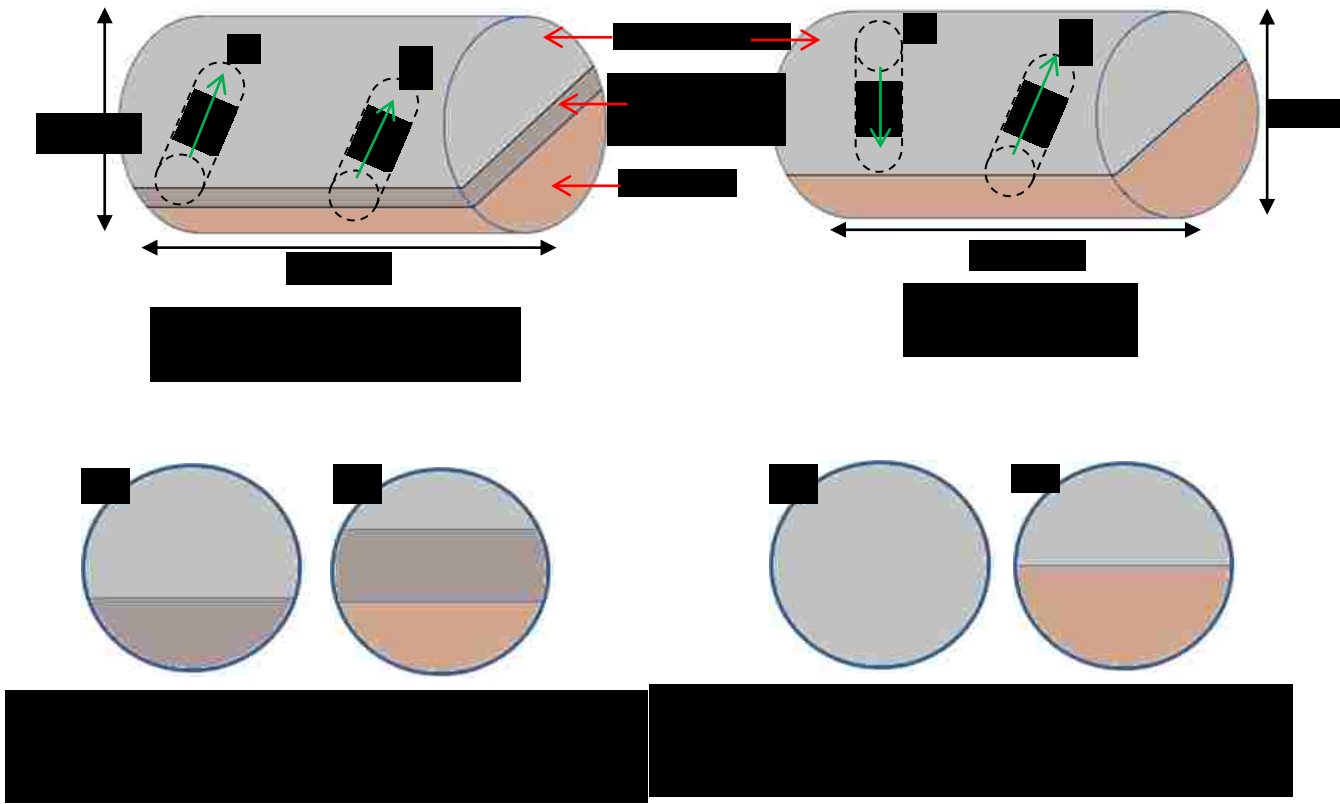
Tomography type	Spatial resolution	Pixel size	Voxel size
Micro-CT	2.5 μm	2.5 μm 2.5 μm	2.5 μm x 2.5 μm x 2.5 μm
Low Resolution CT	300 μm	300 μm 300 μm	300 μm x 300 μm x 300 μm

post core-flood composite core CT images for effective comparison. The longitudinal and cross sectional views of the CT-image of the 0% contaminated composite core (Figure 4.3a) show that a good bond was established between the cement and the rock before the core-flood. Examination of the post core-flood CT images (Figure 4.3b), shows that a good bond was also established between the cement and the rock at the end of the 30 day flow-through experiment. Alteration of the composite core interface due to the core-flood could not be confirmed from the images at the $300\ \mu\text{m} \times 300\ \mu\text{m} \times 500\ \mu\text{m}$ voxel resolution of the scan. The CT-images of the pre core-flood 10% mud contaminated composite core is shown in Figure 4.3c. Examination of the longitudinal and cross sectional images of the composite core showed that a good bond was established between the sandstone and the cement. The composite core was however not scanned at the end of the experiment since we discovered from the 0% composite core scan that the beam hardening effect was interfering with critical data at the interface.

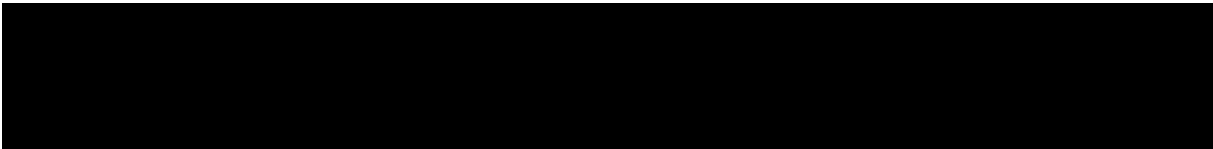
4.3 Micro-CT (High Resolution CT) and Image Based Porosity

Micro-CT was used to examine the composite cores at a much finer scale. The voxel size of the low resolution CT was $300\ \mu\text{m} \times 300\ \mu\text{m} \times 500\ \mu\text{m}$ while that of the Micro-CT was $2.5\ \mu\text{m} \times 2.5\ \mu\text{m} \times 2.5\ \mu\text{m}$. The Micro-CT therefore provides a 2,880,000x decrease in voxel size. Since no specific areas of alteration were observed in the low resolution CT images, the inlet and outlet sections of the composite cores were selected for Micro-CT analyses. Two sets of mini cores were drilled at the inlet and outlet of the composite cores. The first set was drilled to examine the cement-sandstone interface (interface-evaluation mini cores) and the second was drilled to evaluate the depth of cement degradation (cement-evaluation mini cores). Mini cores were also drilled from control samples so that alterations due to the flow-through experiments could be identified. The mini cores were drilled as shown in Figure 4.4.

In carrying out image based porosity calculations, three different subvolumes extracted from each region of the Micro-CT images were used to eliminate bias. For porosity calculations on the subvolumes, three sets of threshold values were also utilized for increased accuracy. Since the 1D resolution of the images was 2.5 μm , only pores larger than 5 μm could be identified⁶⁶. The axial slices presented in Figure 4.5 to Figure 4.7 were chosen to represent typical observations in the imaged volume.



1 and 3: Cement-evaluation mini cores
 2 and 4: Interface-evaluation mini cores
 C1 and C3: Cross sections of cement-evaluation mini cores
 C2 and C4: Cross sections of interface-evaluation mini cores



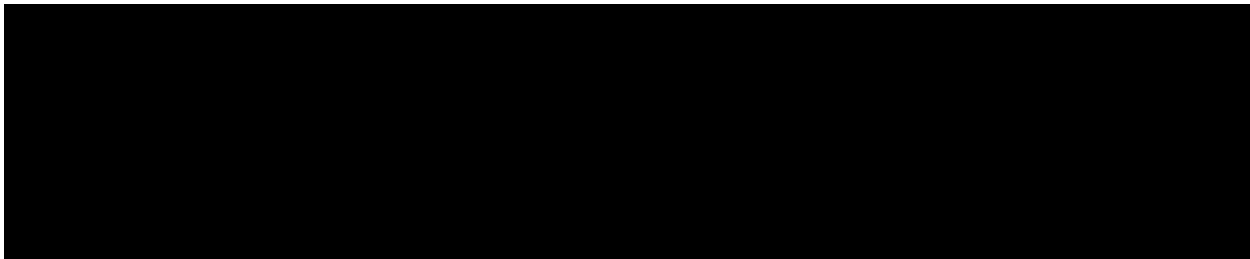
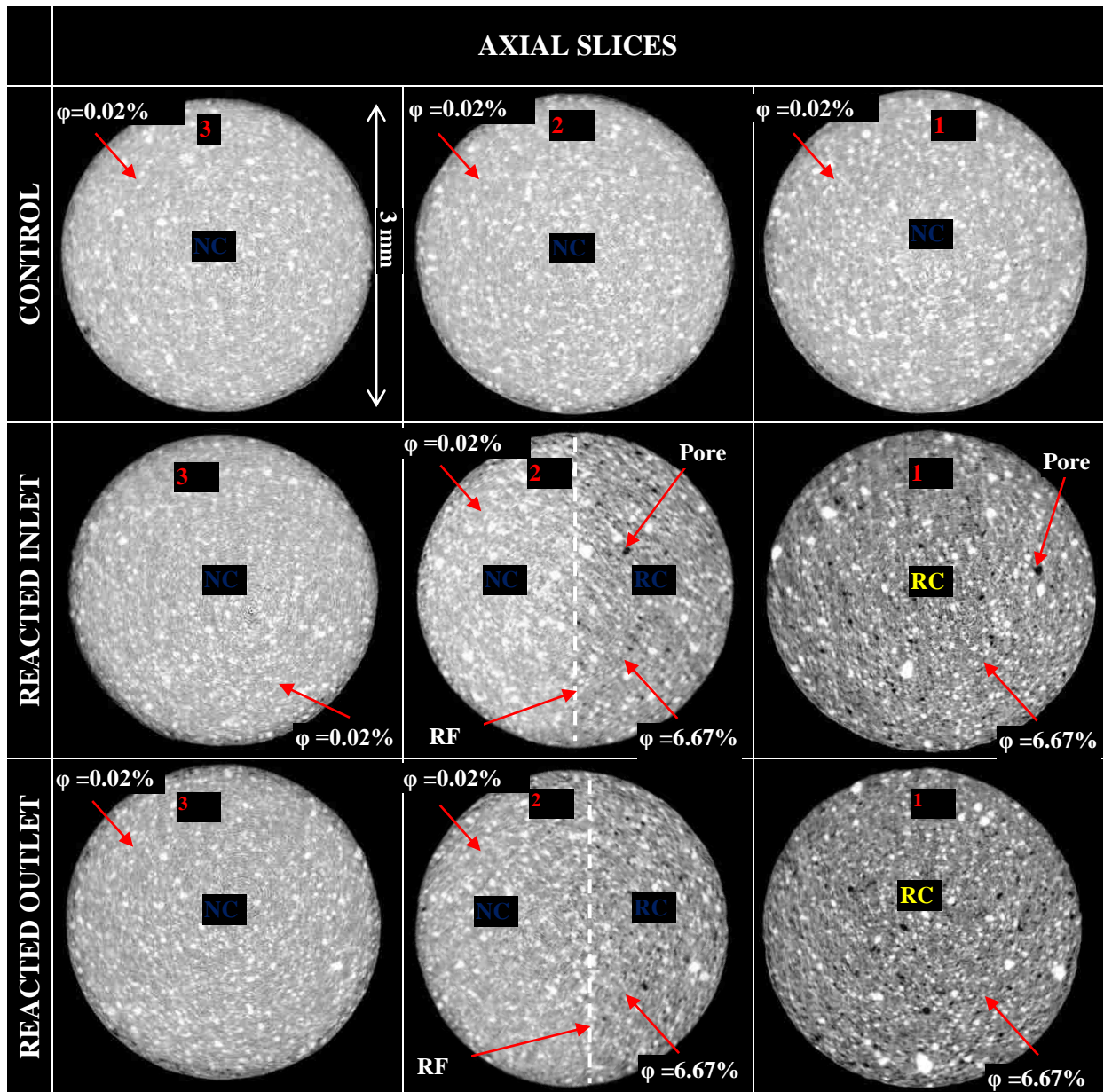
4.3.1 Mud Contamination Experiment [0%]

The Micro-CT images obtained from the 3 mm diameter mini cores are shown in Figure 4.5 and 4.6. For the cement-evaluation mini cores, about 3.84 mm length of each mini core was imaged while about 2.56 mm length of each interface-evaluation mini core was imaged.

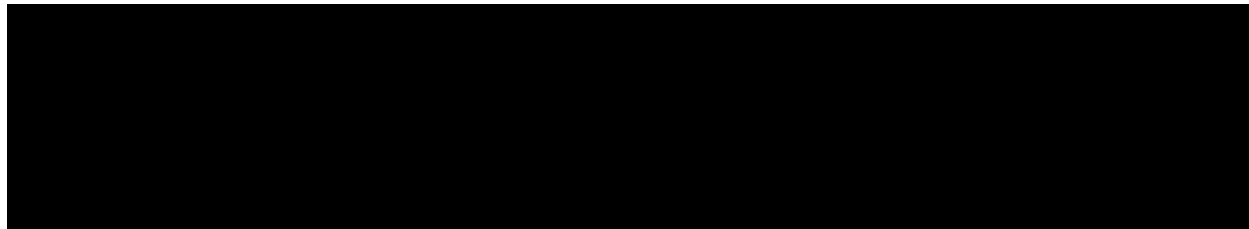
For the control sample, the cement-evaluation mini core showed uniform density throughout the mini core while two distinct zones with different densities were observed in the core-flooded cement-evaluation mini cores as shown in Figure 4.5. The Micro-CT also captured the transition point between the two zones in the core-flooded mini cores. The higher density zone indicated by brighter gray color represents neat cement. The lower density zone was closer to the sandstone and is shown by dark gray color in Figure 4.5; increased number of black spots in the lower density zone show that porosity increased in the zone. The thickness of the lower density region was $\sim 950 \mu\text{m}$ for both the inlet and the outlet mini cores. The lower density region was created due to the leaching of cement by the flowing brine during the flow-through experiment.

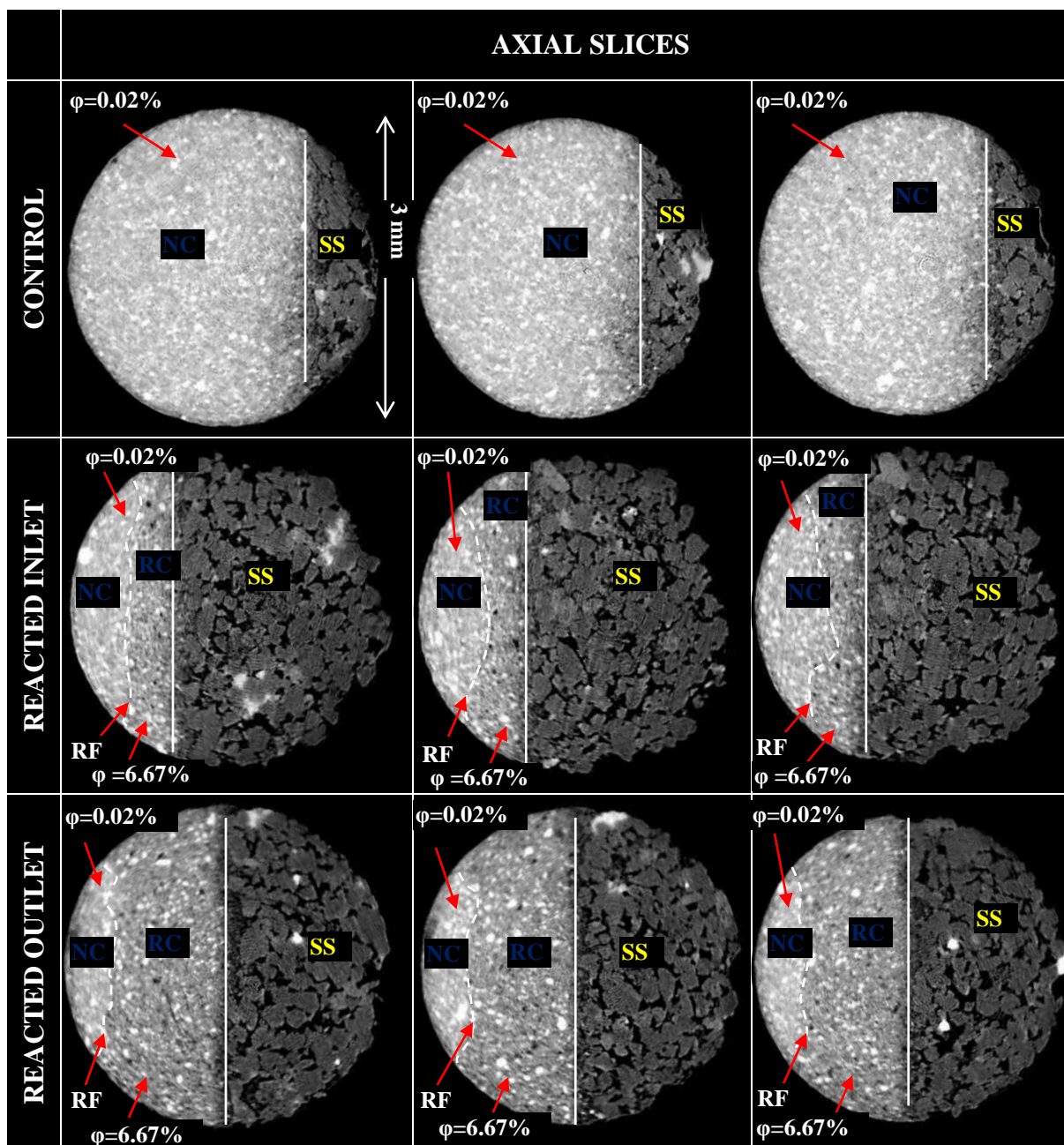
The interface-evaluation mini core from the control sample also showed uniform density in the cement (Figure 4.6). The presence of lower and higher density zones in the core-flooded samples were confirmed by the interface-evaluation mini cores. The area of reduced density was observed to be larger (thickness $\sim 950 \mu\text{m}$) at the outlet than at the inlet (thickness $\sim 370 \mu\text{m}$). The porosity of neat cement was found to be 0.02% while the porosity of the lower density zone was found to be 6.67%.

	WHOLE MINI CORE	ORTHO SLICE OF MINI CORE
CONTROL	<p>Cement-sandstone interface</p> <p>1415 slices</p>	<p>1</p> <p>2</p> <p>3</p> <p>NC</p> <p>1415 slices</p>
REACTED INLET	<p>Cement-sandstone interface</p> <p>1442 slices</p>	<p>1</p> <p>2</p> <p>3</p> <p>RC</p> <p>NC</p> <p>RF</p> <p>1442 slices</p>
REACTED OUTLET	<p>Cement-sandstone interface</p> <p>1438 slices</p>	<p>1</p> <p>2</p> <p>3</p> <p>RC</p> <p>NC</p> <p>RF</p> <p>1438 slices</p>



	WHOLE MINI CORE	ORTHO SLICE OF MINI CORES
CONTROL		
REACTED INLET		
REACTED OUTLET		





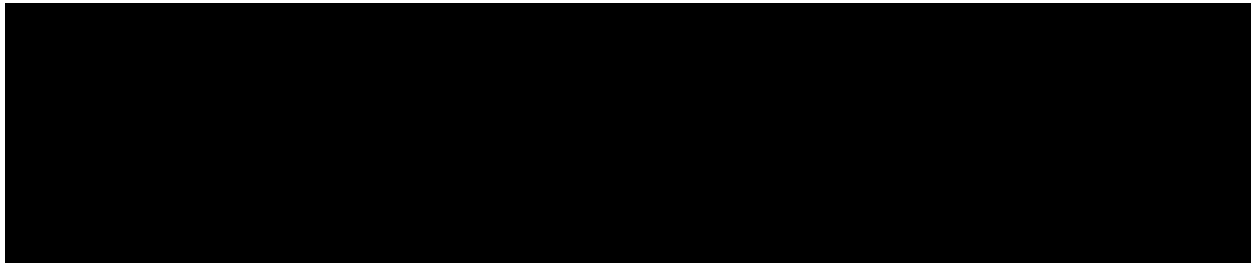
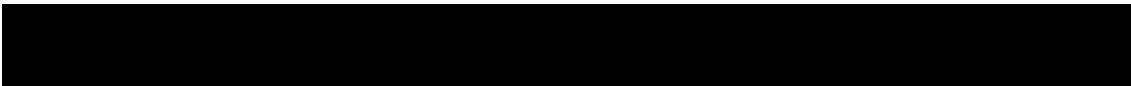
4.3.2 Mud Contamination Experiment [5%]

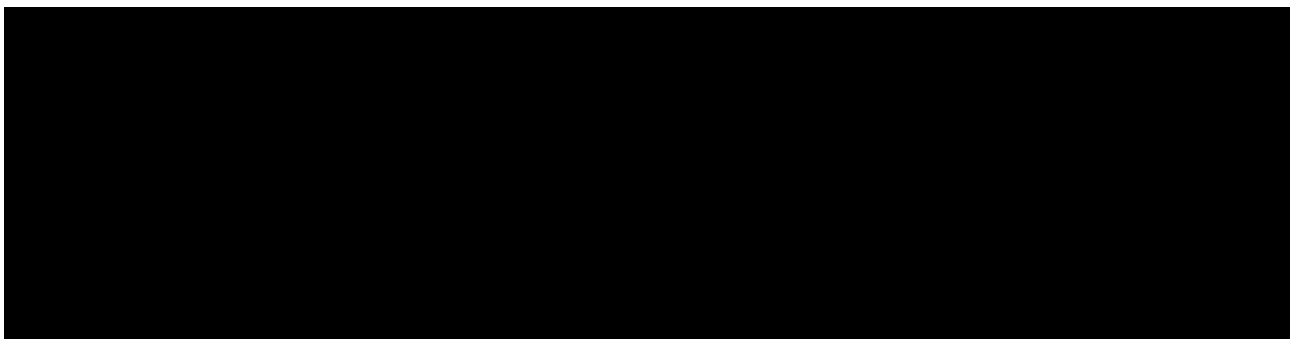
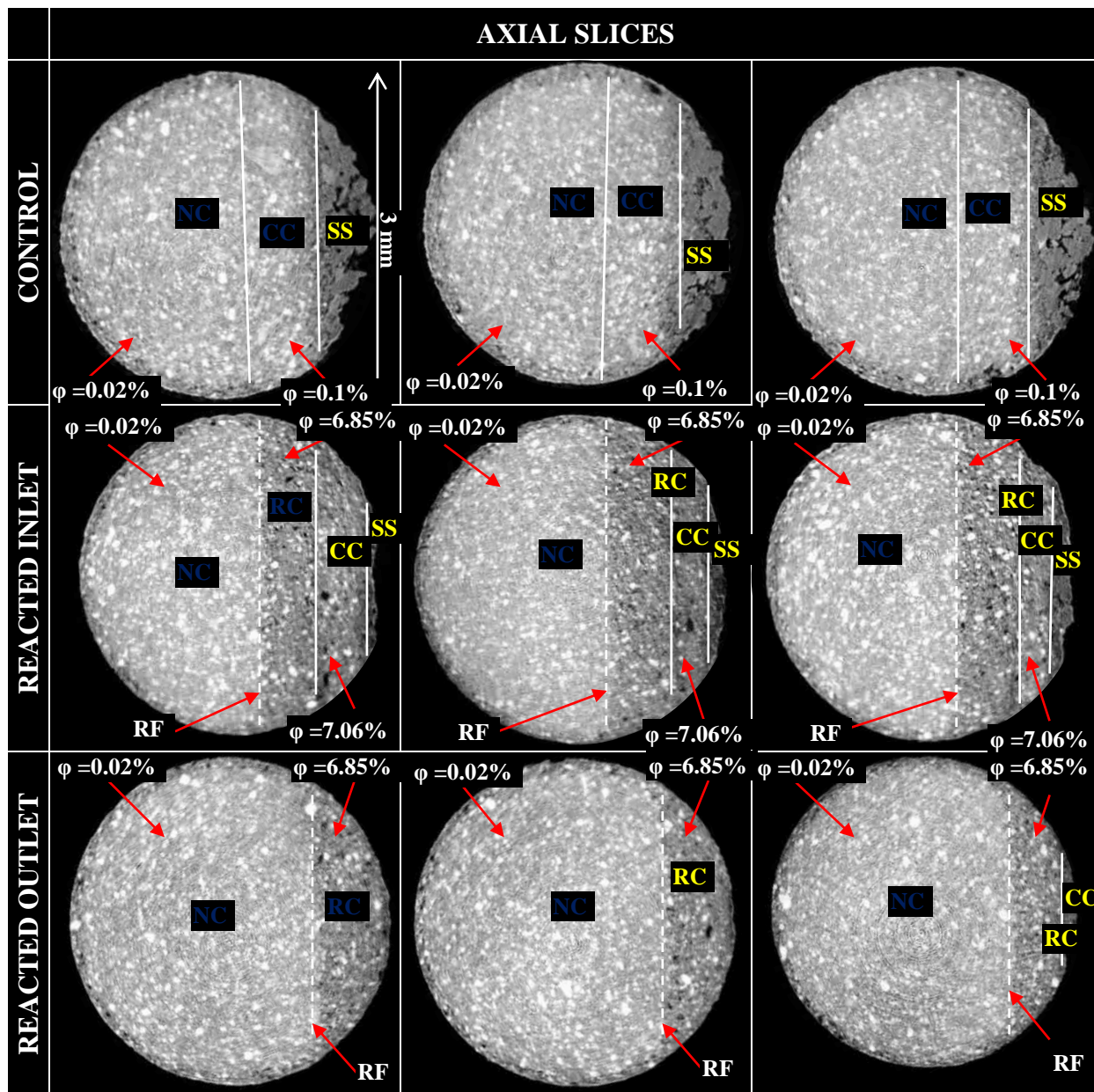
The Micro-CT images obtained from the 3 mm diameter mini cores drilled from the 5% mud contaminated composite core are shown in Figure 4.7 and 4.8. For both the cement-evaluation mini cores and interface-evaluation mini cores, ~2.56 mm length of each mini core was imaged.

In the control sample shown in Figure 4.7, there was no identifiable difference in density between the contaminated and uncontaminated layers of the cement-evaluation mini cores (both showed the same brightness levels). The core-flooded mini cores on the other hand showed reduction in density of the cement close to the sandstone. The density reduction was due to the leaching of cement by the flowing brine during the flow-through experiment. The density reduction, which is indicated by darker gray color, extended ~870 μm into the cement. The density reduction progressed beyond the mud contaminated layer into the neat cement layer.

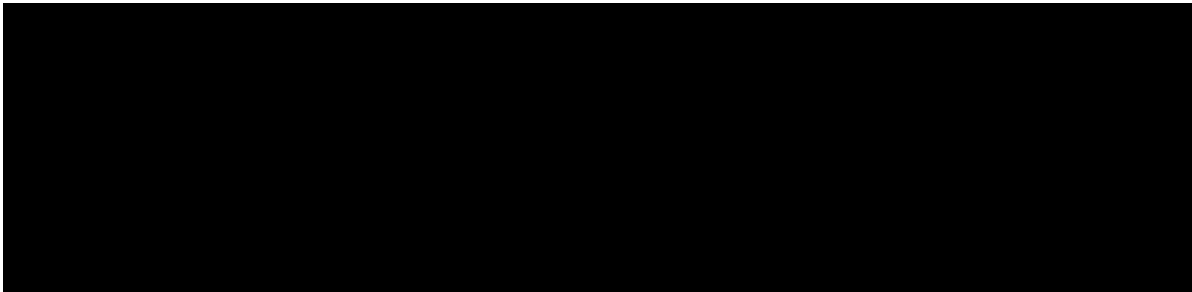
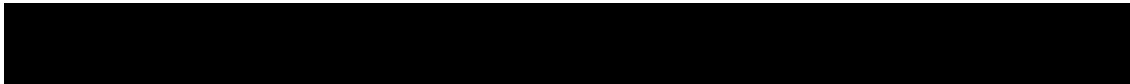
The control sample of the interface-evaluation mini cores did not indicate significant density difference between the contaminated and uncontaminated layers. As with the cement-evaluation mini cores, lower and higher density zones were observed in the interface-evaluation mini cores of the core-flooded samples (Figure 4.8). The lower density region was larger (thickness ~850 μm) in the outlet than at the inlet (thickness ~350 μm); as was observed in the 0% mud contamination composite cores. The porosity of neat cement was found to be 0.02% while the porosity of pre core-flood contaminated cement was found to be 0.1%. At the end of the flow-through experiment, the porosity of the lower density region varied amongst the mini cores. The porosity in the outlet interface-evaluation mini core was highest at 8.77% while the porosity in both inlet and outlet of the cement-evaluation mini cores was lowest at 6.85% as

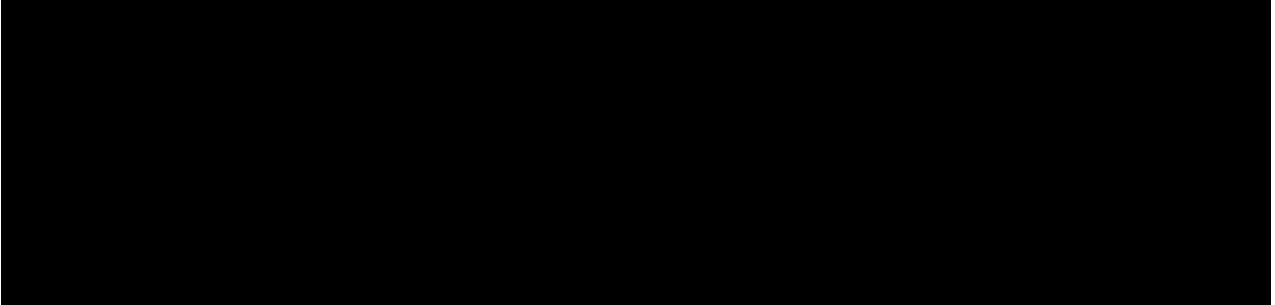
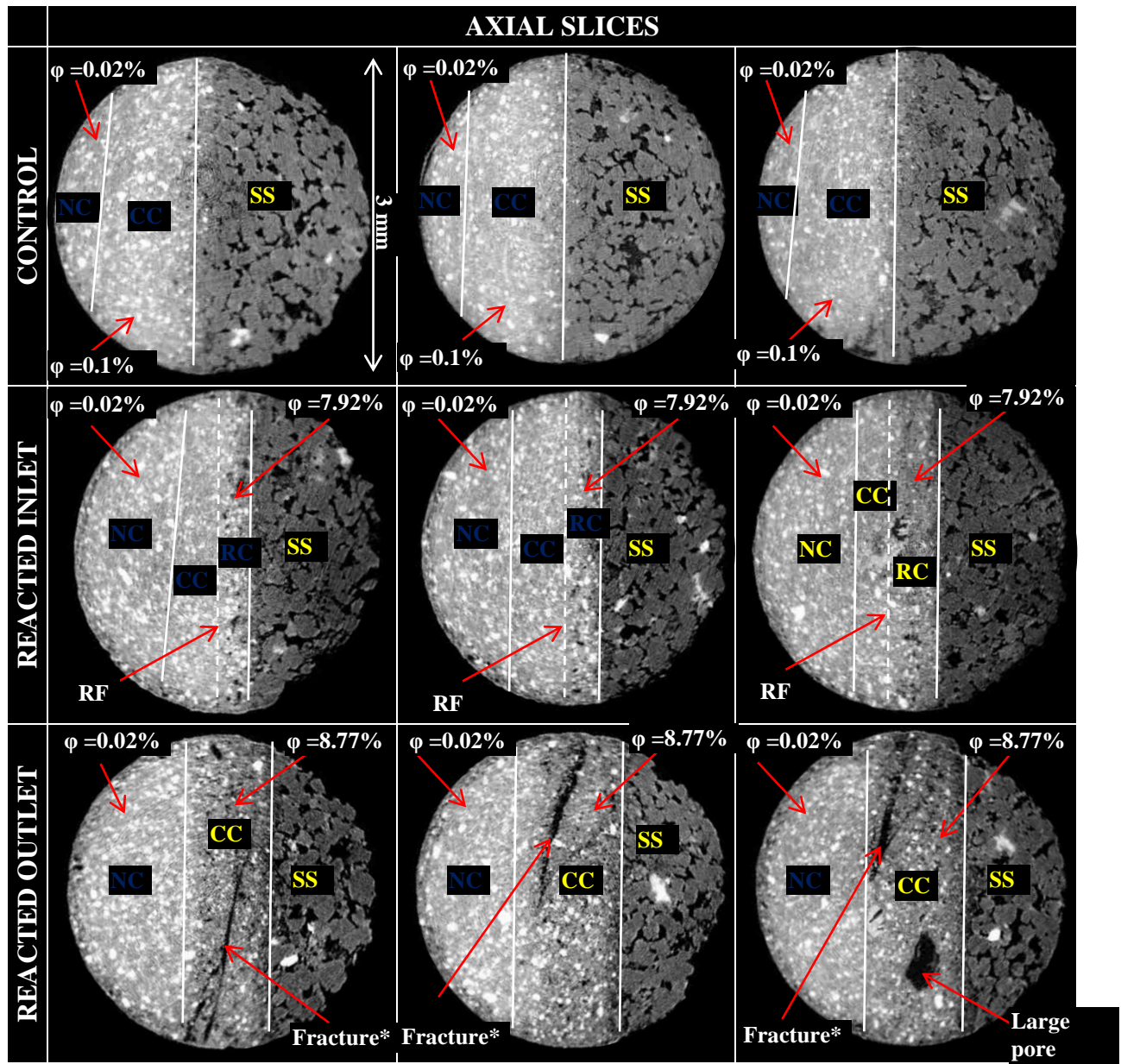
shown in Figure 4.7b and 4.8b. Large pores were also observed in the mud contaminated cement as shown in Figure 4.8a and 4.8b.





	WHOLE MINI CORE	ORTHO SLICE OF MINI CORE
CONTROL		
REACTED INLET		
REACTED OUTLET		





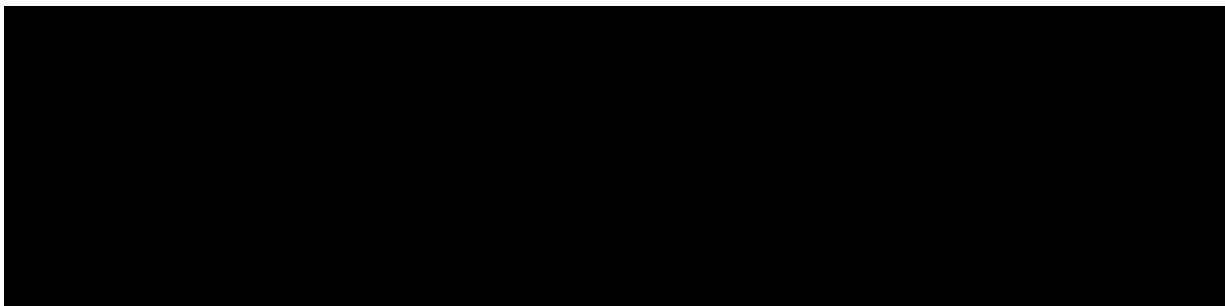
4.3.3 Mud Contamination Experiment [10%]

In the 10% mud contamination experiment, about 3.84 mm length of each cement-evaluation mini core was imaged while ~2.56 mm length of each interface-evaluation mini core was imaged. The cement-evaluation mini core of the control sample showed density gradation between the contaminated and uncontaminated layers of the cement. In the cement-evaluation mini cores from core-flooded composite core, large pores were observed in the mud contaminated region while the neat cement was left intact as shown in Figure 4.9. The large pores are shown as black patches in the Micro-CT images. The large pores were created due to the leaching of the contaminated cement by the flowing brine during the flow-through experiment.

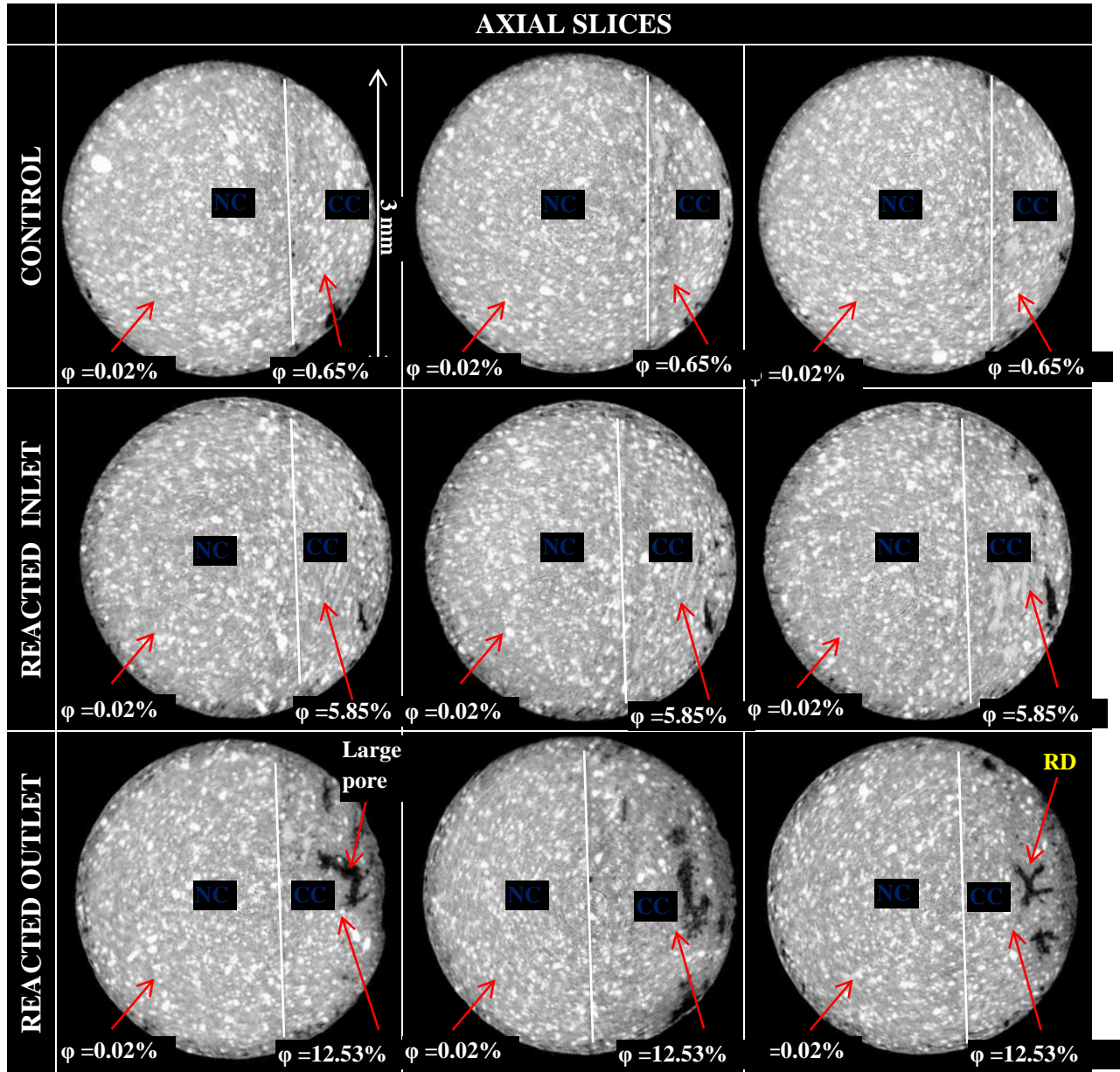
The interface-evaluation mini cores corroborated the observations from the cement-evaluation mini cores as shown in Figure 4.10. The mud contaminated cement closest to the sandstone had very large pores present while the neat cement did not show increased porosity. The large pores were mostly oriented parallel to the sandstone surface, indicating that those areas contained mud which spread out laterally during the wait-on-cement period for the mud contaminated layer.

The porosity of neat cement was found to be 0.02% while the porosity of pre core-flood contaminated cement was found to be 0.65%. At the end of the flow-through experiment, the porosity of the contaminated cement rose to as much as 12.53% in all the mini cores except for the inlet cement-evaluation mini core which had porosity of 5.85% as shown in Figure 4.9b and 4.10b. A zone of low density (dark gray) was also observed around some of the large pores as shown in Figure 4.9b and 4.10b.

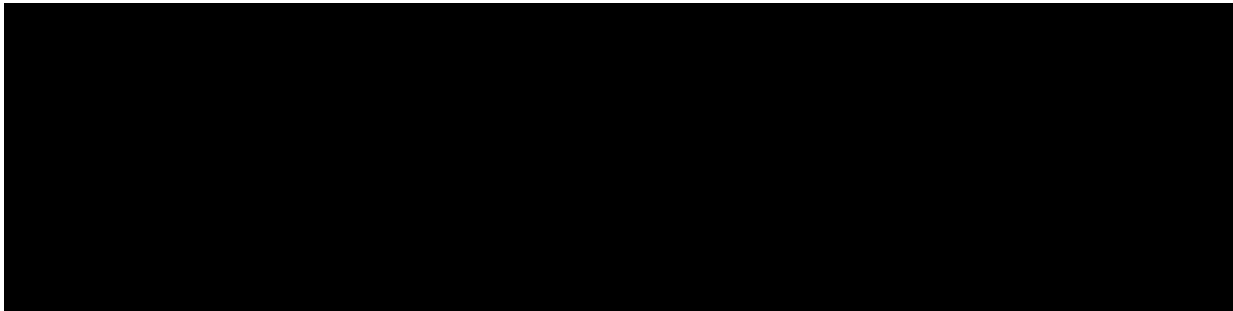
	WHOLE MINI CORE	ORTHO SLICE OF MINI CORE
CONTROL		
REACTED INLET		
REACTED OUTLET		

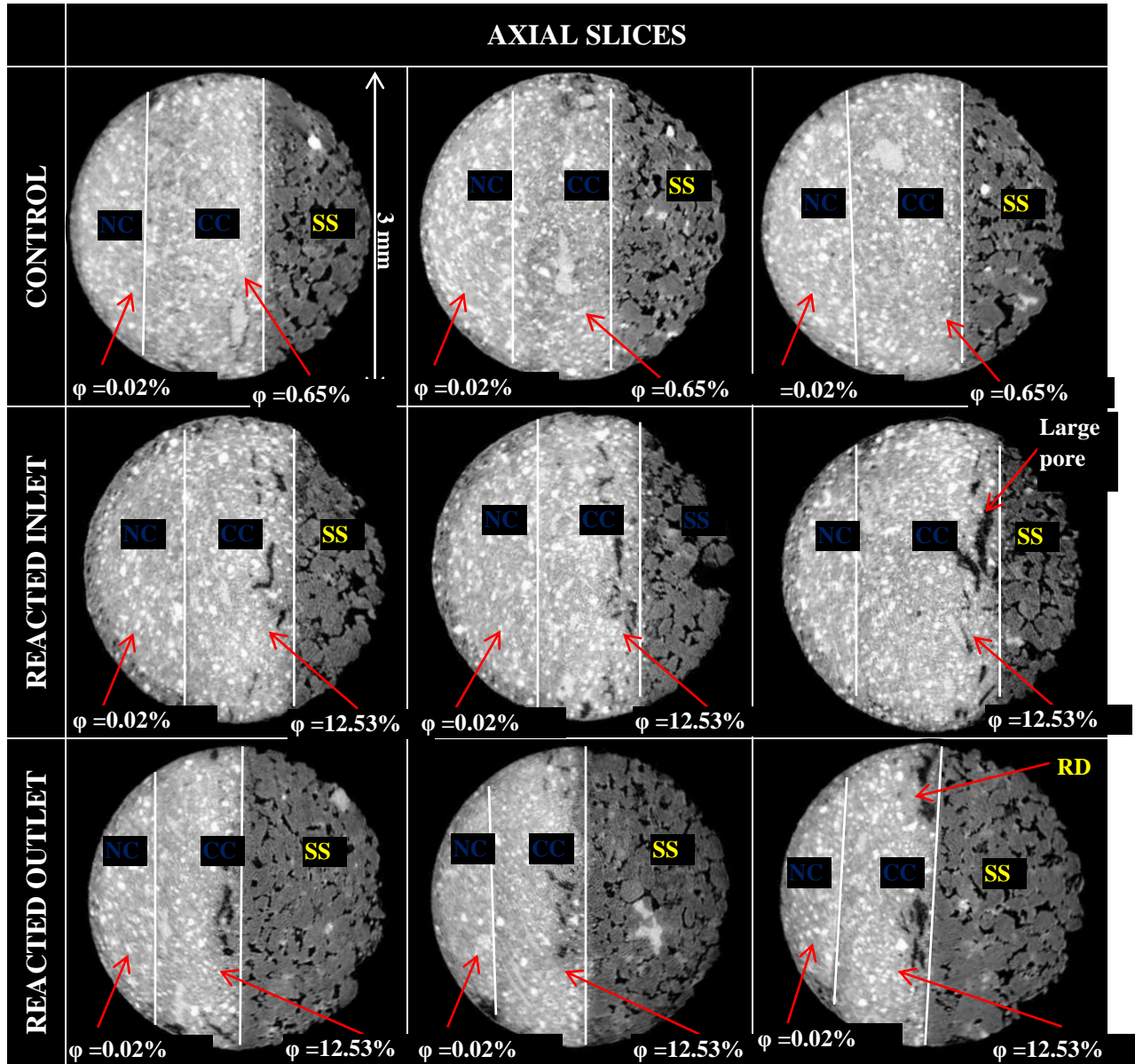


3 mm



	WHOLE MINI CORE	ORTHO SLICE OF MINI CORE
CONTROL		
REACTED INLET		
REACTED OUTLET		





4.4 Pressure Profile

The back pressure was kept at 1350 psi during the flow-through experiments and the varying injection pressure was continuously recorded with the aid of a pressure transducer. The pressure drop values obtained from the three flow-through experiments are plotted in Figure 4.11 as a function of time. The pressure drop profiles show that the three different experiments had three different pressure drop values at the start of the flow-through experiments. The pressure drop at the start of the 0% mud contamination experiment was ~40 psi while that of the 5% and 10% mud contamination experiments were ~15 psi and ~29 psi respectively. These initial pressure drop values were all higher than the 9.8 psi expected from the 300 mD Berea sandstone used. The pore volume of the sandstone was 15.44 cc as shown in Table 4.1 therefore ~93 PV of brine was injected daily throughout each 30-day flow-through experiment.

During the flow-through experiments, the pressure drop showed periodic increase and leveling off as the experiments progressed. However, the 5% and 10% mud contamination experiments showed longer periods of pressure drop stability as shown in Figure 4.11.

Table 4.1: Properties of typical Berea sandstone core used for each composite core.

Property	Value/Description
Shape	Half cylinder
Dimensions	1 in diameter X 12 in length
Bulk volume	77.22 cc
Porosity*	20%
Pore volume	15.44 cc

*Value obtained using image based methods and the value agreed with porosity values reported in literature^{73, 74}.

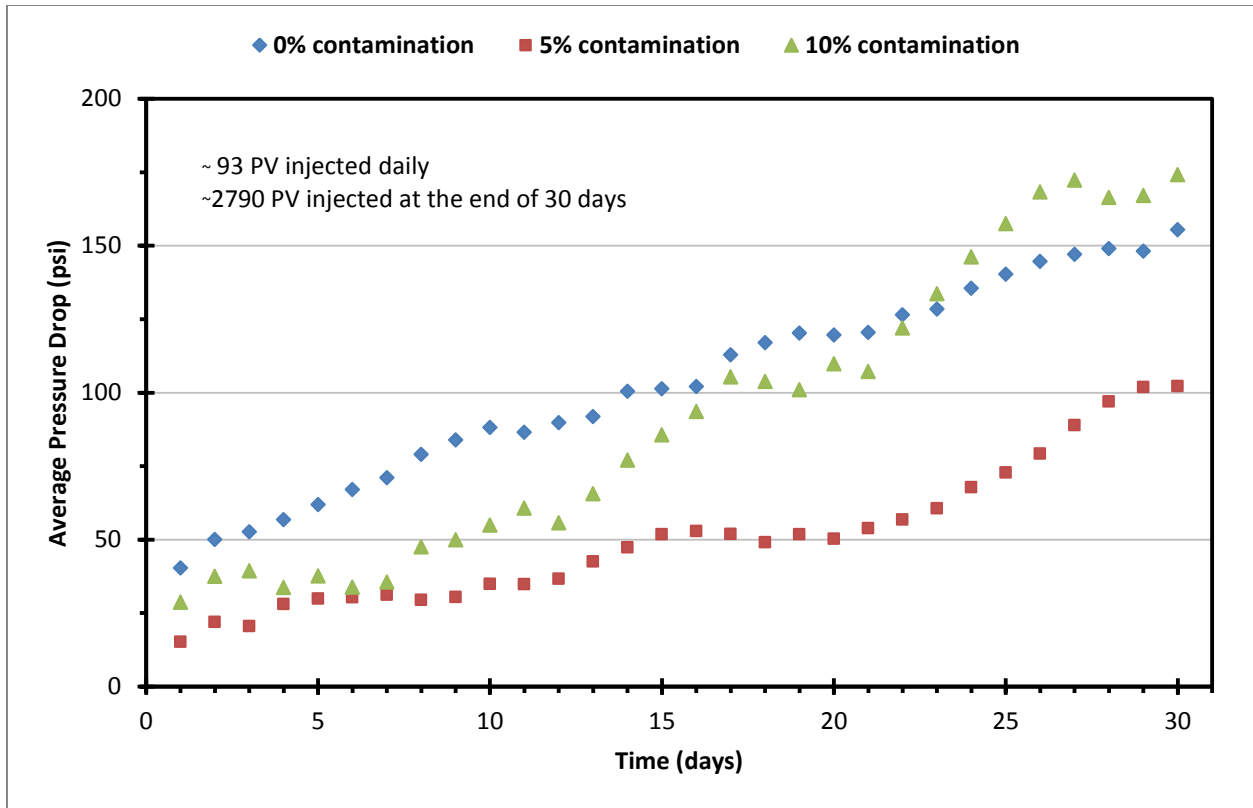
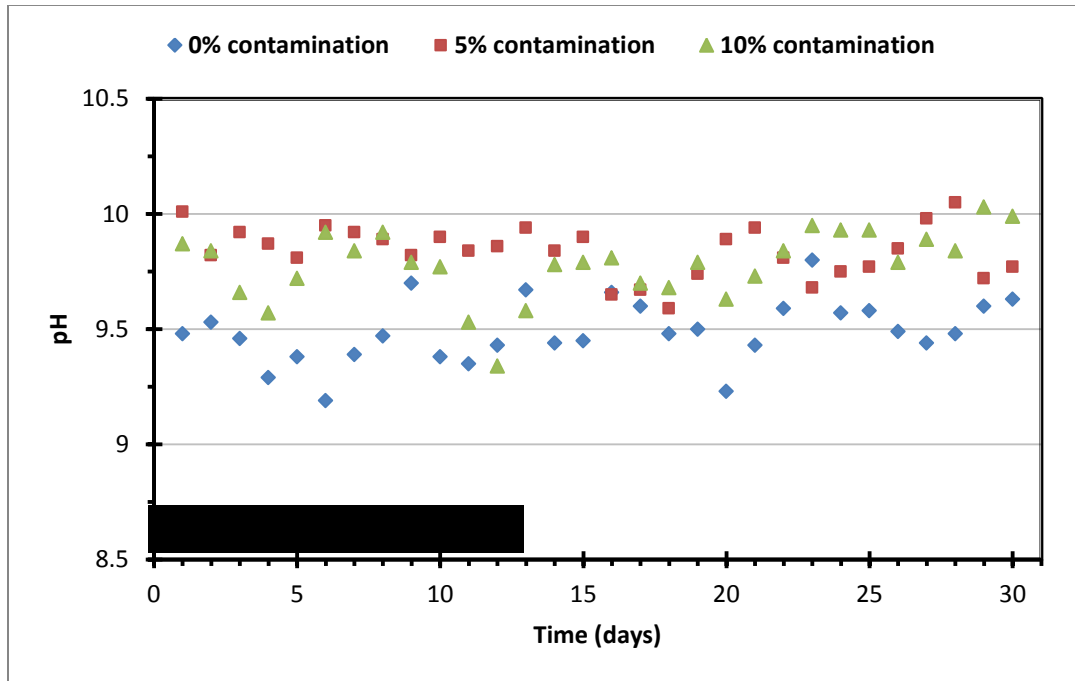


Figure 4.11: Pressure profile of the core-flood experiments. The pressure drop periodically increased and leveled off as the experiments progressed. The periods of pressure drop stability were longer in the 5% and 10% mud contamination experiments.

4.5 pH Measurements

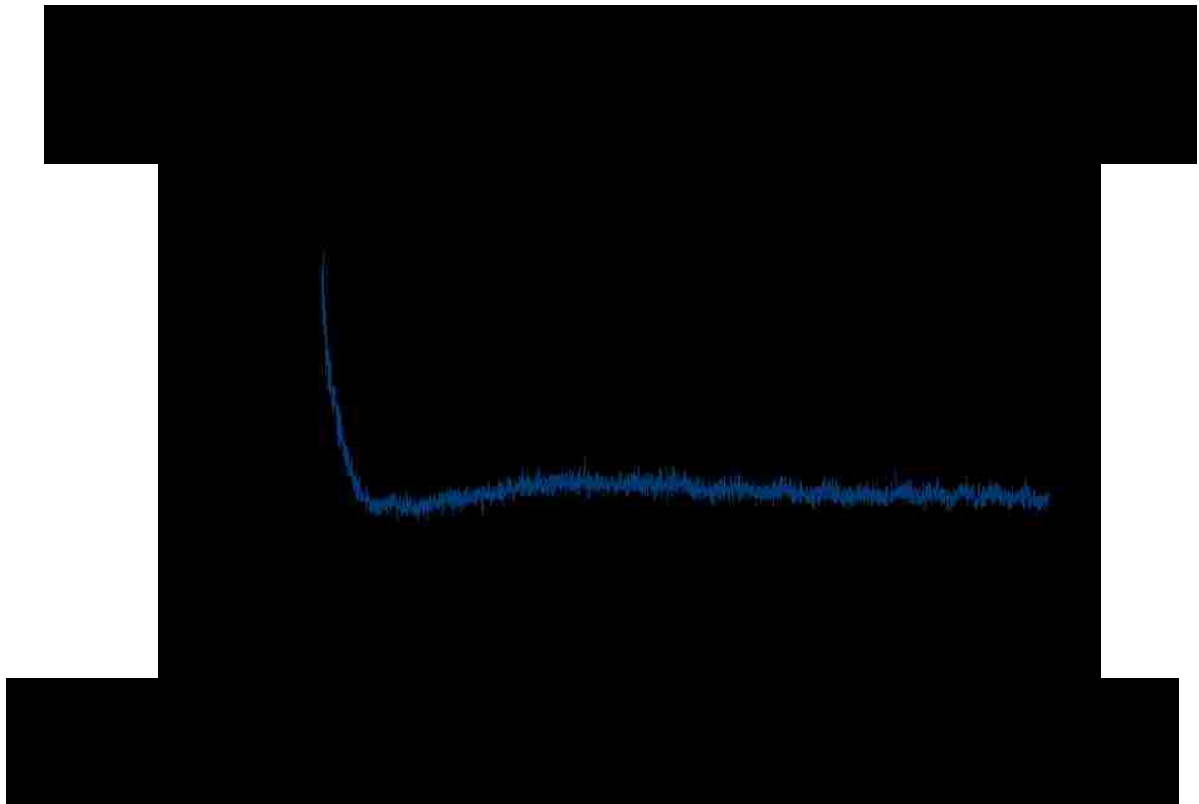
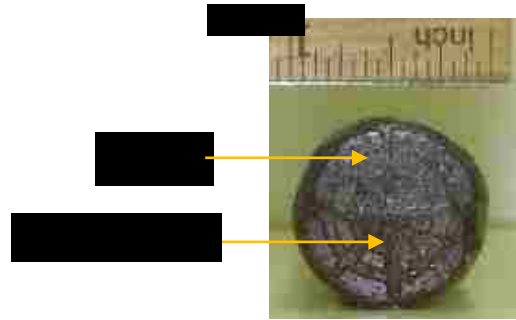
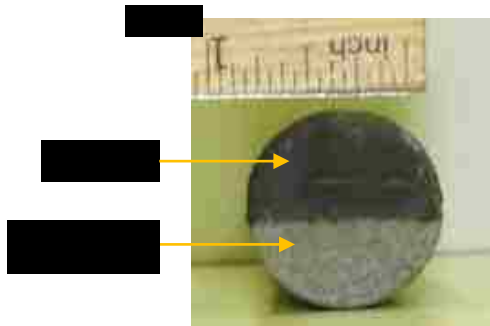
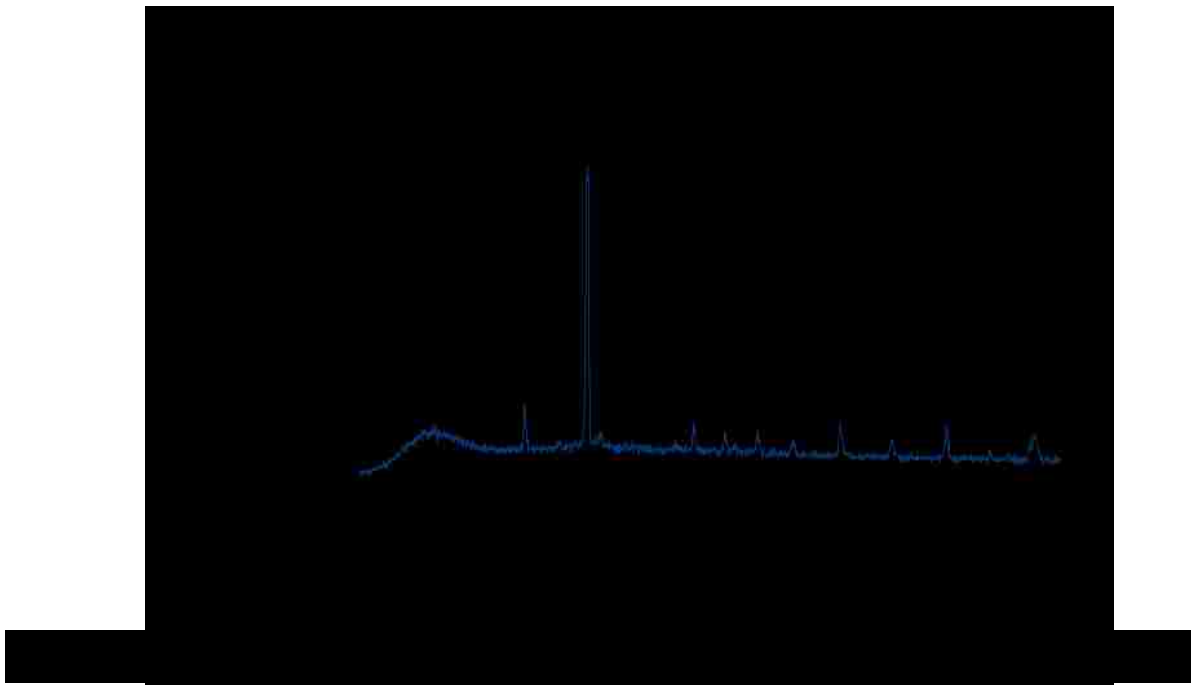
pH measurements were carried out on the effluent brine samples taken daily throughout the three flow-through experiments and the pH measurements are plotted in Figure 4.12. The first pH measurement of the effluent brine was taken 24 hrs after the start of the experiment and subsequent pH measurements were taken after every 24 hrs. The pH of the influent brine and the fresh water mud used were also measured. The pH of the mud was obtained to be 12 ± 0.10 while the pH of the influent brine was $\text{pH } 6.20 \pm 0.20$ throughout the experiments. Since the pH of cement pore water ($\text{pH } \sim 13$) and the fresh water mud ($\text{pH } 12 \pm 0.10$) were much higher than the pH of the influent brine ($\text{pH } 6.20 \pm 0.20$), effluent brine pH was a good indicator of the level of dissolution of the cement. Higher pH values indicate greater cement dissolution. As shown in

Figure 4.12, the pH values of the effluent brine in the 5% and 10% mud contamination experiments were higher than the pH of the effluent brine in the 0% mud contamination experiment. For the 0% contamination experiment, pH increased from 6.2 ± 0.20 to 9.49 ± 0.30 and for the 10% contamination experiment, pH increased from 6.2 ± 0.20 to 9.78 ± 0.40 . The pH of the 5% mud contamination experiment increased from 6.2 ± 0.20 to 9.84 ± 0.30 .



4.6 X-ray Diffraction (XRD) Data

X-ray diffraction was used to analyze the Berea sandstone to ascertain different minerals that were present. Quartz, albite and clays were identified from the diffractogram as shown in Figure 4.13. XRD was also used to evaluate a brown deposit observed at the inlet of all the composite cores at the end of the flow-through experiments (Figure 4.14b). The brown deposit was not present at the inlet of the composite cores at the beginning of the experiments as shown

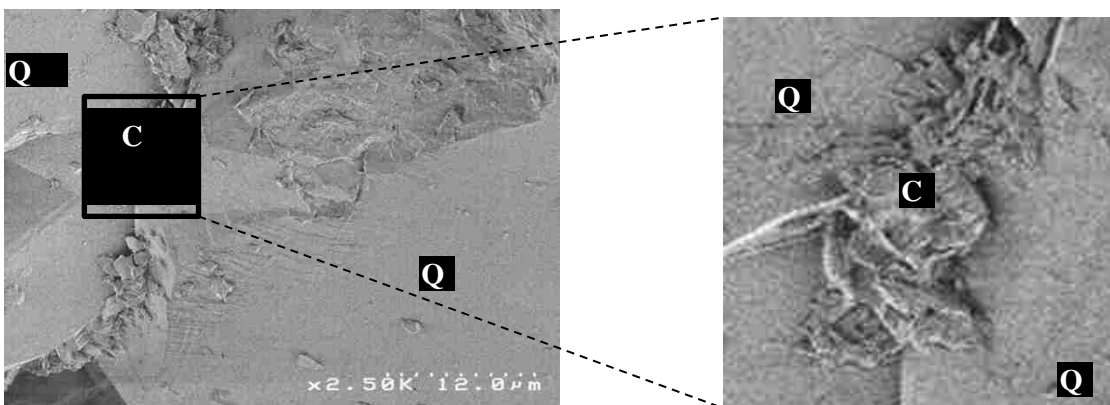


in Figure 4.14a. The diffractogram obtained from XRD of the brown deposit is shown in Figure 4.15. The absence of peaks in the diffractogram shows that the brown deposit is amorphous. Amorphous silica gel is the final stage of cement degradation and several studies have reported the development of a brown layer as the final stage of cement degradation^{23, 75}.

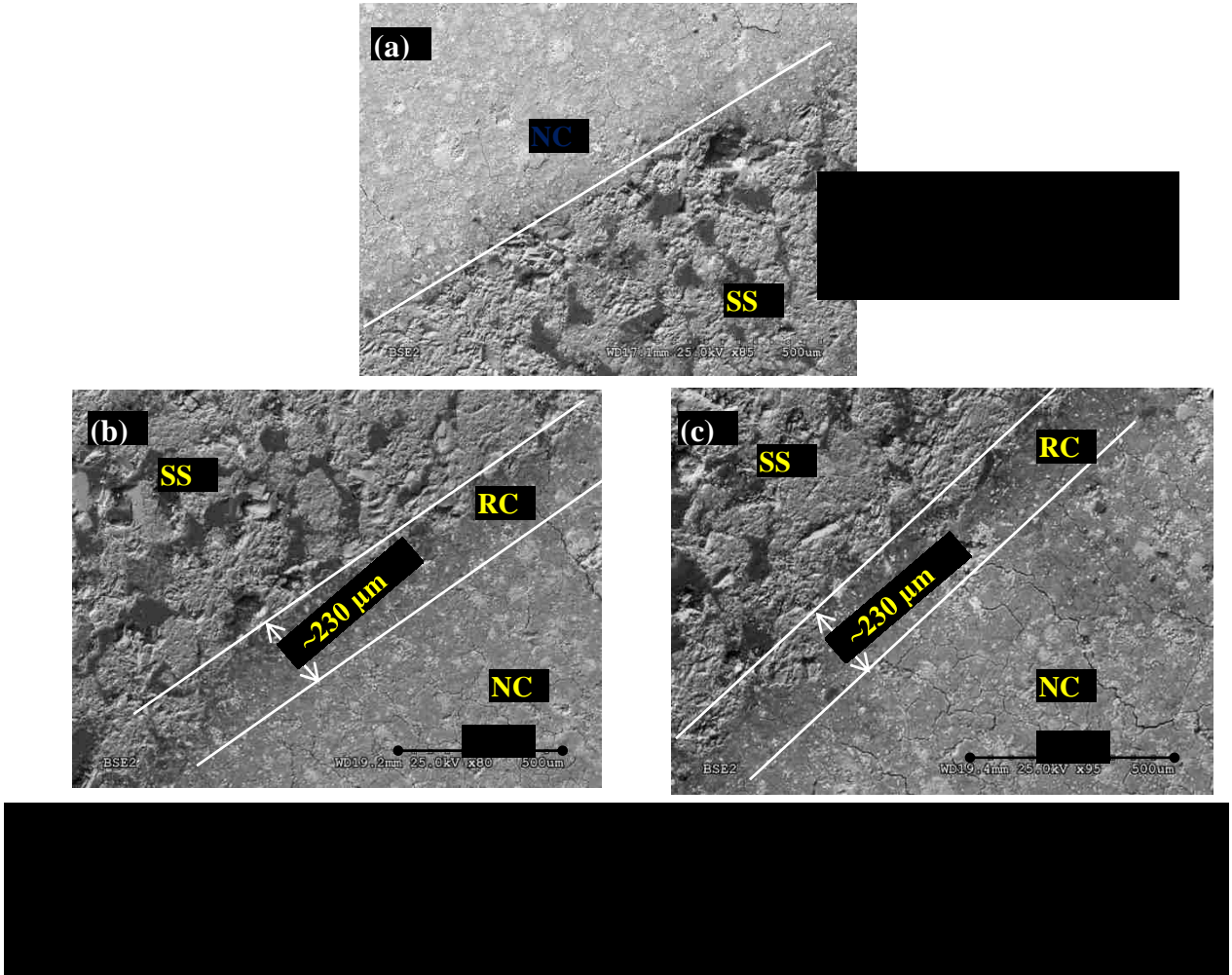
4.7 Scanning Electron Microscopy (SEM) Images

Scanning electron microscopy was carried out to evaluate the composite cores and Berea sandstone to corroborate observations from other analysis techniques. Images of fresh Berea sandstone used in the study were obtained using secondary electron microscopy to evaluate the composition of the sandstone. The images (Figure 4.16) show quartz crystals surrounded by clays. These clays were also confirmed by the XRD diffractogram of the fresh Berea sandstone. The backscattered electron microscopy mode provided density contrast between areas that are calcium rich (Ca=40) and areas that are silicon rich (Si=28). The samples used for back scattered electron microscopy were prepared by impregnating a section of the composite core cut from the inlet, with resin. The samples were also coated with platinum to obtain high quality images.

For the 0% contamination composite core, a zone of reduced density was observed at the cement-sandstone interface at the end of the flow-through experiment. The zone can be identified

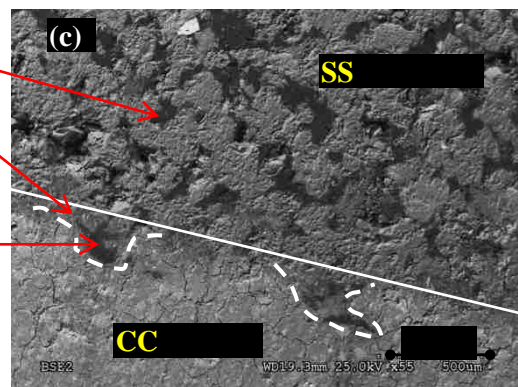
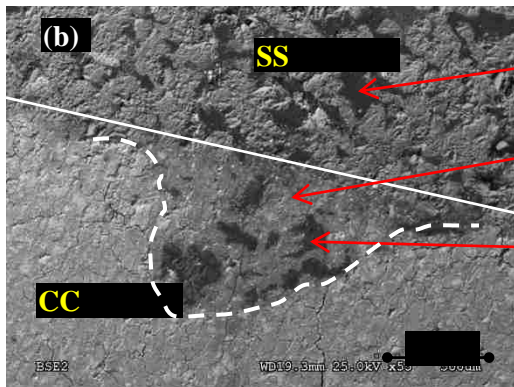
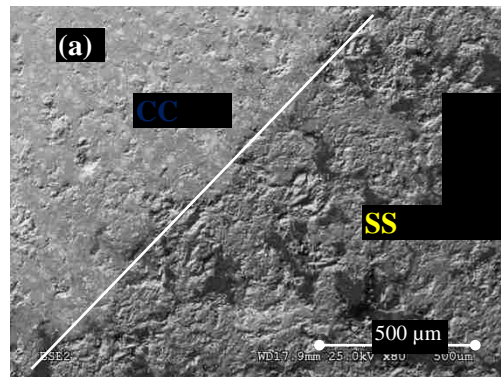


as a dark band that runs along the length of the cement-sandstone interface as shown in Figure 4.17b and Figure 4.17c. This dark zone is absent at the cement-sandstone interface in the control sample shown in Figure 4.17a.



For the post core-flood 10% mud contaminated composite core, the resin filled the interconnected pores of the sandstone as well as the large pores in the contaminated cement at the cement-sandstone interface as shown in Figure 4.18. This shows that there was interconnectivity between the large pores in the contaminated cement and the pores in the sandstone and therefore there was flow of fluids into the large pores. Interconnectivity of the large pores was however not observed and this showed that the large pores did not increase the

effective permeability of the composite core. Resin filled pores are shown as very dark gray in the images. The region surrounding the resin filled pores in the cement also showed density reduction (indicated by dark gray color). No pores were observed in the contaminated cement at the cement-sandstone interface of the control sample.



4.8 Light (Optical) Microscopy

Thin sections of the composite cores measuring about 20 μm thick were prepared and used for optical microscopy. The thin sections were stained for easy identification of minerals present as different minerals show different coloration when stained. The varied coloration can be used to understand the reaction processes that occurred during the flow-through experiments.

Alizarin red was used for calcite staining, therefore calcium rich regions will appear pink and carbonated area will appear red to purple.

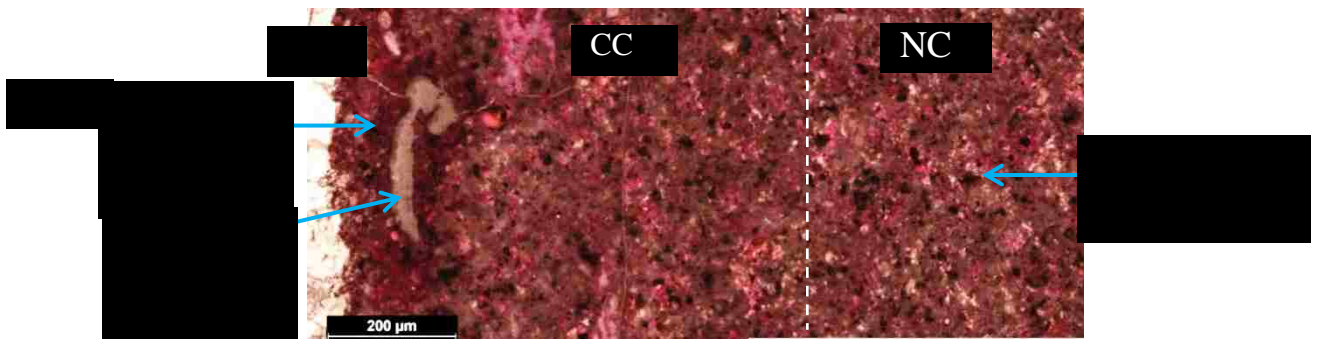
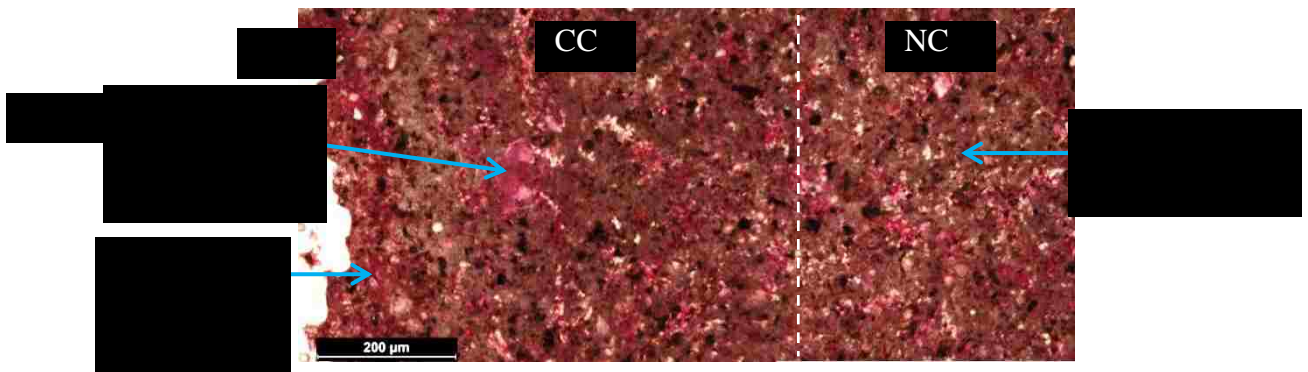
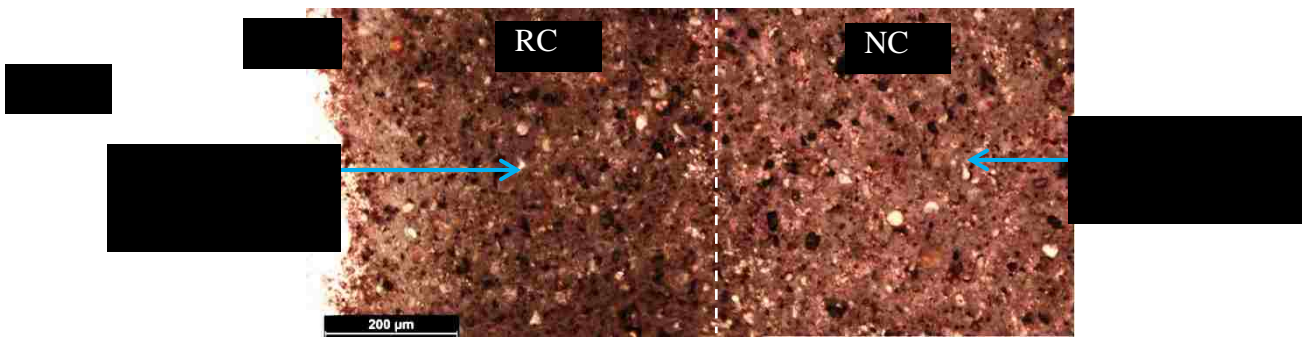
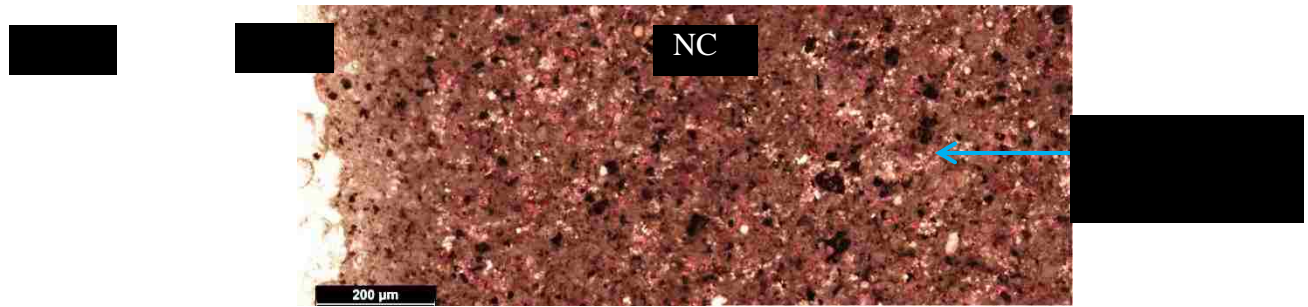
In the optical image of the pre core-flood 0% mud contaminated composite core, extensive pink coloration of the cement was observed as shown in Figure 4.19a. This indicates presence of calcium throughout the cement.

In the post core-flood image, a 600 μm wide region of the cement with reduced calcium content was observed close to the cement-sandstone interface as shown in Figure 4.19b. The reduced calcium content is indicated by the sparse pink coloration in the region. The calcium reduction was the result of leaching of the cement by the injected brine. The rest of the cement retained high calcium content indicated by the extensive pink coloration as shown in Figure 4.19b. The boundary between the reacted cement and neat cement is relatively sharp as could be seen in the image; indicating a consistent dissolution front.

The optical image of the pre core-flood 10% mud contaminated core showed that both the contaminated and neat cement had extensive pink coloration as shown in Figure 4.19c. The dark pink coloration in the contaminated cement closest to the sandstone signified high level of carbonation in that region. Zones with high mud contamination were also identified within the contaminated cement.

For the post core-flood image of 10% mud contaminated core, the contaminated and neat cement also had extensive pink coloration as shown in Figure 4.19d. A carbonated region was also observed close to the sandstone. Zones with high mud contamination were also identified within the contaminated cement. Large pores were however observed within the contaminated cement; one of such pores is shown in Figure 4.19d. The presence of large pores in the contaminated cement of the post core-flood composite core was the major alteration of the

composite core observed at the end of the 30-day core flood as most of the cement appeared unaltered.



4.9 Inductively Coupled Plasma-Optical Emission Spectroscopy (ICP-OES)

ICP-OES analysis was carried out to evaluate the cations present in the brine so that the reactions between the composite core and the injected brine could be delineated. The various cations analyzed and their respective concentrations are presented in Table 4.2. The cations present in the injected brine were first assessed to provide a base for describing the alterations in the flowing brine. The Ca concentration observed in the injected brine was low at 0.2484 mg/L. The Na and K concentrations in the injected brine were high (7110 mg/L and 314.1 mg/L respectively) since NaCl and KCl were used in preparing the brine.

Table 4.2: ICP-OES analysis of influent and effluent brine samples showing the concentration of different cations present. The brine samples analyzed were for the 1st, 15th and 30th day of each flow-through experiment.

Sample ID	Analyte										Comments
	Al	Ca	Fe	K	Mg	Mn	Na	Si	Ti	S	
	-----mg/L-----										
	Influent										
Control	0.906	0.248	ND	314.100	0.052	ND	7110.000	0.500	ND	0.000	All samples were analyzed after 3 times dilution with 2.5% HNO ₃ ; Reported Results were corrected for Dilution
	Effluent										
0% Day 1	1.102	12.030	ND	307.200	0.217	ND	7647.000	3.549	ND	0.342	
0% Day 15	1.051	14.640	ND	281.400	0.276	ND	7371.000	2.763	ND	0.495	
0% Day 30	1.052	18.150	ND	304.200	0.246	ND	7506.000	3.006	ND	0.384	
5% Day 1	0.972	17.760	ND	311.700	0.254	ND	7572.000	2.544	ND	0.251	
5% Day 15	1.109	15.570	ND	165.900	0.349	ND	7437.000	2.565	ND	0.133	
5% Day 30	0.956	15.570	ND	289.500	0.337	ND	7518.000	2.085	ND	0.212	
10% Day 1	1.218	9.978	ND	302.700	0.191	ND	7500.000	3.510	ND	0.059	
10% Day 15	0.950	14.766	ND	310.200	0.314	ND	7482.000	2.607	ND	0.119	
10% Day 30	0.990	14.985	ND	336.600	0.341	ND	7476.000	2.940	ND	0.211	

The Ca content of the effluent brine samples from the three flow-through experiments was much higher than that of the influent brine. The Ca content ranged from 9.978 to 18.15 mg/L. The average Ca content in the effluent was therefore ~60 times that of the influent brine. The high Ca content in the effluent brine was due to cement leaching.

The K content of the effluent was generally slightly lower than the K in the influent brine which suggests that there was a slight net flux of K out of the brine into the cement. The Na concentration was slightly higher in the effluent than in the influent and this indicated that Na was being leached from the cement by the flowing brine. The Mg and Si concentrations in the effluent brine samples were also higher than those of the influent brine. The average Mg and Si content of the effluent brine samples were more than 5 times those of the influent brine. The Si content of the effluent brine samples from the contaminated and uncontaminated composite cores were about the same showing that the increased Si in the effluent brine samples was not primarily from the mud in the mud contaminated cement but rather from the sandstone.

There was no observable difference between the amount of Al in the effluent brine samples and the influent brine showing that Al was not being leached from the composite core. The S content of the effluent brines was also higher than that of the influent brine indicating leaching of S by the flowing brine from the composite core.

4.10 Discussion of Results

4.10.1 pH Increase

The high pH of the effluent brine from the flow-through experiments indicates that dissolution of cement (pH~13) was taking place during the flow-through experiments. The lower pH of the effluent brine of the 0% mud contamination experiment compared to the 5% and 10% mud contamination experiment indicates that less cement dissolution occurred during the 0% mud contamination experiment. When cement comes in contact with low pH brine, there is exchange of ions between the highly alkaline cement pore solution (pH~13) and the slightly acidic brine. The high alkalinity of the cement pore solution is provided by abundant Na^+ , K^+ and OH^- ions in the solution while the brine contains Na^+ , K^+ and Cl^- . The influent brine slightly

acidified by atmospheric CO_2 also contains some CO_3^{2-} and HCO_3^- ions. The incompatibility between the two solutions results in exchange of ions. The ion exchange is an equilibration process that results in the outward diffusion of OH^- ions from the cement pore solution to the leaching brine with consequent reduction in the pH of the cement pore solution. The reduction in the pH of the cement pore solution induces dissolution of $\text{Ca}(\text{OH})_2$ to supply OH^- to maintain equilibrium in the environment. The constant diffusion of OH^- ions into the leaching brine increases the pH of the brine. The neat cement in the 0% contaminated core with its low porosity, provided lower diffusion coefficient for ion exchange than the contaminated cement in the 5% and 10% contaminated cores and therefore had less cement degradation. The pH of the mud used in the experiments was ~ 12 , therefore the mud contributed to the high pH of the effluent brine of the 5% and 10% mud contamination experiments. The large pores observed in the Micro-CT images show that there was significant dissolution of cement. The large pores present in the 5% and 10% mud contaminated cement also provided a large surface area for cement dissolution. The dissolution of $\text{Ca}(\text{OH})_2$ results in decreased pH of the cement and the cement thereby loses its ability to protect the casing from corrosion.

4.10.2 Pressure Drop Increase

Two phenomena likely contributed to pressure drop increase during the flow-through experiments. The first was the deposition of amorphous silica gel at the inlet of the composite cores. In this study, the composite cores were flooded with slightly acidic brine (pH ~ 6.2). The continuation of the cement leaching process explained in section 4.10.1, would lead to total depletion of $\text{Ca}(\text{OH})_2$ leaving the C-S-H with no buffer. This induces the decalcification of C-S-H resulting in the deposition of amorphous silica gel. The XRD diffractogram of the brown layer observed at the inlet of the composite core showed that it is amorphous and such brownish layer

has been observed by Duguid et al²³, Rimmelé et al⁷⁵, Kutchko et al²⁹ and Cheng et al⁷⁶ as the final stage of cement degradation.

The second phenomenon that likely caused the increasing pressure drop was mobilization of clays in the sandstone. The resin filled large pores in the back scattered electron microscopy images of the post core-flood 10% mud contaminated cement showed that there was connectivity between the pores in the sandstone and the pores in the cement but no connectivity was observed among the large pores in the cement. This means that the large pores did not affect the permeability of the composite cores and that flow was through the sandstone. Clays were identified in both the XRD diffractogram and SEM images of the Berea Sandstone used. Studies have shown that Berea sandstone contains high proportion of non-swelling clays (e.g. kaolinite); the kaolinite content of Berea sandstone can be as high as 9.7%^{77, 78}. When Berea sandstone comes in contact with fresh water (e.g. filtrate from fresh water mud), there is formation damage; this occurs due to the weakening of the van der Waals attractive forces and increase in the electrostatic repulsive forces between the pore walls and the clay particles⁷⁸⁻⁸⁰. This results in mobilization of the clay particles which end up plugging the pore throats of the Berea Sandstone and consequently reducing the permeability of the rock. The cement-sandstone composite cores were cured in tap water and this resulted in disruption of the bond between the clay particles and the pore walls. Continuous flooding of the composite core with brine would have mobilized some of the clay and plugged the pore throats in the sandstone. Fines were however not observed in the effluent, showing that occurrence of this phenomenon was not extensive.

4.10.3 Porosity Increase

For the 0% mud contaminated cement, the reduction in density and increase in porosity were caused by the leaching of Ca(OH)_2 as leaching has been shown to reduce porosity in cement⁸¹. The exchange of ions between the cement pore solution and the flowing brine results in the dissolution of Ca(OH)_2 and subsequent transport of Ca^{2+} ions out of the cement. When the CO_3^{2-} ions supplied by the slightly acidic brine combines with the Ca^{2+} in solution, CaCO_3 will be precipitated which tends to decrease porosity. Portlandite (33.1 cc/mol) occupies less volume than calcite (36.9 cc/mol)²⁵ but since the volume of CO_2 in the brine was small, the amount of calcite precipitated was not significant. The porosity of the neat cement was found to be 0.02% while the porosity of the leached cement was found to be 6.67%. The presence of well-defined dissolution front in the cement shows that there was instantaneous dissolution of Ca(OH)_2 to maintain local equilibrium⁸². The leaching rate was dominated by the diffusion rate of ions since the diffusion rate was much slower than the rate of Ca(OH)_2 dissolution⁸². The depth of leaching into the cement is usually estimated using Fick's second law of diffusion with the conditions that there is presence of unaltered cement zone and that the injected brine is of constant composition^{19, 29, 82}

$$L = c \cdot \sqrt{t}$$

where L =leaching depth, t =leaching duration and c is the diffusion coefficient of ions through the cement matrix which depends on the composition of the cement and the environment in which the cement is placed. The value of c varies with cement permeability, porosity, tortuosity and composition²⁹. It is also dependent on the chemical composition of the leaching brine¹⁹. The leaching depth observed for the 0% mud contamination experiment was ~950 μm . This was

close to the 1.4 mm in 3 months and <2 mm in one month observed by Mainguy et al⁸² and Yang et al¹⁹ respectively for 0.4 w/c cement pastes.

In the 10% mud contaminated cement, the porosity of the pre core-flood contaminated cement was 0.65% while the neat cement porosity was 0.02%. The pre core-flood porosity in the contaminated cement was more pronounced in areas with high mud contamination levels. After the core-flood, the porosity of the contaminated cement increased to 12.53%, showing extensive dissolution of the cement. The large pores created in the contaminated cement were caused by preferential dissolution of highly contaminated areas of the cement. The high pre-core flood porosity and the presence of NaOH (NaOH was added to the mud) in the highly contaminated areas resulted in the preferential dissolution of those regions. The high porosity resulted in faster ion diffusion between the cement and the brine when compared with the other sections of the cement that had lower porosity. Also, the solubility of NaOH in water is much higher than the solubility of $\text{Ca}(\text{OH})_2$, while leads to faster dissolution of the cement areas with high NaOH concentration. Leaching was however observed in areas surrounding the large pores; this shows that when the highly contaminated cement was extensively dissolved, the flowing brine started leaching the surrounding cement. In the long term, this may lead to interconnectivity of the large pores and loss of zonal isolation would occur.

In most areas of the 5% mud contaminated cement, the dissolution pattern was similar to the dissolution pattern observed in the 0% mud contamination. Apart from a few large pores, there was uniform dissolution of the cement. This is likely due to the lower volume of mud present in the cement to provide adequate preferential dissolution zones in the cement. The porosity of the pre core-flood contaminated cement was 0.1% while the neat cement porosity

was 0.02%. After the core-flood, the porosity of the leached zone was 8.77% while the porosity of the neat cement remained 0.02%.

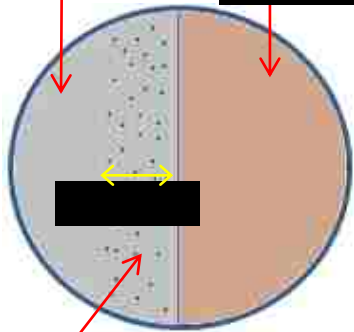
4.10.4 Summary of Observations

Results from the various analysis techniques employed in the study were integrated to obtain a holistic description of the alterations at the cement-sandstone interface in each of the three different composite cores at the end of the 30-day flow-through experiments.

For the 0% mud contaminated composite core, the injected brine leached the Ca(OH)_2 in the cement up to a depth of ~950 μm . There was uniform degradation of the cement with a distinct dissolution front as shown in Figure 4.20a. The leaching depth was similar to that observed in other studies where the leaching depth was found to increase with the square root of time^{19, 82}. The dissolution of the cement increased the porosity of the cement close to the cement-sandstone interface from 0.02% to 6.67% as shown in Tables 4.1, 4.2 and 4.3. Depletion of Ca(OH)_2 in cement reduces cement's ability to protect the casing from corrosive environments. At the end of the 30-day core flood, the cement would still be able to provide zonal isolation since a good bond was still established between the cement and the rock.

Apart from few large pores present, fairly uniform degradation was observed in the contaminated cement of the 5% mud contaminated composite core. The dissolution front was about 850 μm from the contaminated cement-sandstone interface as shown in Figure 4.20b. This is slightly lower than the leaching depth observed in the 0% contamination experiment. The highly contaminated zones in the contaminated cement likely slowed down the progression of the leaching front as they provided preferential dissolution regions. The dissolution of the cement increased the porosity of the contaminated cement from 0.1% to as much as 8.77% as shown in Tables 4.1, 4.2 and 4.3. The large pores present in the contaminated cement may

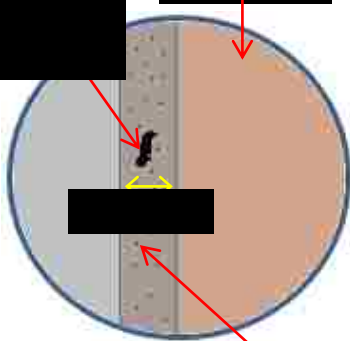
[Redacted]



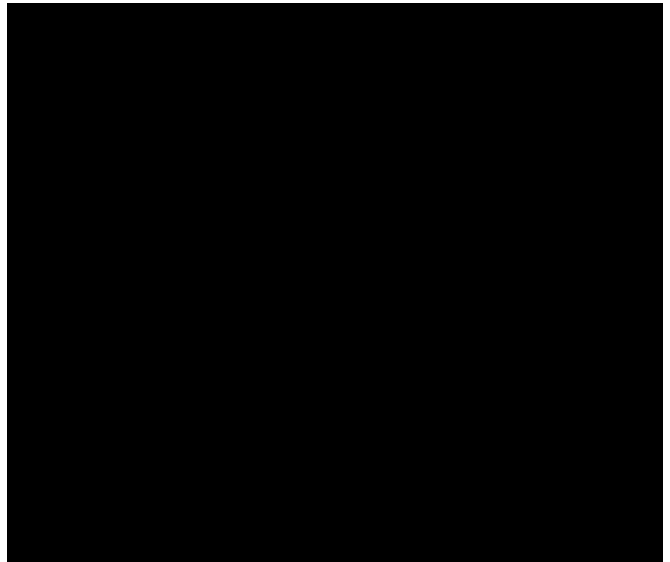
[Redacted]



[Redacted]

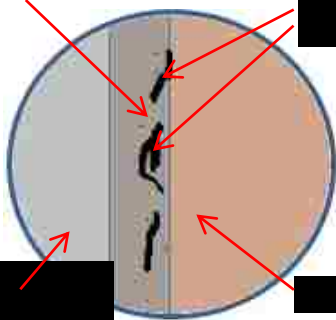


[Redacted]



[Redacted]

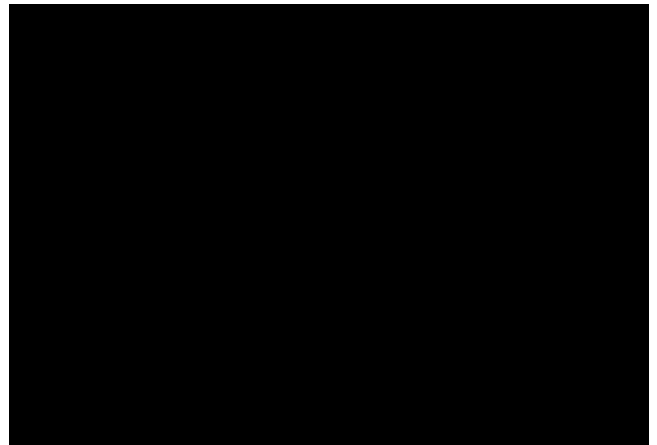
[Redacted]



[Redacted]

[Redacted]

[Redacted]



[Redacted]

reduce the mechanical integrity of the cement-sandstone interface. The cement would still provide zonal isolation as the large pores were few and not connected.

Large pores were observed in the contaminated cement of the 10% mud contaminated composite core as shown in Figure 4.20c. There was no clear dissolution front as the dissolution of cement extended with the depth of the highly contaminated cement areas. Leaching of areas around the large pores was also observed. The dissolution of the cement increased the porosity of the contaminated cement from 0.65% to as much as 12.53% as shown in Tables 4.1, 4.2 and 4.3.

Table 4.3: Pre core-flood porosity of cement in the composite cores.

	Cement-evaluation mini core		Interface-evaluation mini Core	
	Neat Cement	Contaminated Cement	Neat Cement	Contaminated Cement
0% mud contamination	0.02%	N/A	0.02%	N/A
5% mud contamination	0.02%	0.1%	0.02%	0.1%
10% mud contamination	0.02%	0.65%	0.02%	0.65%

Table 4.4: Post core-flood porosity of the cement at the inlet of the composite cores.

	Cement-evaluation mini core		Interface Evaluation mini core	
	Neat Cement	Leached Cement	Neat Cement	Leached Cement
0% mud contamination	0.02%	6.67%	0.02%	6.67%
5% mud contamination	0.02%	6.85% & 7.06%*	0.02%	7.92%
10% mud contamination	0.02%	5.85%	0.02%	12.53%

*Two values were presented because the dissolution front progressed beyond the contaminated cement into the neat cement. The lower value was the porosity of leached neat cement while the higher value was the porosity of leached contaminated cement.

Table 4.5: Post core-flood porosity of the cement at the outlet of the composite cores.

	Cement-evaluation mini core		Interface-evaluation mini core	
	Neat Cement	Leached Cement	Neat Cement	Leached Cement
0% mud contamination	0.02%	6.67%	0.02%	6.67%
5% mud contamination	0.02%	6.85%	0.02%	8.77%
10% mud contamination	0.02%	12.53%	0.02%	12.53%

At the end of the 30-day core-flood, the dissolution pattern left a large area of the cement unaltered thereby retaining cement's ability to protect the casing from corrosion. The numerous large pores would however reduce the mechanical integrity of the cement-sandstone interface and increase the likelihood of mechanical failure of the interface under stress and strain. Continued dissolution of the cement surrounding the large pores may connect the pores and create a fluid migration path.

CHAPTER 5 CONCLUSIONS AND RECOMMENDATIONS

5.1 Conclusions from the Experimental Findings

Three flow-through experiments were conducted to assess the effect of drilling fluid contamination on the integrity of a cement-formation interface using 1 inch by 12 inch cement-sandstone composite cores (half cylinder cement, half cylinder sandstone). One composite core had no contaminated layer and each of the other two composite cores had a (~1.27 mm thickness) layer of contaminated cement with 5% or 10% mud contamination by volume. Each composite core was used for a 30-day flow-through experiment and subsequently characterized to evaluate the alterations that occurred during the experiment. The first objective of the study was to assess the effect of drilling fluid contamination of cement on its ability to provide zonal isolation. The second objective was to investigate the physicochemical alterations at the cement-formation interface to understand the mechanism and kinetics of the alteration process.

At the end of the study the following conclusions were made:

- Dissolution of the cement by the flowing brine as determined from the pH measurements, microscopy images, tomography images, and calculated image based porosity, was the driving mechanism of degradation at cement-formation interface. The leaching of cement (primarily of Ca^{2+}) is due to the pH incompatibility between the composite core fractions (cement pH ~13 and mud pH ~12) and brine pH ~6.2.
- Porosity of the cement adjacent to the formation is increased by the leaching process and presence of mud contamination catalyzes cement dissolution. The large pores created by the preferential dissolution of the highly contaminated zones of the contaminated cement consequently provide large reactive surface areas for further dissolution.

- The presence of large non-circular pores (with as much as ~750 μm length and ~150 μm thickness) in the contaminated cement would likely eventually lead to loss of zonal isolation in the long term when the pores become interconnected due to continued dissolution.
- Within the range of contamination levels used in the study, we can conclude that the presence of 1% mud contamination of cement (10% contamination of 10% of the cement) appears to be a critical contamination level that will result in long term negative effect on zonal isolation and mechanical failure of wellbore cement to much higher degree than uncontaminated cement.

5.2 Recommendations for Future Work

Experiments should be conducted in such a way as to collect intermittent data from the composite cores during the experiment so that the kinetics of the reaction could be better quantified and the diffusion rate of the brine into the cement could be established. With information like diffusion rate, long term behavior of cement could be predicted.

Shear bond tests should be carried out on pre and post core-flood composite cores to quantify the effect of drilling fluid contamination on the cement-formation bond.

In addition, any cement/formation interface is going to be exposed to the geochemistry of the formation waters and the pressure and temperature of the formation, therefore experiments should be designed to test for the different environments.

The effect of mud contamination of cement placed against a shale formation should also be investigated as the shale caprock is the critical zone for fluid containment.

The total suspended solids in the brine should be measured.

REFERENCES

1. Bensted, J., and Barnes, P.: "Structure and Performance Of Cements", Taylor & Francis, New York, 2002.
2. Brandl, A., Cutler, J., Seholm, A., Sansil, M., and Braun, G.: "Cementing Solutions for Corrosive Well Environments", SPE 132228, SPE Drilling & Completion, Issue 2: pp. 208-219, 2011.
3. Nelson, E.B.: "Well Cementing", Schlumberger Educational Services, Sugar Land, Texas, 1990.
4. Tellisi, M., Ravi, K., and Pattillo, P.: "Characterizing Cement Sheath Properties for Zonal Isolation", WPC-18-0865 presented at the 18th World Petroleum Congress, Johannesburg, South Africa, September 25 - 29, 2005.
5. Guen, Y.L., Gouevic, J. L., Chammas, R., Gerard, B., Poupard, O., Van Der Beken, A., and Jammes, L.: "CO₂ Storage: Managing the Risk Associated With Well Leakage Over Long Time Scales" SPE-116424, SPE Projects, Facilities & Construction, Volume 4, Issue 3, pp. 87-96, 2009.
6. Dusseault, M.B., Gray, M. N., and Nawrocki, P.A.: "Why Oilwells Leak: Cement Behavior and Long-Term Consequences", SPE 64733 presented at the SPE International Oil and Gas Conference and Exhibition, Beijing, China, 2000.
7. Cavanagh, P.H., Johnson, C. R., LeRoy-Delage, S., DeBruijn, G. G., Cooper, I., Guillot, D. J., Bulte, H., and Dargaud, B.: "Self-Healing Cement - Novel Technology to Achieve Leak-Free Wells", SPE-105781 presented at the SPE/IADC Drilling Conference, Amsterdam, The Netherlands, 20-22 February 2007.
8. Bourgoyne, A.T., Scott, S.L., and Manowski, W.: "A Review of Sustained Casing Pressure Occurring on the OCS", Final Report submitted to the Mineral Management Services, 2000.
9. Annular Casing Pressure Management for Offshore Wells (Final Rule), Federal Register. p. 23582, May 4, 2010.
10. Kaiser, M., and Kruse III, B.J.: "A Risk-Adjusted Method for Determining OCS Lease Abandonment Liability in the Gulf of Mexico for BOEMRE Supplemental Bonding", SPE 124211, SPE Economics & Management, Volume 3, Issue 1, pp. 22-30, 2011.
11. Ravi, K.M., Beirute, R.M., and Covington, R.L.: "Erodability of Partially Dehydrated Gelled Drilling Fluid and Filter Cake", SPE 24571 presented at the SPE Annual Technical Conference and Exhibition, Washington, D.C., 4-7 October 1992.

12. Zuiderwijk, J.J.M.: "Mud Displacement in Primary Cementation", SPE 4830 presented at the SPE European Spring Meeting, Amsterdam, Netherlands, 29-30 May .1974
13. Clark, C.R. and Carter, G.L.: "Mud Displacement with Cement Slurries", SPE 4090, SPE Journal of Petroleum Technology, Volume 25 Issue 7, pp. 775-783, 1973.
14. Hewlett, P.C.: "Lea's Chemistry of Cement and Concrete", 4th Edition, Elsevier Butterworth-Heinmann, Oxford, 2004.
15. Nelson, E.B. and Guillot, D.: "Well Cementing" 2nd Edition, Schlumberger, Sugar Land, Texas, 2006.
16. Aligizaki, K.K.: "Pore Structure of Cement-based Materials: Testing, Interpretation and Requirements", Taylor & Francis, London, 2006.
17. Chilingar, G.V., Robertson, J.O., and Kumar, S.: "Surface Operations in Petroleum Production, II", Elsevier, Amsterdam, 1989.
18. Tian, B. and Cohen, M.D.: "Does Gypsum Formation During Sulfate Attack on Concrete Lead to Expansion?", Cement and Concrete Research, Volume 30 Issue 1, pp. 117-123, 2000.
19. Yang, H., Jiang, L., Zhang, Y., Pu, Q., and Xu, Y.: "Predicting the Calcium Leaching Behavior of Cement Pastes in Aggressive Environments", Construction and Building Materials, Volume 29, p. 88-96, 2012.
20. Ekström, T.: "Leaching of Concrete: Experiments and Modeling", Report TVBM-3090, Lund Institute of Technology, Division of Building Materials, 2001.
21. Jain, J. and Neithalath, N.: "Analysis Of Calcium Leaching Behavior of Plain and Modified Cement Pastes in Pure Water", Cement and Concrete Composites, Volume 31 Issue 3, pp. 176-185, 2009.
22. Kutchko, B.G., Strazisar, B. R., Dzombak, D. A., Lowry, G. V., and Thaulow, N.:, "Degradation of Well Cement by CO₂ under Geologic Sequestration Conditions", Environ. Sci. Technol., Volume 41 Issue 13, pp. 4787-4792, 2007.
23. Duguid, A. and Scherer, G.W.: "Degradation of Oilwell Cement Due to Exposure to Carbonated Brine", International Journal of Greenhouse Gas Control, Volume 4 Issue 3, pp. 546-560, 2010.
24. Yalcinkaya, T., Radonjic, M., Hughes, R. G., Willson, C. S., and Kyungmin, H.: "The Effect of CO₂-Saturated Brine on the Conductivity of Wellbore-Cement Fractures", SPE-139713, SPE Drilling & Completion, Issue 3, pp. 332-340. 2011.

25. Glasser, F.P., Marchand, J., and Samson, E.: "Durability of concrete — Degradation Phenomena Involving Detrimental Chemical Reactions", *Cement and Concrete Research*, Volume 38 Issue 2, pp. 226-246, 2008.
26. Yurtdas, I., Xie, S. Y., Burlion, N., Shao, J. F., Saint-Marc, J., and Garnier, A.: "Influence of Chemical Degradation on Mechanical Behavior of a Petroleum Cement Paste", *Cement and Concrete Research*, Volume 41 Issue 4, pp. 412-421, 2011.
27. Xie, S.Y., Shao, J.F. and Burlion, N. "Experimental Study Of Mechanical Behaviour of Cement Paste Under Compressive Stress and Chemical Degradation", *Cement and Concrete Research*, Volume 38 Issue 12, pp. 1416-1423, 2008.
28. Duguid, A.: "An Estimate of the Time to Degrade the Cement Sheath in a Well Exposed To Carbonated Brine", *Energy Procedia*, Volume 1 Issue 1, pp. 3181-3188, 2009.
29. Kutchko, B.G., Strazisar, B. R., Lowry, G. V., Dzombak, D. A., and Thaulow, N.: "Rate of CO₂ Attack on Hydrated Class H Well Cement under Geologic Sequestration Conditions", *Environ. Sci. Technol.*, Volume 42 Issue 16, pp. 6237-6242, 2008.
30. Bachu, S. and Bennion, D.B.: "Experimental Assessment of Brine and/or CO₂ Leakage Through Well Cements at Reservoir Conditions", *International Journal of Greenhouse Gas Control*, Volume 3 Issue 4, pp. 494-501, 2009.
31. Brandvoll, Ø., Regnault, O., Munz, I. A., Iden, I. K., and Johansen, H.: "Fluid–Solid Interactions Related to Subsurface Storage of CO₂ Experimental Tests of Well Cement", *Energy Procedia*, Volume 1 Issue 1, pp. 3367-3374, 2009.
32. Carey, J.W., Wigand, M., Chipera, S. J., WoldeGabriel, G., Pawar, R., Lichtner, P. C., Wehner, S. C., Raines, M. A., and Guthrie Jr, G. D.: "Analysis And Performance Of Oil Well Cement with 30 Years of CO₂ Exposure From the SACROC Unit, West Texas, USA", *International Journal of Greenhouse Gas Control*, Volume 1 Issue 1, pp. 75-85, 2007.
33. Bourgoyne, A.T.: "Applied Drilling Engineering", *SPE Textbook Series*, Volume 2, Richardson, 1986.
34. American Society of Mechanical Engineers Shale Shaker Committee: "Drilling Fluids Processing Handbook", Elsevier, 2005.
35. Southwest Research Institute: "Fall Velocity of Synthetic-Based Drilling Fluids in Seawater - Final Report", *Minerals Management Service*, 2007.
36. Burke, C.J. and Veil, J.A.: "Potential Environmental Benefits from Regulatory Consideration of Synthetic Drilling Muds", *U.S. Department of Energy*, 1995.

37. Ladva, H.K.J., Bernadette, C., Timothy, G. J., Garry, G., and David, S.: "The Cement-to-Formation Interface in Zonal Isolation", SPE 88016, SPE Drilling & Completion, Volume 3, pp. 186-197, 2005.
38. Crawshaw, J.P. and Frigaard, I.: "Cement Plugs: Stability and Failure by Buoyancy-Driven Mechanism", SPE 56959 presented at the Offshore Europe Oil and Gas Exhibition and Conference, Aberdeen, United Kingdom, 7-10 September 1999.
39. Fosso, S.W., Tina, M., Frigaard, I. A., and Crawshaw, J. P.: "Viscous-Pill Design Methodology Leads to Increased Cement Plug Success Rates; Application and Case Studies from Southern Algeria", SPE 62752 presented at the IADC/SPE Asia Pacific Drilling Technology, Kuala Lumpur, Malaysia, 2000.
40. Smith, R.C.: "Improved Method of Setting Successful Cement Plugs", SPE 11415, SPE Journal of Petroleum Technology, Issue 11, pp. 1897-1904, 1984.
41. Caenn, R., Darley, H., and Gray, G.R.: "Composition and Properties of Drilling and Completion Fluids", Gulf Professional Publishing, 2011.
42. Muhammad, N.: "Hydraulic, Diffusion, and Retention Characteristics of Inorganic Chemicals in Bentonite", Doctoral Dissertation, University of South Florida, 2004.
43. Wallender, W.W. and Land, D.P.: "Nanoscale Adsorbed Water Layer and Macroscopic Soil Properties: Kearney Foundation of Soil Science: Understanding and Managing Soil-Ecosystem Functions Across Spatial and Temporal Scales, 2006-2011 Mission, 2009.
44. Kaufhold, S. and Dohrmann, R.: "Stability Of Bentonites in Salt Solutions III — Calcium Hydroxide", Applied Clay Science, Volume 51 Issue 3, pp. 300-307, 2011.
45. Savage, D., Walker, C., Arthur, R., Rochelle, C., Oda, C., and Takase, H.: "Alteration of Bentonite by Hyperalkaline Fluids: A Review of the Role of Secondary Minerals", Physics and Chemistry of the Earth, Parts A/B/C, Volume 32 Issue 1-7, pp. 287-297, 2007.
46. Gates, W.P. and Bouazza, A.: "Bentonite Transformations in Strongly Alkaline Solutions", Geotextiles And Geomembranes, Volume 28 Issue 2, pp. 219-225, 2010.
47. Fernández, R., Cuevas, J., and Mäder, U.K.: "Modeling Experimental Results of Diffusion of Alkaline Solutions Through a Compacted Bentonite Barrier", Cement and Concrete Research, Volume 40 Issue 8, pp. 1255-1264, 2010.
48. Gaucher, E.C. and Blanc, P.: "Cement/Clay Interactions – A Review: Experiments, Natural Analogues, And Modeling", Waste Management, Volume 26 Issue 7, pp. 776-788, 2006.

49. Read, D., Glasser, F. P., Ayora, C., Guardiola, M. T., and Sneyers, A.: "Mineralogical and Microstructural Changes Accompanying the Interaction of Boom Clay with Ordinary Portland Cement", *Advances in Cement Research*, pp. 175-183, 2001.
50. El-Sayed, A.A. H.: "Effect of Drilling Muds Contamination on Cement Slurry Properties", *Fourth Saudi Engineering Conference*, pp. 287-295, 1995.
51. Bradford, B.B.: "Setting Cement Plugs Requires Careful Planning", *Oil & Gas Journal*, pp. 102, 1982.
52. Tasong, W.A., Lynsdale, C.J., and Cripps, J.C.: "Aggregate-Cement Paste Interface. II: Influence of Aggregate Physical Properties", *Cement and Concrete Research*, Volume 28 Issue 10, pp. 1453-1465, 1998.
53. Tasong, W.A., Lynsdale, C.J., and Cripps, J.C.: "Aggregate-Cement Paste Interface: Part I. Influence of Aggregate Geochemistry", *Cement and Concrete Research*, Volume 29 Issue 7, pp. 1019-1025, 1999.
54. Ollivier, J.P., Maso, J.C. and Bourdette, B.: "Interfacial Transition Zone in Concrete", *Advanced Cement Based Materials*, Volume 2 Issue 1, pp. 30-38, 1995.
55. Scrivener, K.L., Crumbie, A.K., and Laugesen, P.: "The Interfacial Transition Zone (ITZ) Between Cement Paste and Aggregate in Concrete", *Interface Science*, Volume 12 Issue 4, pp. 411-421, 2004.
56. Peterson, B.: "Bond Of Cement Compositions For Cementing Wells", WPC-10123 presented at the 6th World Petroleum Congress, Frankfurt am Main, Germany, June 19 - 26, 1963.
57. Evans, G. W. and Carter, L.G.: "Bounding Studies of Cementing Compositions to Pipe and Formations", API 62-072 , *Drilling and Production Practice*, 1962.
58. Yong, M., Rong, C. M., Yang, G., Qing, S., and Li, L.: "How To Evaluate the Effect of Mud Cake on Cement Bond Quality of Second Interface?", SPE-108240 presented at the SPE/IADC Middle East Drilling and Technology Conference, Cairo, Egypt, 22-24 October, 2007.
59. Recommended Practice For Testing Oil-Well Cements And Cement Additives, API Recommended Practice 10B, Twentieth Edition, American Petroleum Institute, April, 1977.
60. Yalcinkaya, T.: "Experimental Study on Single Cement Fracture Exposed to CO₂ Saturated Brine Under Dynamic Conditions", Master's Thesis, Louisiana State University, 2010.

61. Stout, K. and Blunt, L.: " Three-dimensional Surface Topography". Penton Press (Kogan Page Ltd), London, 2000.
62. Bennett, J.M. and Mattsson, L.: "Introduction to Surface Roughness and Scattering", Optical Society of America, 1989.
63. Herman, G.T.: "Fundamentals of Computerized Tomography: Image Reconstruction from Projections", Springer-Verlag, London, 2009.
64. Amelinckx, S., Van Dyck, D., Van Landuyt, and Van Tendeloo, G.: "X-Ray Microtomography - Handbook of Microscopy Set", Wiley-VCH Verlag GmbH, pp. 149-161, 2008.
65. Betz, O., Wegst, U., Weide, D., Heethoff, M., Helfen, L., Lee, W., and Cloetens, P.: "Imaging Applications of Synchrotron X-Ray Phase-Contrast Microtomography In Biological Morphology And Biomaterials Science. I. General Aspects of the Technique and its Advantages in the Analysis Of Millimetre-Sized Arthropod Structure", Journal of Microscopy, Volume 227 Issue 1, pp. 51-71, 2007.
66. Al-Raoush, R.I.: "Extraction of Physically-Realistic Pore Network Properties from Three-Dimensional Synchrotron Microtomography Images of Unconsolidated Porous Media", Doctoral Dissertation, Louisiana State University, 2002.
67. Rasband W.S., ImageJ - Version 1.45s, U.S. National Institutes of Health. Available: <http://rsb.info.nih.gov/ij/>. Bethesda, Maryland.
68. Goldstein, D.J.: "Understanding the Light Microscope: A Computer-Aided Introduction", Academic Press, London, 1999.
69. Goldstein, J., Newbury, D., Joy, David., Lyman, C., Echlin, P., Lifshin, E., Sawyer, L., and Michael, J.: "Scanning Electron Microscopy and X-Ray Microanalysis", Third Edition, Kluwer Academic/Plenum Publishers, New York, 2003.
70. Suryanarayana, C. and Norton, M. G.: "X-Ray Diffraction: A Practical Approach", Plenum Press, New York, 1998.
71. Verbal Communication with Dr Varshni Singh, Center for Advanced Microstructures and Devices, Baton rouge, Louisiana
72. Akin, S. and Kovscek, A.R.: "Computed Tomography in Petroleum Engineering Research", Geological Society London - Special Publications, Volume 215 Issue 1, pp. 23-38, 2003.
73. Iglauer, S., Wu, Y., Shuler, P., Tang, Y., and Goddard III, W. A.: "New Surfactant Classes for Enhanced Oil Recovery and Their Tertiary Oil Recovery Potential", Journal of Petroleum Science and Engineering, Volume 71 Issue 1-2, pp. 23-29, 2010.

74. Li, K.: "Determination of Resistivity Index, Capillary Pressure, and Relative Permeability", presented at the Thirty-Fifth Workshop on Geothermal Reservoir Engineering, Stanford, California, February 1-3, 2010.
75. Rimmelé, G., Barlet-Gouédard, V., Porcherie, O., Goffé, B., and Brunet, F.: "Heterogeneous Porosity Distribution In Portland Cement Exposed To CO₂-Rich Fluids", *Cement and Concrete Research*, Volume 38 Issue 8-9, pp. 1038-1048, 2008.
76. Cheng, K.Y., Bishop, P., Isenburg, J.: "Leaching boundary in cement-based waste forms", *Journal of Hazardous Materials*, Volume 30 Issue 3, pp. 285-295, 1992.
77. Shaw, J.C., Churcher, P.L. and Hawkins, B.F.: "The Effect of Firing on Berea Sandstone", SPE 18463, *SPE Formation Evaluation*, Issue 1, pp. 72-78, 1991.
78. Mohan, K.K., Vaidya, R. N., Reed, M. G., and Fogler, H. S.: "Water Sensitivity Of Sandstones Containing Swelling and Non-Swelling Clays", *Colloids and Surfaces A: Physicochemical and Engineering Aspects*, Volume 73, pp. 237-254, 1993.
79. Gray, D.H. and Rex, R.W.: "Formation Damage in Sandstones Caused by Clay Dispersion and Migration", *Fourteenth National Conference on Clay and Clay Minerals*, pp. 355-366, 1966.
80. Vaidya, R.N. and Fogler, H.S.: "Formation Damage Due to Colloidally Induced Fines Migration", *Colloids and Surfaces*, Volume 50, pp. 215-229, 1990.
81. Van Gerven, T., Cornelis, G., Vandoren, E., and Vandecasteele, C.: "Effects Of Carbonation And Leaching on Porosity in Cement-Bound Waste", *Waste Management*, Volume 27 Issue 7, pp. 977-985, 2007.
82. Mainguy, M., Tognazzi, C., Torrenti, J., and Adenot, F.: "Modelling of Leaching in Pure Cement Paste and Mortar", *Cement and Concrete Research*, Volume 30 Issue 1, pp. 83-90, 2000.

APPENDIX

Additional ICP-OES data

Table: ICP-OES analysis of influent and effluent brine samples showing the concentration of different cations present. The brine samples analyzed were for the 1st, 15th and 30th day of each flow-through experiment. The additional ICP analysis was carried out to validate the initial ICP-OES carried out during the study. The purple color represents values that are below confidence limits.

Sample ID	Analyte									
	Ca	Fe	K	Li	Mg	Mn	Na	B	Al	Sr
	mg/L									
	Influent									
Control	-0.017	0.119	193.985	0.015	0.034	-0.003	7450.000	-0.041	-0.035	0.069
	Effluent									
0% Day 1	15.716	0.052	208.985	0.018	0.222	-0.011	7880.000	0.596	0.277	0.328
0% Day 15	21.016	0.012	191.985	0.005	0.260	-0.035	7950.000	0.295	0.040	0.209
0% Day 30	19.716	0.031	198.985	0.004	0.230	-0.029	7970.000	0.345	0.173	0.210
5% Day 1	19.316	0.026	212.985	0.012	0.262	-0.020	8070.000	0.181	-0.123	0.295
5% Day 15	16.516	0.006	229.985	0.003	0.374	-0.020	7890.000	0.028	-0.060	0.235
5% Day 30	15.916	0.025	182.985	0.013	0.323	-0.005	7790.000	0.035	-0.034	0.282
10% Day 1	11.716	0.081	205.985	0.021	0.175	-0.021	7900.000	0.641	0.238	0.247
10% Day 15	15.416	0.013	203.985	0.019	0.327	-0.027	7790.000	-0.017	0.133	0.092
10% Day 30	16.516	0.020	101.985	0.010	0.373	-0.014	7830.000	-0.022	0.141	0.083

VITA

Nnamdi Agbasimalo was born in Obosi, Nigeria, in May 1983. He received his Bachelor of Engineering degree in Electrical and Electronic Engineering from Federal University of Technology, Owerri (F.U.T.O), Imo State, Nigeria, in 2005. He spent some time in the banking industry and then proceeded to Louisiana State University where he is currently pursuing his Master of Science degree. His research interests include drilling and completions. The degree of Master of Science in Petroleum Engineering will be conferred in August 2012.

During his stay at Louisiana State University, he authored two papers that were presented at the 46th ARMA Rock Mechanics/Geomechanics Symposium, Chicago and the 31st International Conference on Ocean, Offshore and Arctic Engineering (OMAE 2012), Brazil. He presented a poster at the 2011 Microscopy and Microanalysis Conference, Tennessee and his paper was also accepted for the Greenhouse Gas Control Technologies Conference (GHGT-11), Japan. He placed first in the 15th Annual Gulf of Mexico Deepwater Technical Symposium student poster competition and second in the 2012 Gulf Coast Regional SPE paper contest. He also mentored Lekendra Fusilier in research work.